

# **The Effect of different Filler Systems on Silicone Elastomers**

## **Dissertation**

With the aim of achieving the doctoral degree  
at the Faculty of Mathematics, Informatics and Natural Sciences

Department of Chemistry  
University of Hamburg

Submitted by

**Wolf J. Ammann**

Hamburg 2022



The experimental work described in this thesis was carried out from November 2015 to April 2019 at the Institute of Technical and Macromolecular Chemistry, University of Hamburg in the research group of Professor Dr. Gerrit A. Luinstra.

The following examiners recommend the admission of the dissertation:

1. Examiner: Professor Dr. Gerrit A. Luinstra
2. Examiner: Dr. Werner Pauer

Examination commission:

1. Prof. Dr. Gerrit A. Luinstra
2. Prof. Dr. Volker Abetz
3. Dr. Christoph Wutz

Date of thesis defense: 17.11.2023



# Table of Contents

Table of Contents .....	I
List of Abbreviations.....	IV
Abstract .....	1
Zusammenfassung.....	3
1 Introduction and Background.....	5
1.1 Synthetic Rubber.....	5
1.2 Silicone Rubber.....	6
1.2.1 Structure and Characteristics.....	6
1.2.2 Production .....	7
1.2.3 Crosslinking .....	9
1.2.4 Applications .....	9
1.3 Fillers in Rubber Compounds .....	10
1.4 Rubber Reinforcement .....	12
1.5 Aramid Fibres.....	14
1.5.1 Structure and Characteristics.....	14
1.5.2 Production .....	16
1.5.3 Applications .....	17
1.6 Halloysite Nanotubes .....	18
1.6.1 Structure and Characteristics.....	18
1.6.2 Applications .....	19
1.7 Carbon Nanotubes .....	21
1.7.1 Structure and Characteristics.....	21
1.7.2 Production .....	22
1.7.3 Applications .....	23
2 Motivation .....	24
3 Results and Discussion.....	25

## Table of Contents

---

3.1	Modification and Characterisation of Fillers.....	25
3.1.1	Aramid Fibres.....	25
3.1.2	Halloysite Nanotubes .....	28
3.1.3	Carbon Nanotubes .....	32
3.2	Preparation of Rubber Compounds .....	34
3.3	Silicone Aramid Composites.....	36
3.3.1	Vulcanisation behaviour.....	36
3.3.2	Thermal properties .....	38
3.3.3	Mechanical properties .....	39
3.4	Silicone HNT Composites.....	43
3.4.1	Vulcanisation behaviour.....	43
3.4.2	Thermal properties .....	46
3.4.3	Mechanical properties .....	48
3.5	Silicone CNT Composites.....	54
3.5.1	Vulcanisation behaviour.....	54
3.5.2	Thermal properties .....	55
3.5.3	Electrical properties.....	55
3.5.4	Mechanical properties .....	57
3.6	Composites with Filler Combinations.....	61
3.6.1	Vulcanisation behaviour.....	62
3.6.2	Mechanical properties .....	64
4	Summary .....	66
5	Experimental Part.....	68
5.1	Materials and Chemicals .....	68
5.2	Filler Modification .....	68
5.3	Rubber Processing.....	69
5.4	Rubber Testing .....	70
5.5	Characterisation.....	71

## Table of Contents

---

6	Safety Data .....	73
7	Bibliography.....	75
8	Appendix .....	82
	Declaration on Oath.....	83

## List of Abbreviations

AF	aramid fibres
BR	butadiene rubber
CNT	carbon nanotube
Demin	demineralised
DSC	dynamic scanning calorimetry
EPDM	ethylene propylene diene monomer
GE	glycerol triglycidyl ether
HNT	halloysite nanotube
HTV	high-temperature vulcanising silicone rubber
IIR	isobutylene-isoprene rubber
IR	infrared
LD	laser diffraction
LSR	liquid silicone rubber
MDR	moving die rheometer
$M_H$	maximum torque
$M_L$	minimum torque
MWCNT	multi-wall carbon nanotube
NBR	acrylonitrile butadiene rubber
NMR	nuclear magnetic resonance
NR	natural rubber
PDMS	polydimethylsiloxane
p-HNTs	pristine halloysite nanotubes



## List of Abbreviations

---

phr	parts per hundred rubber
PMA	3-(trimethoxysilyl)propyl methacrylate
PMIA	poly( <i>m</i> -phenylene isophthalamide)
PPTA	poly( <i>p</i> -phenylene terephthalamide)
RH	resorcinol-hexamethylenetetramine complex
RTV	room-temperature vulcanising silicone rubber
SBR	styrene-butadiene rubber
SEM	scanning electron microscopy
SiR	silicone rubber
SWCNT	single-wall carbon nanotube
T <sub>5%</sub>	temperature at 5% weight loss
T <sub>50%</sub>	temperature at 50% weight loss
t <sub>90</sub>	vulcanisation time when 90% of crosslinking is reached
T <sub>final</sub>	temperature at finalised weight loss
TGA	thermogravimetric analysis
UHMWPE	ultra-high molecular weight polyethylene
USD	United States dollar
VMQ	vinyl-methyl silicone rubber
XRD	x-ray diffraction



## Abstract

Silicone rubber (SiR) products are omnipresent in everyday life. They are used in many different areas of application due to their high temperature stability, high chemical resistance, high gas permeability and good processability.<sup>[1]</sup> In terms of their mechanical stability, however, silicone elastomers are inferior to other rubber types, limiting the possible applications.

The properties of rubber compounds are commonly adjusted by the incorporation of fillers. This work addresses the impact of different filler system on the characteristics of silicone rubber. Mechanical properties and thermal stability serve as criteria to evaluate the reinforcing effect of the used fillers. Furthermore, the vulcanisation behaviour and, if appropriate, the electrical conductivity were examined. Aramid fibres (AF), halloysite nanotubes (HNTs) and carbon nanotubes (CNTs) are used as fillers.

To validate the applicability of AF, HNTs and CNTs as reinforcing fillers for HTV SiR, composites with filler contents in the range of 0.1 to 10 phr were produced using an internal mixer. The incorporation of untreated AF increased the hardness and the Young's modulus compared to unfilled SiR by up to 13% and 101%, respectively. However, this was accompanied by a decrease in tensile strength and elongation at break, which is owed to the weak adhesion of the aramid fibres to the silicone matrix. An epoxy-silane coating was applied to the AF in order to improve the adhesion to silicone. The modification caused a reduction in the crosslinking density, which increased the tear resistance compared to unfilled SiR by 22%. However, the other mechanical properties were adversely affected.

Silicone-HNT composites were prepared using pristine HNTs and HNTs modified with a complex based on resorcinol and hexamethylenetetramine (RH). The RH complex acts as an adhesion promoter, due to the formation of a phenol-formaldehyde resin during the vulcanisation process. The incorporation of the RH modified HNTs (RH-HNTs) resulted in an increased crosslinking density, an accelerated vulcanisation time and an improved compression set without impairing other mechanical properties.

Four different types of CNTs were used purchased from the manufacturers Nanocyl SA, Kumho Petrochemical Co. and OCSiAl. Among them were three types of multi-wall CNTs (MWCNTs) and one type single-wall CNTs (SWCNTs). The latter showed a greater

reinforcing effect, which is attributed to the significantly smaller diameter of the SWCNTs and the larger surface area. A composite with 2 phr SWCNT showed an electrical conductivity of 1.4 S/m and a 29% increase in tear resistance compared to the unfilled SiR.

Novel multi-filler composites were prepared using RH modified HNTs in combination with untreated aramid fibres and SWCNTs, respectively. A further mechanical reinforcement was not achieved by the filler combinations. Only single parameters such as M100 in case of the aramid-HNT combination or tear strength in case of the CNT-HNT combination were improved. However, this was accompanied by weakening of other mechanical properties. The adverse effect of the insufficient adhered or dispersed AF and SWCNTs was not compensated by the reinforcing effect of the RH-HNTs.

## Zusammenfassung

Produkte aus Silikonkautschuk (SiR) sind im täglichen Leben allgegenwärtig. Sie werden aufgrund ihrer hohen Temperaturstabilität, hohen Chemikalienbeständigkeit, hohen Gasdurchlässigkeit und guten Verarbeitbarkeit in vielen unterschiedlichen Anwendungsgebieten eingesetzt.<sup>[1]</sup> Hinsichtlich ihrer mechanischen Eigenschaften sind Silikonelastomere anderen Gummiarten allerdings unterlegen, was die Anwendungsmöglichkeiten begrenzt.

Die Eigenschaften von Gummimischungen werden üblicherweise durch den Einsatz von Füllstoffen angepasst. Diese Arbeit befasst sich mit dem Einfluss unterschiedlicher Füllstoffsysteme auf die Eigenschaften von Silikonkautschuk. Als Kriterien zur Beurteilung der Verstärkungswirkung der verwendeten Füllstoffe dienen gängige mechanische Parameter und die Temperaturstabilität. Außerdem werden das Vulkanisationsverhalten und die elektrische Leitfähigkeit betrachtet. Als Füllstoffe werden Aramidfasern (AF), Halloysit-Nanoröhren (HNTs) und Kohlenstoff-Nanoröhren (CNTs) verwendet.

Um die Eignung von AF, HNTs und CNTs als verstärkende Füllstoffe für HTV SiR zu untersuchen, wurden Komposite mit Füllstoffgehalten im Bereich von 0.1 bis 10 phr im Innenmischer hergestellt. Durch die Inkorporation von unbehandelten Aramidfasern wurden die Härte sowie der Elastizitätsmodul im Vergleich zu ungefülltem Silikonkautschuk um bis zu 13% bzw. 101% erhöht. Dies ging allerdings mit einer Abnahme der Zugfestigkeit und Bruchdehnung einher, was der schwachen Anbindung der Aramidfasern an die Silikonmatrix geschuldet ist. Um die Anbindung zu erhöhen, wurden die Fasern mit einer Epoxy-Silan-Beschichtung modifiziert. Die Modifikation der Aramidfaser rief eine Erniedrigung der Netzwerkdicke hervor, wodurch die Weiterreißfestigkeit im Vergleich zu ungefülltem SiR um 22% erhöht, die anderen mechanischen Eigenschaften allerdings beeinträchtigt wurden.

Es wurden Silikon-HNT-Komposite mit unbehandelten HNTs und HNTs, die mit einem Komplex basierend auf Resorcin und Hexamethylentetramin (RH) modifiziert wurden, hergestellt. Dabei wirkt der RH-Komplex als Haftvermittler, was auf der Bildung eines Phenol-Formaldehyd-Harzes während der Vulkanisation beruht. Durch die Inkorporation der RH modifizierten HNTs (RH-HNTs) wurden eine Erhöhung der Netzwerkdicke, eine Verkürzung der Vulkanisationszeit und eine Verbesserung des Druckverformungsrests erreicht, ohne andere mechanische Eigenschaften zu beeinträchtigen.

Vier verschiedene CNT-Typen der Hersteller Nanocyl SA, Kumho Petrochemical Co. und OCSiAl wurden eingesetzt, darunter drei Typen mehrwandige CNTs (MWCNTs) und eine Type einwandige CNTs (SWCNTs). Die SWCNTs zeigten dabei eine höhere Verstärkungswirkung, was auf den deutlich geringeren Durchmesser der SWCNTs und die damit zusammenhängende größere Oberfläche zurückzuführen ist. Der Komposit mit 2 phr SWCNTs wies eine elektrische Leitfähigkeit von 1.4 S/m und im Vergleich zu ungefülltem SiR eine um 29% erhöhte Weiterreißfestigkeit auf.

Durch eine Kombination der RH-HNTs mit AF bzw. SWCNTs wurden neuartige Mehrkomponenten-Komposite hergestellt. Die Füllstoffkombinationen resultieren allerdings nicht in einer weiteren Verstärkung der Komposite. Nur einzelne Parameter wurden verbessert, wie M100 im Fall der AF-HNT-Kombination oder die Weiterreißfestigkeit im Fall der CNT-HNT-Kombination. Dies wurde jedoch von einem Verlust anderer mechanischer Eigenschaften begleitet. Die negative Auswirkung der unzureichend angebundenen oder dispergierten AF und SWCNTs wurde durch die verstärkende Wirkung der RH-HNTs nicht kompensiert.

# 1 Introduction and Background

## 1.1 Synthetic Rubber

Rubber is one of the most important industrial materials and is used in many areas such as automotive industry, construction, medical applications and household goods. In 2018 the worldwide production volume of rubber was 29.13 million tons, of which synthetic rubber accounted for over 52%.<sup>[2,3]</sup> The demand for synthetic rubber has been increasing continuously for decades (Figure 1).

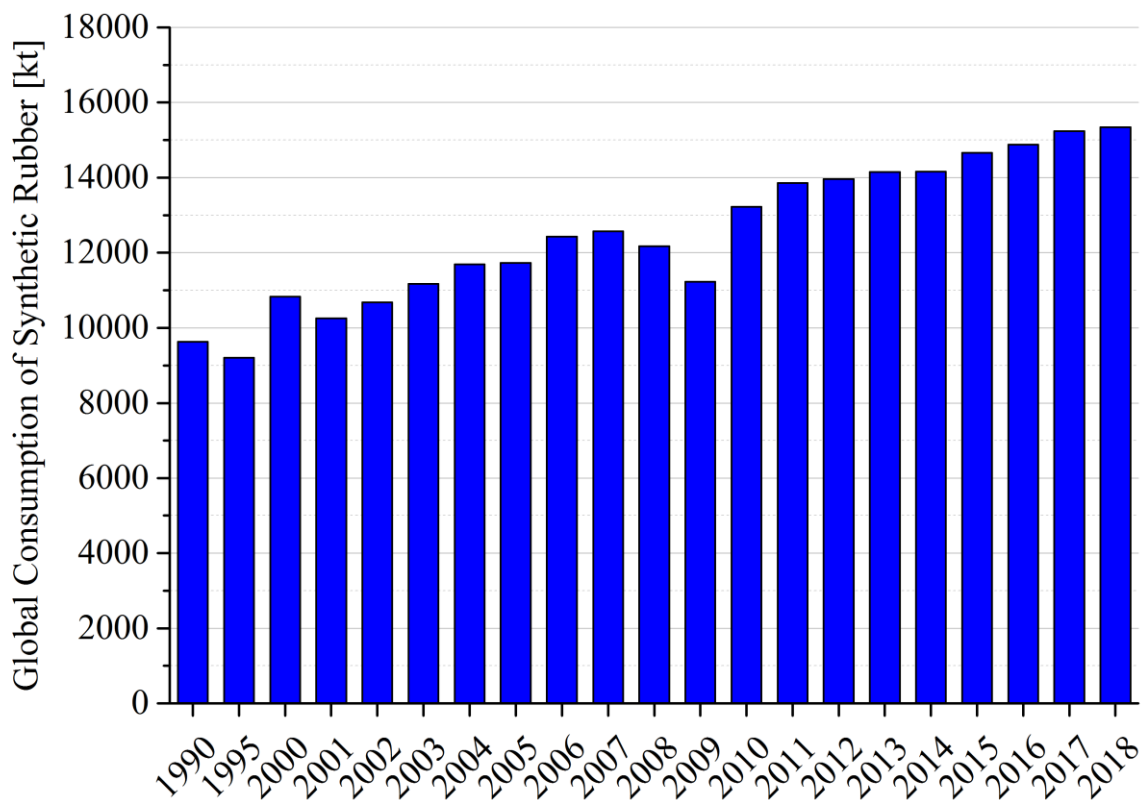


Figure 1. Global consumption of synthetic rubber from 2000 to 2018.<sup>[4]</sup>

With a share of over 55% of the global consumption of synthetic rubber, butadiene rubber (BR) and styrene-butadiene rubber (SBR) are still the most important synthetic rubbers.<sup>[5,6]</sup> One of the fastest growing rubber markets in recent years, however, is the silicone rubber market. According to recent market research the market share of silicone rubber amounted to 6.38 billion USD in 2018 and is estimated to grow an average of 6.7% per year between 2018 and 2023.<sup>[7]</sup>

## 1.2 Silicone Rubber

Silicone rubber (SiR) is a well-known and commercially important synthetic elastomer. The applications range from ordinary household goods to specialised high performance rubber goods. Silicone rubber products are widely used in large industries such as construction, automotive industry, health care, electronics, coatings and paints as well as consumer care.

### 1.2.1 Structure and Characteristics

Silicones (or polysiloxanes) are composed of siloxane as repeating unit, in which silicon atoms with at least one alkyl substituent are bound via oxygen atoms (Figure 2). This inorganic backbone gives silicone its extraordinary properties.

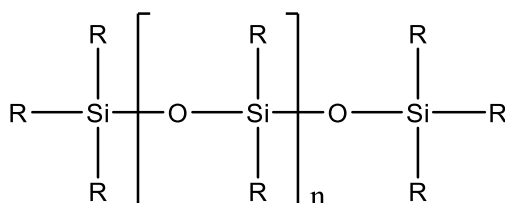


Figure 2. General structure of silicones (polysiloxanes).

The most common type of silicones is polydimethylsiloxane (PDMS), in which the alkyl substituents are methyl groups. The polysiloxane backbone shows a high thermal and oxidative stability due to the higher bond dissociation energy of the silicon-oxygen bond (373 kJ/mol) compared to that of the carbon-carbon bond (343 kJ/mol). The relatively obtuse bond angle of the silicon-oxygen-silicon bond (140 °) and the low intermolecular interaction of the polysiloxane chains allow a high mobility of the chain segments resulting in a low glass transition temperature (-123 °C for PDMS).<sup>[1]</sup> Further the alkyl substituents are on the periphery and thereby shield the polar silicon-oxygen bonds which accounts for the very hydrophobic nature of silicones.<sup>[8]</sup>

Depending on molecular weight, fillers and other additives, silicones are available as silicone oil, silicone grease or silicone rubber. Silicone rubbers are produced with different molecular weights with regards to their further processing. The molecular weight ranges from 70,000 to 100,000 g/mol for liquid silicone rubbers and from 250,000 to 900,000 g/mol for solid silicone rubbers.<sup>[1]</sup> Solid silicone rubbers typically contain a certain amount of fumed silica



dispersed by the manufacturer. The properties of the silicone rubbers can be adjusted by incorporating siloxanes with different substituents into dimethyl siloxane. The labelling of the different silicone rubbers depends on the present siloxanes (Table 1).

**Table 1. Labelling of silicone rubbers<sup>[1]</sup>**

Labelling according to ISO 1629	Structure
Q	Polysiloxane
MQ	Polydimethylsiloxane
VMQ	Copolymer from dimethyl- and vinylmethylsiloxane
PMQ	Copolymer from dimethyl- and phenylmethylsiloxane
PVMQ	Terpolymer from dimethyl-, phenylmethyl- and vinylmethylsiloxane
FVMQ	Terpolymer from dimethyl- trifluoropropylmethyl- and vinylmethylsiloxane

### 1.2.2 Production

Precursor for the production of silicone rubber is dimethyl dichlorosilane, which is produced according to the direct process by Müller and Rochow.

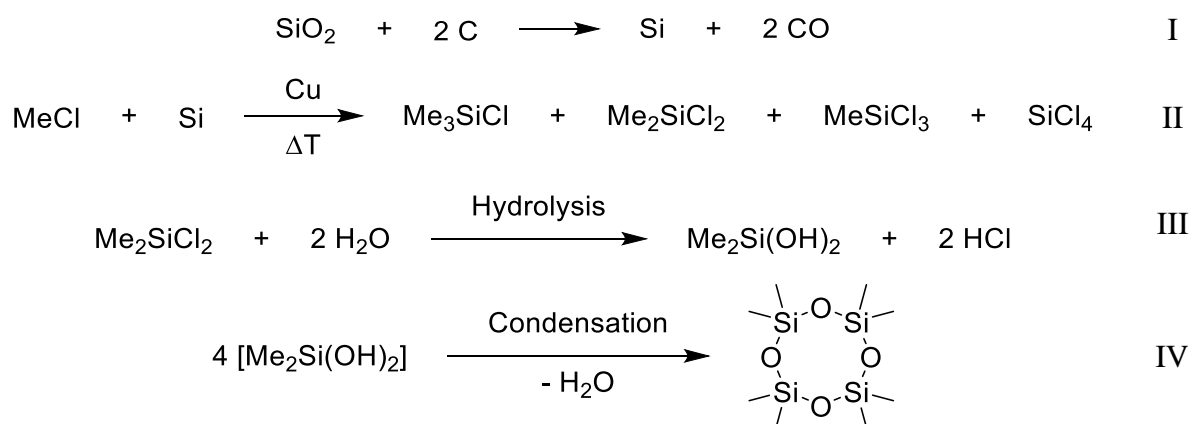


**Figure 3. Production of octamethyl cyclotetrasiloxane.<sup>[1]</sup>**

Starting material for the silicone rubber production is high-grade elemental silicon, which is obtained by smelting quartz sand with carbon (Figure 3 I). The copper-catalysed reaction of powdered silicon and chloromethane yields dimethyl dichlorosilane as main product (II). The byproducts are removed by fractional distillation. Dimethyl dichlorosilane is hydrolysed in the presence of acids leading to the formation of silanols (III), which are unstable in acidic medium and condensate to linear and cyclic oligomeric dimethyl siloxanes (IV). In order to produce high molecular polydimethyl siloxanes the hydrolysis is set to form predominantly cyclic dimethyl siloxanes. After obtaining the tetrameric dimethyl siloxane by distillation, a catalysed ring-opening polymerisation is performed. In case of using bases as catalysts, the cyclosiloxane is in equilibrium with the linear polymer (Figure 4). Remaining siloxanes are removed by distillation.<sup>[1]</sup>

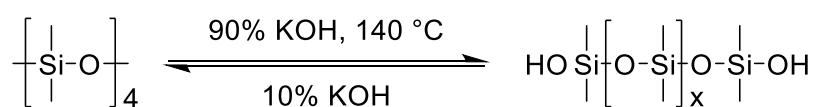


Figure 4. Ring-opening polymerisation of cyclosiloxane ( $x = 3000-10000$ ).<sup>[1]</sup>

The reaction is stopped by the addition of monofunctional silanes or water. Depending on the manufacturing process, the terminal groups can be methyl, vinyl or hydroxyl groups.<sup>[1]</sup> The manufacturing process of silicone is illustrated in Figure 5.

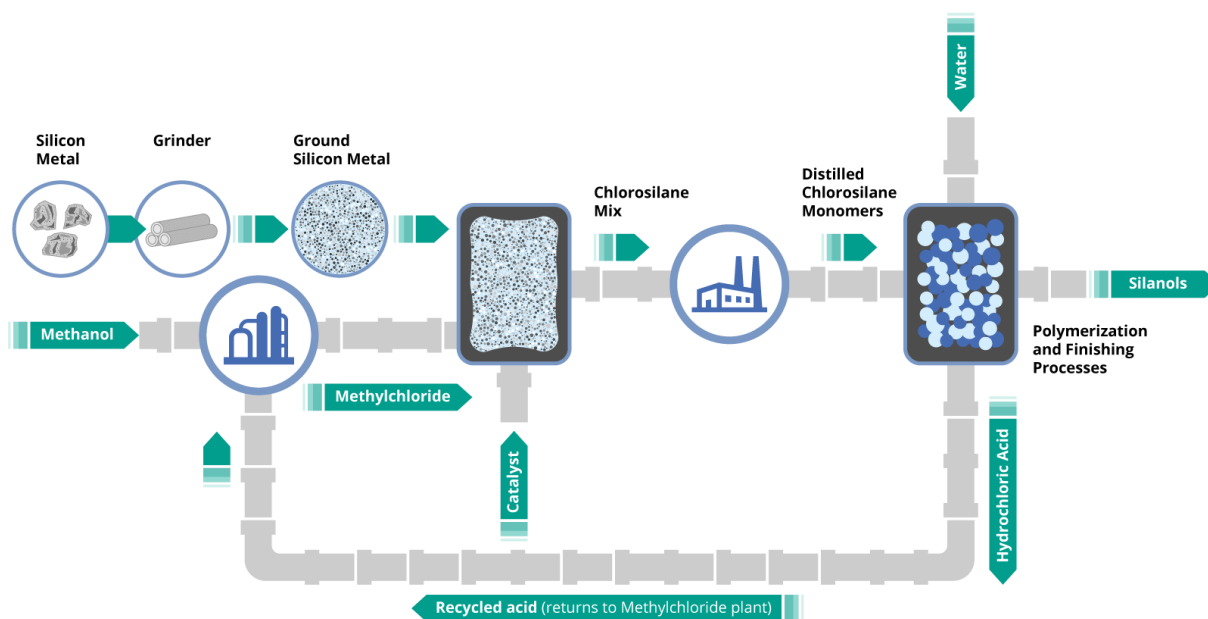


Figure 5. Diagram of the silicone manufacturing process.<sup>[9]</sup>

### 1.2.3 Crosslinking

Commercial silicone rubbers are classified according to their curing systems: high-temperature vulcanising solid silicone rubber (HTV), high-temperature vulcanising liquid silicone rubber (LSR) and room temperature-vulcanising silicone rubber (RTV). HTV are primarily cured radically by peroxide curing agents, whereas addition- or condensation-curing systems are used for LSR and RTV.<sup>[1]</sup>

The Peroxide curing of HTV involves the use of organic peroxides. These decompose at elevated temperatures forming reactive radicals, which crosslink the polymer chains. The pathway of peroxide curing is shown in Figure 6.

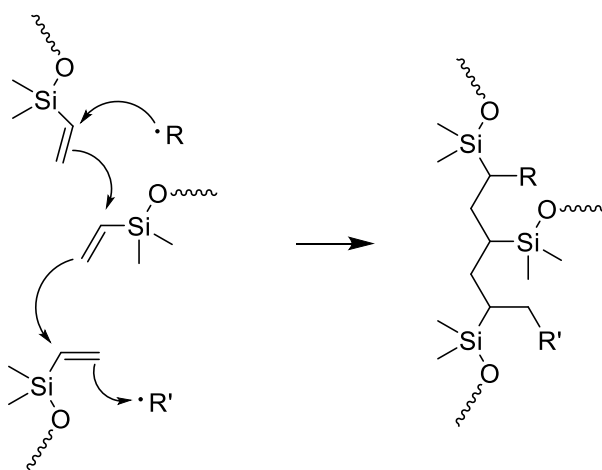


Figure 6. Crosslinking pathway of peroxide curing.<sup>[10]</sup>

LSR with vinyl groups can be crosslinked by addition curing using platinum compounds as catalysts. Silicone rubbers with terminal hydroxy groups can be crosslinked by condensation reactions with polyfunctional alkoxy silanes.<sup>[1]</sup>

### 1.2.4 Applications

Elastomers made of silicone rubber show thermal stability over a wide temperature range (-100 to +250 °C), good low-temperature flexibility, high elasticity as well as good weathering and aging properties.<sup>[11]</sup> Because of these properties, silicone rubber products are extensively used in insulations, coatings, gaskets, sealants, hoses and cosmetics. Additionally,

they are approved as materials for the contact with food and drinking water and due to their physiological compatibility applied in medical products.<sup>[12–14]</sup>

However, compared to other common rubbers, SiR has inferior mechanical properties, such as tensile strength, tear resistance, compression set and abrasion resistance (Table 2). This aspect limits the application range of silicone rubbers.

**Table 2. Relative properties of standard rubbers<sup>[15]</sup>**

<b>Parameter</b>	<b>NR</b>	<b>BR</b>	<b>SBR</b>	<b>IIR</b>	<b>EPDM</b>	<b>SiR</b>
<b>Durometer Range</b>	30-90	40-90	40-80	40-90	40-90	30-90
<b>Tensile max [psi]</b>	4500	3000	3500	3000	2500	1500
<b>Tear resistance</b>	A	B	C	B	C	C-B
<b>Compression set</b>	A	B	B	B	B-A	B-A
<b>Abrasion resistance</b>	A	A	A	C	B	B

A = excellent, B = good, C = fair

NR = Natural rubber, BR = Butadiene rubber, SBR = Styrene-butadiene rubber (SBR), IIR = Isobutylene-isoprene rubber, EPDM = Ethylene propylene diene monomer

### 1.3 Fillers in Rubber Compounds

Fillers are used in almost all rubber compounds and essentially determine their properties. They are mainly used to enhance the physical properties, but also to lower the formulation cost and generate specific characteristics. Fillers can be categorised into reinforcing (active) fillers and non-reinforcing (inactive) fillers. Reinforcing fillers interact with the rubber matrix and thereby affect the viscoelastic properties. They increase the viscosity and improve the fracture behaviour, such as tensile strength, tear strength and abrasion resistance. Non-reinforcing fillers mainly serve as extenders for the rubber compound. While the addition of

these fillers cause features like fracture energy to decrease, other properties such as processability and gas permeability can be improved. The effect of reinforcing and non-reinforcing fillers on selected properties is shown in Figure 7. Reinforcing fillers and non-reinforcing fillers can be also distinguished by their particle size. Reinforcing fillers have particle sizes between 10 and 100 nm, whereas non-reinforcing fillers have particle sizes between 500 and 1000 nm.<sup>[1]</sup>

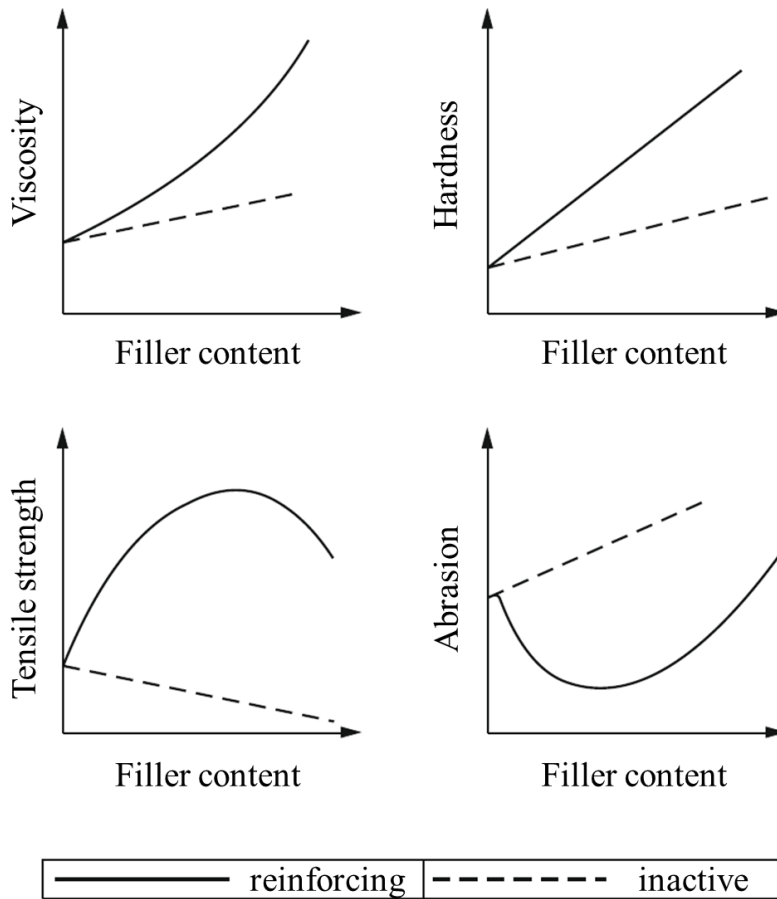


**Figure 7. Depiction of the effects of reinforcing and non-reinforcing fillers on selected properties of amorphous rubber.<sup>[1]</sup>**

The conventional fillers in general purpose elastomers are carbon black, precipitated silica, clays and natural carbonates. Less used but still of importance are silicates, talc and metal oxides. For more specialised applications, a variety of other fillers like macroscopic fibres, such as glass or aramid fibres, or carbon nanomaterials are used.<sup>[16]</sup>

## 1.4 Rubber Reinforcement

Rubber reinforcement refers to the improvement of one or more physical properties of a rubber, regardless whether it is crosslinked or not. The considered physical properties are usually tensile strength, tear strength, modulus and abrasion resistance. Further the improvement is sought to be achieved without impairing other properties such as compression set.<sup>[16]</sup> As criterion to evaluate the reinforcing effect of fillers Wiegand introduced the fracture energy, which is the integral of the stress-strain curve.<sup>[17]</sup> For reinforcing fillers, the fracture energy rises to a maximum with increasing filler content, while decreasing steadily for non-reinforcing fillers.<sup>[1]</sup>

According to Wiegand, the reinforcing effect of a specific filler is defined by a combination of its structure, contact surface and surface activity.<sup>[17]</sup> The structure describes the morphology of the filler particles and includes the size, form and size distribution. The smallest units that fillers are composed of are referred to as primary particles. These particles can be strongly attached to each other by intergrowth or fusion, building up the so called aggregates.<sup>[16]</sup> Aggregates are the smallest stable structural units that cannot be degraded by shear forces. Under the influence of van der Waals forces, several primary particles and aggregates can form anisotropic agglomerates. Agglomerates are referred to as secondary particles and are weaker structures, which are easily broken down during the mixing process. A lower degree of agglomeration means a higher available surface area for interaction with the rubber. Since solely the filler surface that is in contact with the rubber has an impact on the reinforcing effect, the dispersion of the filler in the rubber matrix is of great significance for the reinforcement.<sup>[1]</sup>

The surface activity describes the interactions between filler and rubber and is influenced by functional groups and free radicals on the filler surface. These interactions include van der Waals forces, dipole-dipole interactions, hydrogen bonds and covalent chemical bonds. Due to adsorption of the polymer molecules on the filler surface, the polymer chains are immobilized in the area of the filler surface. Depending on the strength of the interactions and the distance from the particle surface, a firmly bound, immobile rubber layer and an outer, more loose bound layer can be distinguished. These two states are called bound rubber and rubber shell.<sup>[1]</sup> Bound rubber is referred to the part of the rubber that cannot be extracted using a suitable solvent.<sup>[18]</sup> The surface activity of the fillers has a substantial influence on the rubber reinforcement.<sup>[1]</sup> On the other hand, strong interactions between filler particles

promote agglomeration and the formation of a filler network, which is particularly important at higher filler contents. This network is, however, strongly affected by deformation. Heavy deformations cause the network to collapse leading to a sharp decrease of the modulus, which is called Payne effect (Figure 8).<sup>[1]</sup>

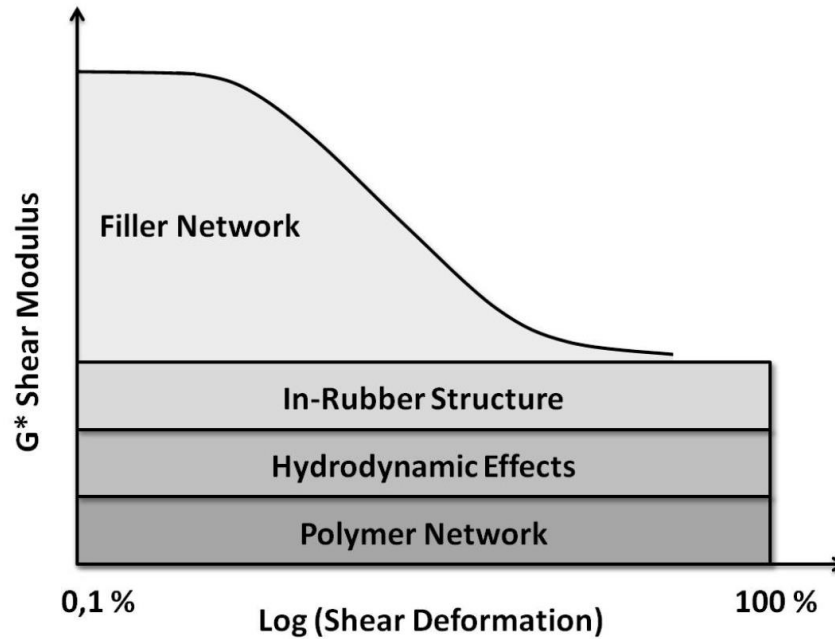


Figure 8. Contributions to the modulus of a rubber composite filled with a particulate filler.<sup>[19]</sup>

The effects of the main filler properties on the properties of filled elastomers are listed in Table 3.

Table 3. Effects of specific filler properties on those of filled elastomers<sup>[16]</sup>

<b>Elastomer property</b>	<b>Particle size (decreasing)</b>	<b>Structure (increasing)</b>	<b>Dispersion (increasing)</b>	<b>Interaction (increasing)</b>
<b>Hardness</b>	++	++	-	+
<b>Tensile strength</b>	++	little	+	+
<b>300% modulus</b>	+	++	little	++
<b>Elongation at break</b>	-	--	++	-
<b>Tear resistance</b>	++	little	little	little
<b>Hysteresis</b>	++	+	-	--
<b>Abrasion resistance</b>	++	+	++	++

+ = small increase, ++ = strong increase, - = small decrease, -- = strong decrease

## 1.5 Aramid Fibres

Aromatic polyamides, called aramids, are a polymer class with high mechanical stability and thermal resistance. They are commercially produced in form of yarns, films, papers and pulp. The most widely known applications of aramids are in fabrics for protective gear, such as bulletproof vests and fire protective clothing. Nevertheless, the use of aramid fibres as reinforcements in composite materials is also of great importance.

### 1.5.1 Structure and Characteristics

Aramids are linear polymers that are composed of aromatic units linked by amide bonds. This definition allows for various different polymers depending on the positions of the substituents on the aromatic rings. However, mainly two types of aramids are commercially produced, namely poly(*m*-phenylene isophthalamide) (PMIA), under the trade names Nomex and Teijinconex, and poly(*p*-phenylene terephthalamide) (PPTA), under Kevlar and Twaron (Figure 9).

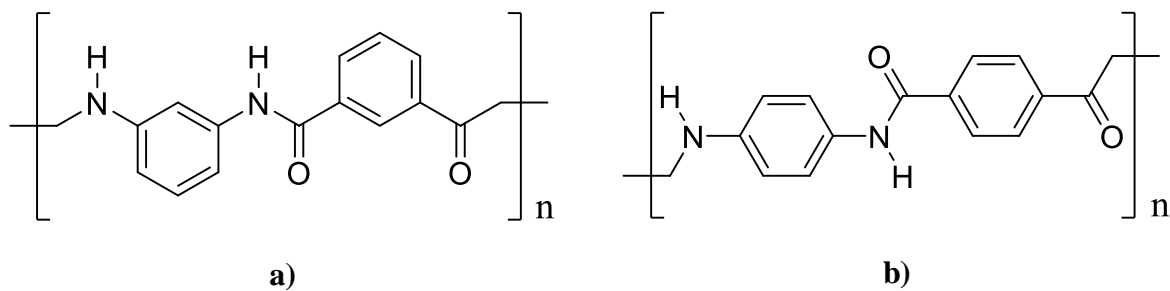
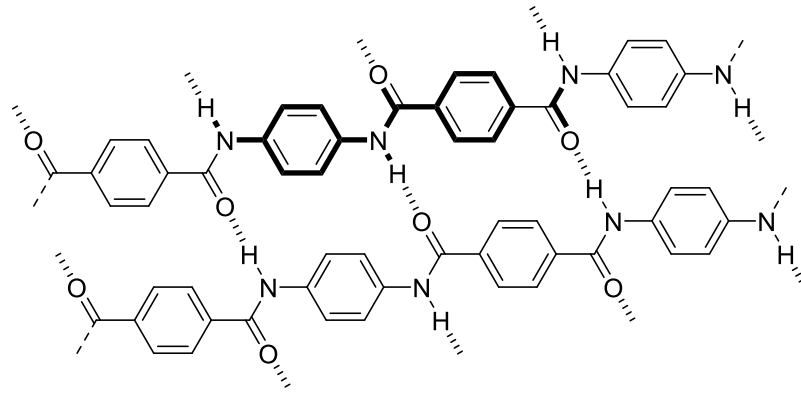


Figure 9. a) Poly(*m*-phenylene isophthalamide) and b) poly(*p*-phenylene terephthalamide).

Both aramids are characterised by their rigid backbone, made of planar aromatic rings and amide bonds. In this configuration the flexibility of the polymer chains is quite low due to the lacking possibility of rotation around the Ar-C and Ar-N bonds. Moreover, intermolecular hydrogen bonds between adjacent polymer strands cause a fixation of the extended molecular chains in longitudinal direction resulting in a highly aligned and highly crystalline structure of the filaments (Figure 10).<sup>[20]</sup> In PPTA the dominant crystalline domains alternate periodically with crystalline defect layers. However, this affects the strength of the fibre only to a small extent, since the defect layers are bridged by extended polymer chains. According to Northolt the structure of PPTA can be considered as paracrystalline.<sup>[21]</sup>





**Figure 10. PPTA strands with hydrogen bonds.**

PPTA fibres contain several levels of micro- and macroscopic structures. In the literature it is suggested that PPTA fibres consist of fibrils, which are oriented along the fibre axis and are 600 nm wide and several centimetres long.<sup>[22]</sup> These fibrils form radially arranged pleated sheets in longitudinal direction.<sup>[23]</sup> Another aspect of the PPTA morphology is the structural difference between the surface layer, the so-called skin, and the core of the fibres. The fibrils in the surface layer are uniformly axially oriented, while the ones in the core are imperfectly packed and ordered. It was found that these skin-core structures are roughly circular cylinders with a diameter of 30-50 nm.<sup>[22]</sup>

The structural details of the aramid fibres directly affect their mechanical and thermal properties. The impact of the structure becomes obvious when comparing the mechanical properties of the rigid PPTA and the more flexible PMIA (Table 4). PPTA shows significantly higher mechanical stability, while PMIA has much higher extensibility (around factor 10).

**Table 4. Mechanical properties of aramid fibres by Teijin Aramid<sup>[24]</sup>**

	Density [g/cm <sup>3</sup> ]	Tensile strength [GPa]	Tenacity [N/tex]	Elongation at break [%]
<b>Twaron (PPTA)</b>	1.44 – 1.45	2.7 – 3.6	1.9 – 2.5	2.3 – 4.2
<b>Teijinconex (PMIA)</b>	1.38	0.51 – 0.86	0.37 – 0.62	28 – 45

Compared to other common fibres in polymer reinforcement, PPTA fibres offer high tensile strength and temperature stability at low density (Table 5). They might be outperformed by carbon and ultra-high molecular weight polyethylene (UHMWPE) fibres, however, these have

much higher costs and for the UHMWPE a lower melting point. Additionally, PPTA fibres have a high glass transition temperature (around 530 °C), high decomposition temperature (around 530 °C), low flammability and good electrical insulation capabilities.<sup>[20]</sup>

**Table 5. Properties of various fibres used in reinforcement<sup>[25]</sup>**

	Density [g/cm <sup>3</sup> ]	Tensile strength [GPa]	Young's modulus [GPa]	Melting temp. [°C]
<b>PPTA (Kevlar 981)</b>	1.44	4.5	120	500
<b>E-Glass</b>	2.55	3.4	72.4	<1725
<b>Carbon (HS)</b>	1.50	5.7	280	3700
<b>Carbon (HM)</b>	1.50	1.9	530	3700
<b>UHMWPE</b>	0.97	2.6	120	147

HS = high strength, HM = high modulus

## 1.5.2 Production

The production of aramid fibres follows several steps, beginning with the synthesis of the polymer, then preparation of the spinning solution and finally the spinning process.<sup>[20]</sup>

Aramids are synthesised by polycondensation in solution using aromatic diamines and aromatic diacid chlorides. The reaction is carried out at low temperature (from 0 to -40 °C) in order to avoid side reactions. Common solvents are polar, aprotic solvents, like *N,N*-dimethylacetamide (DMAc) and *N*-Methylpyrrolidone (NMP). In case of the PPTA synthesis the addition of calcium chloride as solubilising aid has proven useful, as PPTA shows lower solubility in amide-type solvents.<sup>[25]</sup>

Precursors for the synthesis of PMIA are *m*-phenylenediamine and isophthaloyl dichloride, which react with elimination of hydrochloric acid (Figure 11).

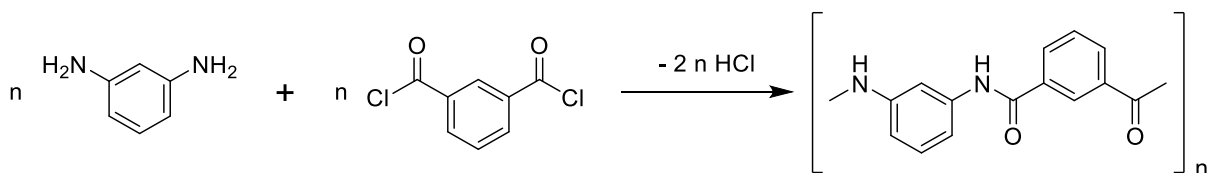


**Figure 11. Synthesis of poly(*m*-phenylene isophthalamide).**

For the synthesis of PPTA *p*-phenylenediamine and terephthaloyl dichloride are used (Figure 12).

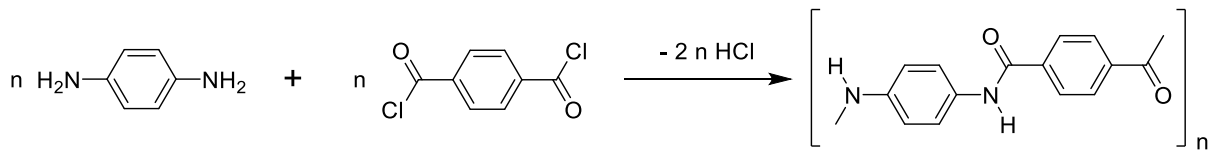


Figure 12. Synthesis of poly(*p*-phenylene terephthalamide).

In case of PMIA the synthesised polymer can be spun into yarns from isotropic NMP and DMAc solutions by dry spinning.<sup>[26]</sup> However, the fibre fabrication of PPTA is more challenging. After synthesis PPTA is isolated, washed and dried. To prepare a dope for fibre spinning PPTA is then dissolved in concentrated sulfuric acid, giving a solution with typical lyotropic properties. Oriented domains are formed at concentrations above 12 wt% and the solutions viscosity reaches its minimum at around 20 wt%.<sup>[20]</sup> Thus a concentration of 20 wt% is chosen for the PPTA spinning solution.<sup>[25]</sup>

According to Blades invention, PPTA fibres are manufactured from anisotropic solutions using the dry-jet wet spinning method.<sup>[27]</sup> This technique involves the extrusion of the PPTA solution through a small air gap (approx. 0.5 or 1 cm) into a coagulation bath. Choosing the right gap size is important to ensure a reorientation of the polymer molecules after leaving the spinneret. Finally the coagulated filaments are washed, neutralised and dried. The high orientation of the filaments is essential for the mechanical properties of the PPTA fibres.<sup>[20]</sup>

### 1.5.3 Applications

Due to their remarkable properties aramids fibres can be found in a wide variety of applications. They are used in friction materials, gaskets, ropes, cables, prosthetics, and sport equipment as well as in protective gear, such as bulletproof vests and fire protective clothing.<sup>[28]</sup> Furthermore, aramid fibres are used as composite reinforcement, for example in tires, pipes and pressure vessels. The reinforcing effect of aramid fibres has been studied in combination with many different polymers. They have been successfully incorporated in thermoplastics such as polyester, vinyl ester and epoxy resins as well as polyurethanes and in elastomers such as NR, SBR, NBR and SiR.<sup>[25,29–33]</sup> In some cases, a modification of the fibre surface was necessary to improve the adhesion to the polymer matrix. Moreover, PPTA fibres

are increasingly used in cement composites due to their low density and high specific strength.<sup>[20]</sup>

## 1.6 Halloysite Nanotubes

### 1.6.1 Structure and Characteristics

Halloysite is a naturally occurring aluminosilicate clay mineral with the chemical formula  $\text{Al}_2\text{Si}_2\text{O}_5(\text{OH})_4 \cdot 2\text{H}_2\text{O}$  at a fully hydrated state. It is a phyllosilicate, or sheet silicate, and belongs along with the minerals kaolinite, dickite and nacrite to the kaolinite group.<sup>[34]</sup> Regarding their structure and composition halloysite is similar to kaolinite, but the aluminosilicate layers are separated by a monolayer of water molecules. The structure consists of alternating octahedral alumina ( $\text{AlO}_6$ ) and tetrahedral silica ( $\text{SiO}_4$ ) sheets, that are bound via oxygen atoms.<sup>[35]</sup> A mismatch in the periodicity of these alumina and silica sheets cause the layers to roll up into a tubular shape, referred to as halloysite nanotubes (HNTs).<sup>[36]</sup> In these tubes the external surface of each HNT is composed of siloxane ( $\text{Si-O-Si}$ ) groups, whereas the internal surface consists of aluminol ( $\text{Al-OH}$ ) groups.<sup>[35]</sup> The crystalline structure of halloysite and the structure of halloysite nanotubes are depicted in Figure 13.

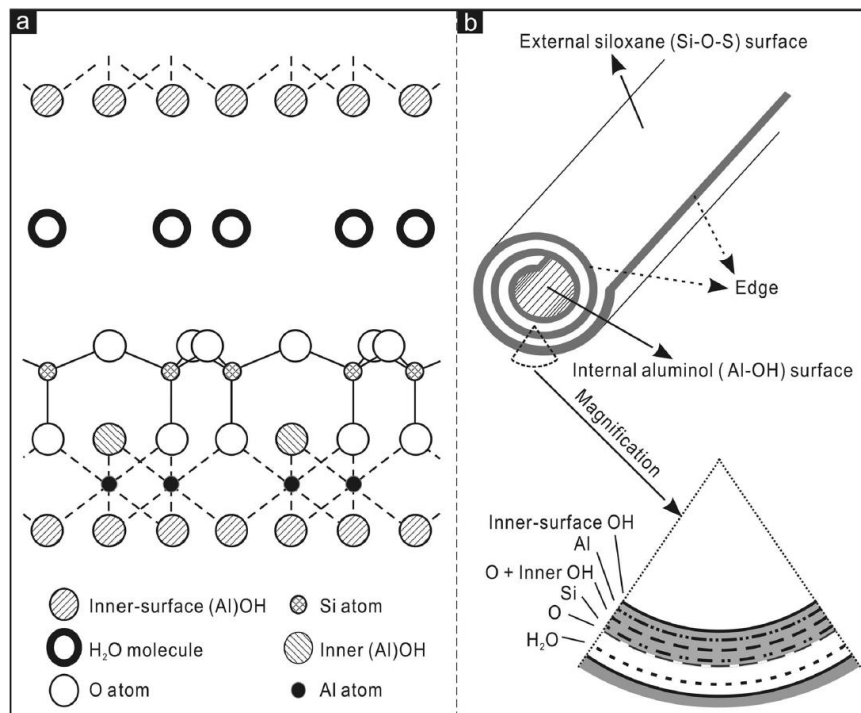


**Figure 13. Schematic diagram of a) the crystalline structure of halloysite and b) the structure of a halloysite nanotube.<sup>[35]</sup>**

HNTs exhibit a length of 50-5000 nm with external diameters of 20-200 nm and internal diameters of 10-70 nm.<sup>[37]</sup> The tubule walls generally consist of about 15-20 aluminosilicate layers with a basal spacing of around 1.0 nm or 0.7 nm for the hydrated or dehydrated state.<sup>[38]</sup>

### 1.6.2 Applications

Besides kaolinite, halloysite is one of the base materials for ceramics and is mined annually in millions of tons.<sup>[34]</sup> Because of its easy accessibility, high aspect ratio and extraordinary tubular structure, HNTs have been the topic of interest in various research activities. Due to their tubular, hollow structure they are relevant in the medical sector as, for example, a drug delivery system and many other applications.<sup>[39]</sup> However, the use of HNTs as a filler in different kinds of polymers has a much larger dimension.

For example, modified HNTs were incorporated into polypropylene (PP) by melt blending. The obtained nanocomposite showed increased thermal stability and flame retardant properties. These enhancements were ascribed to barrier effects in heat and mass transport as well as the presence of iron in HNTs.<sup>[40]</sup>

For linear low density polyethylene (LLDPE), HNTs showed to be a promising reinforcing nano-filler as the incorporation increased the thermal stability, flame retardancy as well as the mechanical properties. The tensile and flexural strength increased continuously with higher HNT loading. These properties could be further improved by grafting of PE copolymer enhancing the dispersion and interfacial bonding.<sup>[41]</sup>

In another study, the suitability of halloysite nanotubes as a fire retardant for nylon 6 was investigated. Composites with 5-30 wt% HNTs were prepared by a simple melt extrusion process. It has shown that relatively high concentrations of filler ( $\geq 15$  wt%) were required to obtain the desired fire-retardant effect. The easy dispersibility of HNTs in polymers compared to other nanoclays was ascribed to the tubular structure and low available hydroxy groups at the surface of the nanotubes.<sup>[42]</sup>

Untreated and surface-treated HNTs were tested as reinforcing filler in epoxy composites using 0-25 wt% respectively. The applied surface treatment was a sol-gel reaction between Si-OH groups on the HNT surface and TEOS to form SiO<sub>2</sub> particles on the HNTs. The test results showed an improvement in flexural strength for the HNT composites. Here, the

surface-treated HNTs showed better performance especially at higher HNT loading (20-25 wt%). In addition, the HNT epoxy composites exhibited enhanced thermal properties.<sup>[43]</sup>

The results of another study on HNT epoxy composites revealed that epoxy blended with 2.3 wt% HNTs increased the impact strength by the factor 4 without losing flexural modulus and strength, as well as thermal stability. It was proposed that the HNTs stabilized damaged areas with large numbers of micro-cracks through bridging.<sup>[44]</sup>

HNTs were also used as reinforcing filler in styrene-butadiene rubber (SBR). Here, they were incorporated by direct blending. Methacrylic acid and sorbic acid were used to modify the HNTs and thus improve the performance of the nanocomposites. Both modifications enhanced the interfacial bonding of the HNTs with the rubber matrix and yielded a significantly improved dispersion. This resulted in significantly increased tensile strength, 300% modulus, elongation at break and tear strength.<sup>[45,46]</sup>

Acrylonitrile-butadiene rubber (NBR) nanocomposites with 0-7 phr HNTs were prepared using a two-roll mill. It has been shown that the scorch time and cure time decreased with increasing HNT content. Furthermore, the tensile strength, tensile modulus at 100% elongation (M100) and elongation at break increased up to an optimum HNT loading of 5 phr. These improvements were ascribed to good dispersion of HNTs in the NBR matrix and strong interactions between HNTs and the NBR chains.<sup>[47]</sup>

In ethylene propylene diene monomer (EPDM), HNTs were incorporated with a content of 0-100 phr. It was found that the mechanical properties such as tensile strength, elongation at break, tensile modulus (M100) and crosslink density were significantly increased with higher HNT loading. The improvement in mechanical properties was ascribed to the homogenous dispersion of HNTs, the strong interactions between HNTs and EPDM as well as the formation of zig-zag structures by the HNTs. Moreover, the nanocomposites showed enhanced thermal stability and flame retardancy, which was attributed to entrapment of degradation products.<sup>[48]</sup>

Composites of natural rubber (NR) and 0-10 phr HNTs were prepared using a two-roll mill. Studies of vulcanisation showed an increase in scorch time and curing time as well as maximum torque with higher HNT loading. These findings were ascribed to restricted molecular motion of the polymer chains. The tensile strength and elongation at break could be improved and showed an optimum at 5 phr HNT loading. The highest tensile moduli (M100

and M300) were found at the highest HNT loading. Good dispersion and strong interfacial interactions were the suggested explanation for these results.<sup>[49]</sup>

## 1.7 Carbon Nanotubes

Carbon nanotubes are considered to be the most promising nanomaterial due to their outstanding qualities. CNTs show high flexibility, high aspect ratio and exceptional mechanical, electrical and thermal properties making them highly desired for the production of composites.

### 1.7.1 Structure and Characteristics

Carbon nanotubes (CNTs) consist of a hexagonal lattice of covalently bonded carbon atoms with a tubular shape. They can be considered as rolled-up graphene sheets with capped ends. CNTs occur in two basic types: single-wall carbon nanotubes (SWCNTs) consisting of a single graphene layer and multi-wall carbon nanotubes (MWCNTs) consisting of at least two coaxial cylinders (Figure 14). The length of CNTs ranges usually from a few micrometres up to millimetres, while the diameter varies between a few nanometres in case of SWCNTs and several tens of nanometres in case of MWCNTs.<sup>[50]</sup> The interlayer spacing in MWCNTs is 0.32-0.35 nm which is similar to the interlayer distance in graphite (0.34 nm).<sup>[51]</sup>

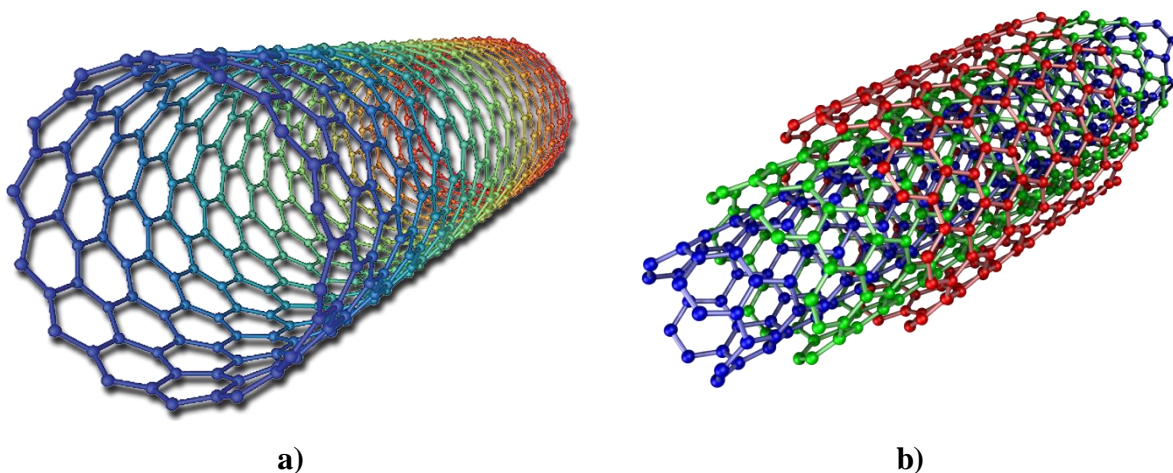


Figure 14. Schematic illustration of a) SWCNT and b) MWCNT.<sup>[52,53]</sup>

The interest in CNTs began as Iijima reported on them in 1991 and continued to grow due to their unique mechanical and electrical properties.<sup>[54]</sup> Individual MWCNTs have higher tensile

strength (11-63 GPa) and Young's modulus (270-950 GPa) than steel as well as higher electrical conductivity ( $10^7$ - $10^8$  S/m) than copper.<sup>[55,56]</sup> For individual SWCNTs tensile strength values of 13-52 GPa and Young's modulus values of 320-1470 GPa were reported.<sup>[57]</sup> The electrical conductivity of SWCNTs depends strongly on their helicity. There are three different configurations of SWCNTs possible: armchair, zigzag and chiral (Figure 15). While all SWCNTs with armchair configuration and one third of all zigzag SWCNTs are metallic, the rest are semiconducting.<sup>[58]</sup> Another important feature of CNTs is the thermal conductivity. An individual MWCNT was reported to exhibit values of  $>3000$  W/mK at room temperature, which is remarkably higher than that of diamond (2200 W/mK) or graphite (2000 W/mK).<sup>[59-61]</sup>

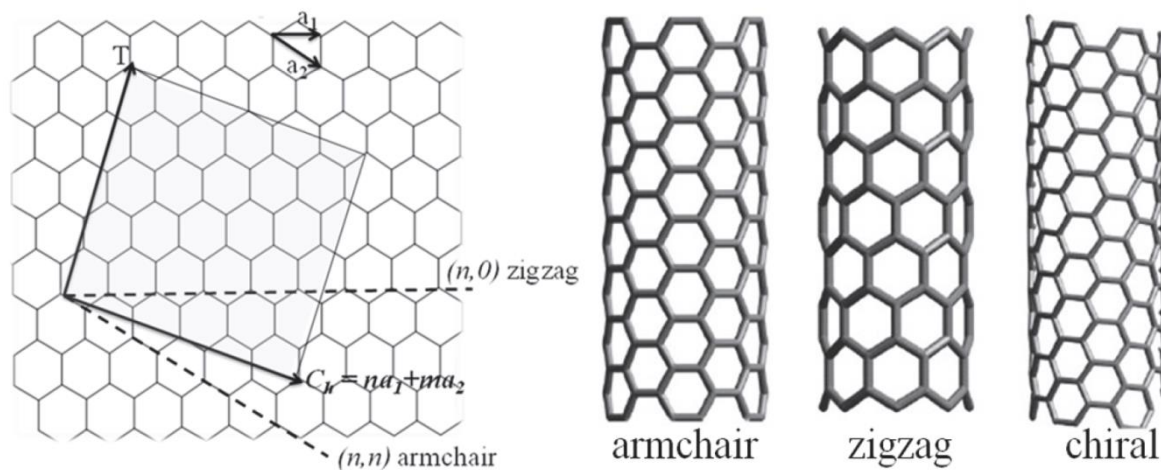


Figure 15. Diagram of graphene with lattice vectors of the different conformations of SWCNTs.<sup>[50]</sup>

## 1.7.2 Production

CNTs can be prepared using different methods including arc discharge, laser ablation and various chemical vapour depositions (CVD). The arc discharge method uses an arc discharge between two graphite electrodes at higher temperatures ( $>1700$  °C). The CNTs form on the negative electrode, while the positive electrode is consumed.<sup>[62]</sup> Laser ablation is based on the vaporisation of a graphite target at 1200 °C with following condensation of the carbon particles in the form of mainly SWCNTs on a cooled collector.<sup>[62]</sup> Both of these methods produce high-quality MWCNTs and SWCNTs, but are limited by their scale-up capabilities.<sup>[50]</sup> In the process of the catalysed CVD (CCVD) a hydrocarbon, e.g. methane, ethane, ethylene or acetylene, and a metal catalyst are introduced into the reaction chamber. The CNTs form on a substrate under catalytic decomposition of the carbon source. This



method is carried out at relatively low temperatures (<800 °C) compared to the other methods. CCVD has become the standard production method for CNTs due to large-scale access, easy process control and high purity of the obtained CNTs.<sup>[62]</sup>

### 1.7.3 Applications

Due to their outstanding mechanical and electrical properties, CNTs have great potential for various different applications. They are used in electronics, such as field emission displays or field-effect transistors, in electrochemical devices, such as batteries or supercapacitors, as well as in drug-delivery systems and as sensors. In polymer composites CNTs show great reinforcement qualities due to their excellent mechanical properties and large surface area. Additionally, the high electrical conductivity and high aspect ratio of CNTs enable electrical percolation in composites at relatively low loadings leading to antistatic properties and therefore preventing electrostatic discharge (ESD).<sup>[63]</sup>

The first report on polymer composites using CNTs as fillers was published in 1994.<sup>[64]</sup> Since then CNTs have been applied in all kinds of different polymers. In thermoplastics, such as PP, PE or PMMA, CNTs have been incorporated mainly by solution processing, melt mixing or in-situ polymerisation. Nanocomposites prepared by incorporating CNTs showed increased mechanical properties, e.g. Young's modulus, tensile strength, elongation at break, hardness as well as increased electrical and thermal conductivity. The reinforcing effects were attributed to good dispersion and good interaction with the polymer matrix, which can be enhanced by chemically modification of the CNT surface.<sup>[65-67]</sup>

CNTs have been used in combination with probably all common rubbers, such as NR, SBR, EPDM and SiR for the preparation of composites.<sup>[68-72]</sup> They are usually incorporated into the rubber matrix by mixing in a two-roll mill or internal mixer. Due to strong-van-der-Wall interaction and the inert surface CNTs tend to form strong agglomerates. Hence many manufacturers offer masterbatches with CNTs dispersed at high concentrations in a polymer matrix. Another method to improve the dispersion in the rubber matrix is the modification of the CNTs.<sup>[73,74]</sup> CNT composites based on elastomers show increased Young's modulus, tensile strength, elongation at break, hardness as well as increased electrical and thermal conductivity.

## 2 Motivation

The aim of this work is the improvement of the mechanical and electrical properties of silicone rubber by the incorporation of different filler systems to broaden its scope of application. Composites were prepared by mixing different fillers with varying filler contents and filler combinations into silicone rubber. The fillers, aramid fibres, halloysite nanotubes and carbon nanotubes, were, if necessary, chemically modified to increase the compatibility to silicone. The prepared composites were analysed with regard to their mechanical, electrical and thermal properties as well as their vulcanisation behaviour.

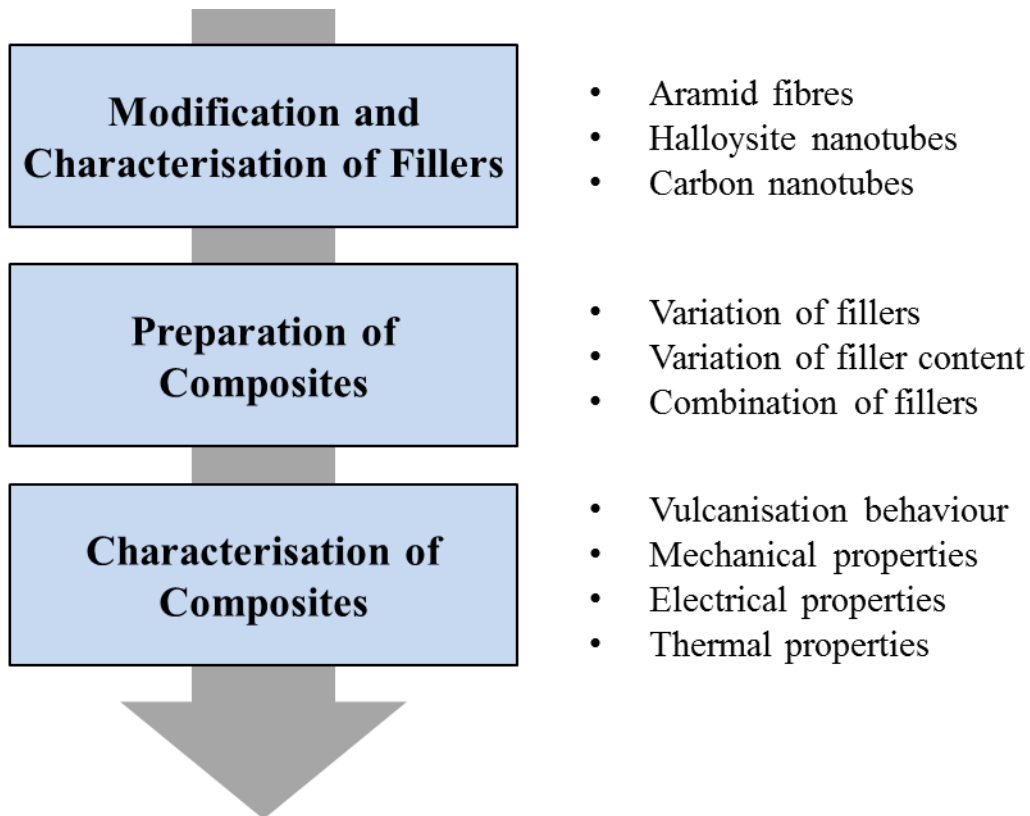


Figure 16. Flow chart with the approach in this thesis.

## 3 Results and Discussion

### 3.1 Modification and Characterisation of Fillers

In this work, aramid fibres (AF), halloysite nanotubes (HNTs) and carbon nanotubes (CNTs) were used as fillers for silicone rubber. This chapter addresses the chosen fillers including their modification and characterisation.

#### 3.1.1 Aramid Fibres

Aramid fibres were chosen for the reinforcement of silicone rubber because of their high tear resistance and temperature stability. The incorporation of aramid fibres into silicone rubber aimed at combining the beneficial properties of both materials. The use of aramid fibres as rubber reinforcement has been reported repeatedly in the literature.<sup>[75–77]</sup> The reinforcement of SBR with aramid pulp using ionic liquids as compatibilisers was described. For one composite, a 340% increase in tensile strength was found compared to that of SBR.<sup>[78]</sup> In this work, commercially available dry *para*-aramid pulp (Twaron 1095 by Teijin Aramid) was used. This type of aramid fibre is fibrillated and thus has an enlarged specific surface area and provides the possibility of interlocking of the filaments. The technical data of the applied aramid pulp is listed in Table 6. The size applied by the manufacturer was removed by Soxhlet extraction with ethanol before use.

**Table 6. Technical data of the used aramid pulp<sup>[79]</sup>**

Specific surface area	Fibre length	Diameter	Aspect ratio (L/D)
5 – 8 m <sup>2</sup> /g	0.75 – 1.2 mm	~ 12 μm	~ 80

The morphology of the aramid pulp was investigated using scanning electron microscopy (SEM). Individual fibre strands and the fibrillation of the aramid pulp can be clearly identified (Figure 17).

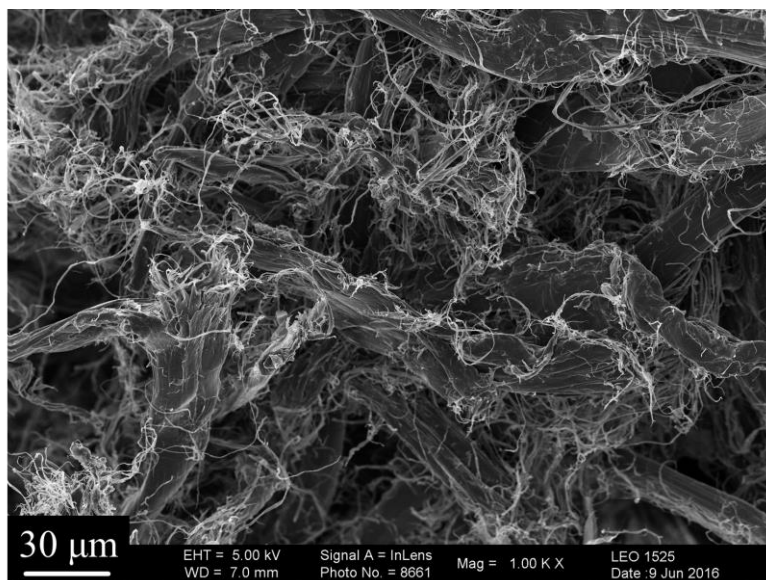


**Figure 17. SEM image of aramid pulp.**

The temperature stability of aramid fibres can be verified from the TGA curve (Figure 18). The small weight loss below 100 °C occurs due to the release of adsorbed water, which amounts to 2.2%. The thermal degradation of aramid takes place through one rapid degradation step between roughly 525 and 600 °C with a weight loss of 55%. Above 600 °C the weight loss is very slow. The total weight loss at 800 °C is 65%.

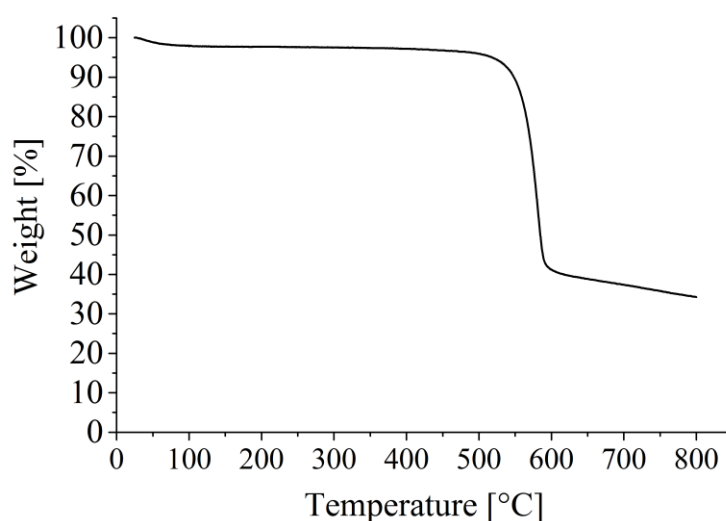


**Figure 18. TGA curve of aramid pulp.**

The poor adhesion between the polar amid groups of aramid and the methyl groups of silicone is well-known and it was expected that the aramid surface would require modification to

develop a reinforcing effect. Aramid short fibres and aramid pulp were used as reinforcement for liquid silicone rubber (LSR).<sup>[30]</sup> The aim was to improve the adhesion by roughening the aramid surface and using bifunctional organosilanes as adhesion promoter. An increase in modulus at low strain and decreased tensile strength and elongation at break was reported. However, the effect of modified aramid pulp on the tear strength and compression set of SiR has not been reported.

The aramid pulp was chemically modified following the method from Michiels, which includes the application of an epoxy undercoat and an organosilane topcoat onto the fibres.<sup>[80]</sup> Two-coat adhesive systems involving an epoxy compound were reported in the literature to give good adhesion to aramid.<sup>[81]</sup> The epoxy compound was glycerol triglycidyl ether (GE) and 3-(trimethoxysilyl) propyl methacrylate (PMA) was chosen as organosilane because of its good availability and low cost. The success of the fibre coating was examined by IR spectroscopy. In Figure 19 the IR spectra of the neat AF, the epoxy coated AF and the used triglycidyl ether are presented. In the spectrum of the neat AF, the characteristic absorption bands of the amide bond can be observed at  $3313\text{ cm}^{-1}$  for N-H stretching vibrations, at  $1643\text{ cm}^{-1}$  for C=O stretching vibrations, at  $1541\text{ cm}^{-1}$  for the combination of C-N stretching and N-H bending vibrations and at  $1313\text{ cm}^{-1}$  for the combination of C-N stretching and N-H bending vibrations.<sup>[82]</sup> The signals at  $1514$ ,  $1016$  and  $822\text{ cm}^{-1}$  arise due to the C-H vibrations of the aromatic ring. In the spectrum of the epoxy coated AF, new signals are visible. The signals at  $2999$ ,  $2916$  and  $2874\text{ cm}^{-1}$  are ascribed to C-H stretching vibrations of the GE methylene groups. The signal of the epoxy group at  $985\text{ cm}^{-1}$  is covered by the wide absorption band of the C-O-C group at  $1094\text{ cm}^{-1}$  and only visible as a small shoulder.<sup>[83]</sup> Nevertheless, the signals indicate a successful epoxy modification.

Figure 20 shows the IR spectra of the epoxy coated AF, the PMA modified AF (m-AF) and PMA. Most of the distinctive absorption bands of PMA overlap with those from aramid or the epoxy coating. The signal at  $1178\text{ cm}^{-1}$  is recognisable as a small shoulder and corresponds to the Si-O-C bond, suggesting that the PMA coating took place, but only to a very small extent.<sup>[84]</sup> It was envisioned, that even this minor modification would have an impact on the adhesion between aramid and silicone.

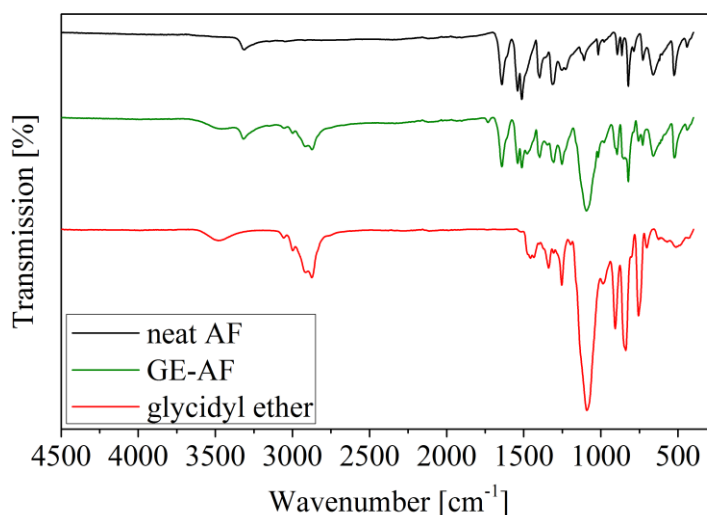


Figure 19. IR spectra of the neat AF, epoxy coated AF (GE-AF) and GE.

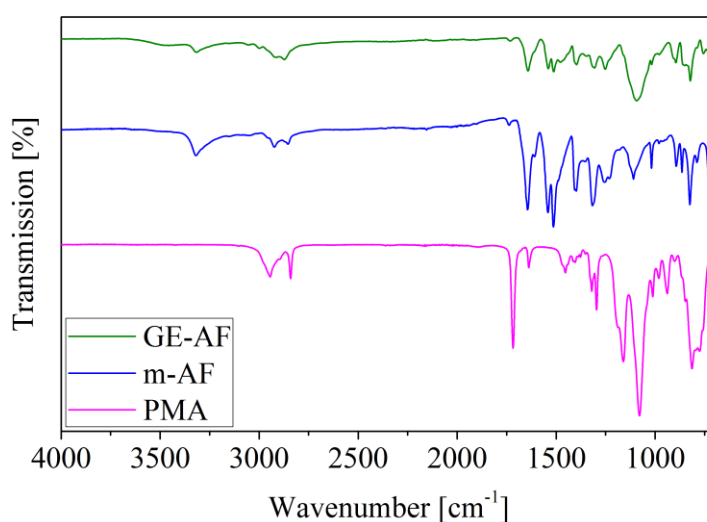


Figure 20. IR spectra of the epoxy coated AF, PMA coated AF and PMA.

### 3.1.2 Halloysite Nanotubes

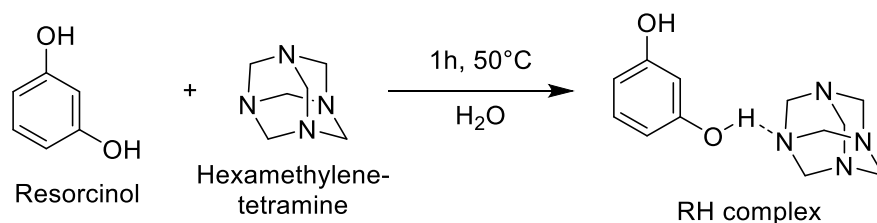
The use of HNTs for the preparation of rubber nanocomposites has been extensively described in the literature. A variety of modifications of HNTs and the incorporation into various rubber types have been reported.<sup>[85]</sup> The HNTs used in this work were Dragonite-HP from Applied Minerals, Inc. According to the manufacturer this product grade offers optimal mechanical performance at loadings of 1-3%. The technical data of the HNTs is shown in Table 7.

**Table 7. Technical data of the applied HNTs<sup>[86]</sup>**

Length [ $\mu\text{m}$ ]	Outside diameter [nm]	Inside diameter [nm]	Aspect ratio (L/D)	BHT surface area [ $\text{m}^2/\text{g}$ ]	Bulk density [ $\text{g}/\text{mL}$ ]
0.2-2	50-70	15-45	10-20	35-65	~0.25

HNTs like other nanomaterials tend to form agglomerates. Therefore, a modification of the HNTs was sought to improve the dispersion of the HNTs in the silicone matrix as well as the adhesion of the HNT surface to the silicone molecules. A complex of resorcinol and hexamethylenetetramine (RH complex) was used, which is a common adhesion promoter in the rubber industry.<sup>[87]</sup> Its use has been reported in several studies over the past decades. For example, it was applied for the preparation of sisal fibre NR composites in 1994, montmorillonite NBR composites in 2006 and HNT SBR composites in 2009.<sup>[88-90]</sup> The RH complex was also used for the preparation of silicone rubber HNT nanocomposites. The study revealed increased Young's modulus, tensile strength and accelerated cure kinetics compared to unfilled silicone rubber.<sup>[91]</sup>

The modification of HNTs was carried out following an established procedure.<sup>[91]</sup> The formation of the RH complex takes place in water at around 50 °C (Figure 21) and is driven by the proton donor activity of resorcinol and the proton acceptor function of hexamethylenetetramine. Hence, in the complex the resorcinol and hexamethylenetetramine molecules are connected by hydrogen bonds between the hydroxy groups of resorcinol and the nitrogen atoms of hexamethylenetetramine.<sup>[92]</sup> The RH complex also provides the possibility to form hydrogen bonds between the hydroxy groups of resorcinol and the HNT surface.

**Figure 21. Formation of RH complex.**

In the following chapters the pristine HNTs are referred to as HNTs or p-HNTs and the RH modified HNTs are referred to as RH-HNTs. The tubular structure of HNTs could be made

visible using SEM (Figure 22). Furthermore it can be seen that some p-HNTs and RH-HNTs are present in agglomerates (Figure 23).

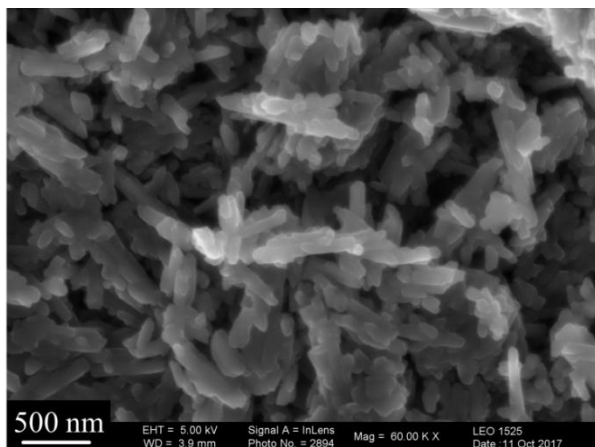


Figure 22. SEM image of p-HNTs.

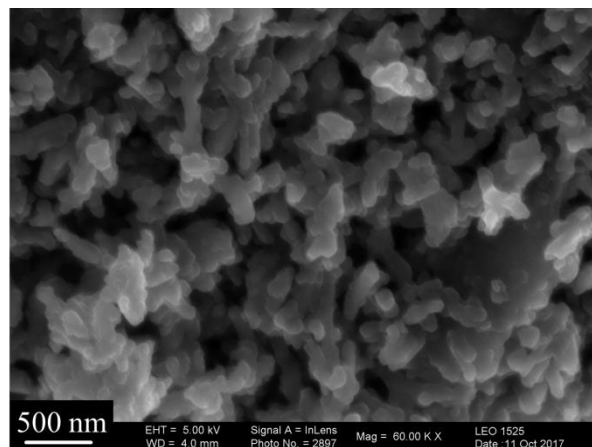


Figure 23. SEM image of RH modified HNTs.

The success of the modification was investigated using energy-dispersive X-ray spectroscopy (EDX). According to the EDX spectra, RH-HNTs show significantly increased O/Al and C/Al ratios plus the appearance of nitrogen, which confirms the RH complex modification on the RH-HNTs (Figure 24). Intercalated calcium atoms as well as a part of the iron atoms were apparently washed out during the modification process.

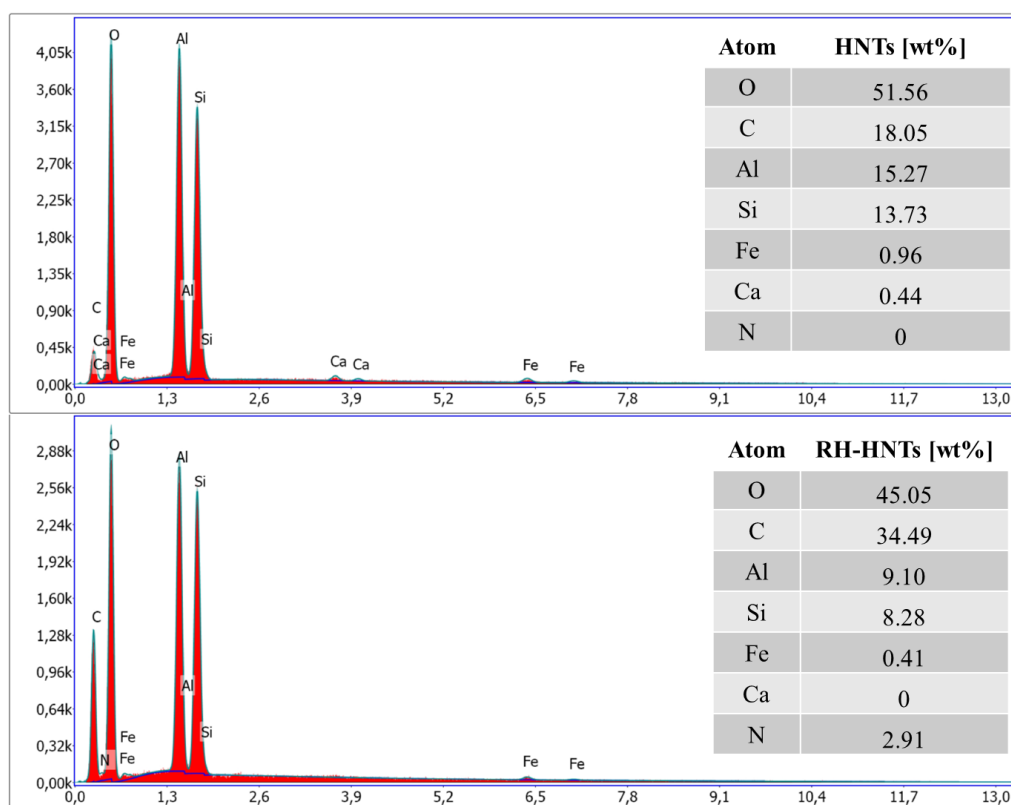


Figure 24. EDX spectra and chemical compositions of p-HNTs and RH-HNTs.



In Figure 25 the IR spectra of p-HNTs and the modified RH-HNTs are shown. The adsorption bands at 3693 and 3621  $\text{cm}^{-1}$  are ascribed to stretching vibrations of inner-surface Al-OH bonds and inner Al-OH bonds respectively. The inner Al-OH bonds also account for the band at 905  $\text{cm}^{-1}$ , which is due to bending vibrations. The peak at 1649  $\text{cm}^{-1}$  is attributed to O-H deformation vibrations of adsorbed water. The bands at 1119, 1029, 795, 750 and 681  $\text{cm}^{-1}$  are assigned to stretching vibrations of the Si-O bonds. The bands at 522, 459 and 426  $\text{cm}^{-1}$  are attributed to deformation vibrations of the Al-O-Si, Si-O-Si and Si-O bonds respectively.<sup>[93,94]</sup> Compared to the spectrum of p-HNTs, the spectrum of the modified RH-HNTs shows that new peaks appeared between 1200 and 1700  $\text{cm}^{-1}$ . The peak at 1614  $\text{cm}^{-1}$  can be assigned to N-H bending vibrations of the RH complex and the peak at 1451  $\text{cm}^{-1}$  to the deformation vibrations of the methylene groups.<sup>[91]</sup>

The basal spacing of HNTs could be determined using powder X-ray diffraction (XRD). The XRD patterns show peaks at 11.8 and 12.0 ° respectively (Figure 26). According to Bragg's law (Equation 1) this results in a basal spacing of 0.75 nm for HNTs and 0.74 nm for RH-HNTs. As mentioned in chapter 1.6.1, the interlayer distance of HNTs depends on the state of hydration. Accordingly, the used HNTs occur in mostly dehydrated form. The fact that there is no significant increase in the interlayer distance after the modification indicates that no intercalation between the rolled up sheets occurred. When some of the RH complex has formed inside the cavity of the nanotubes, no major changes of structure are expected.

$$n\lambda = 2d \sin \theta \quad (1)$$

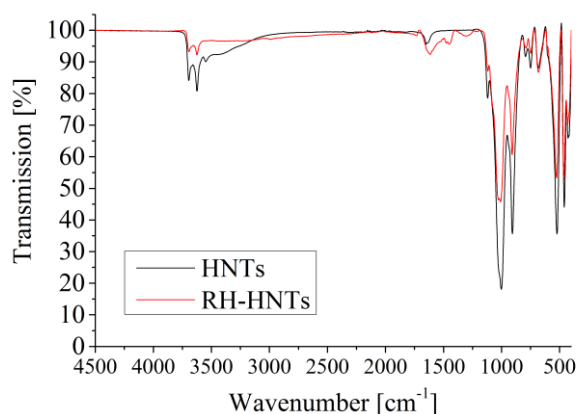


Figure 25. IR spectra of p-HNTs and RH-HNTs.

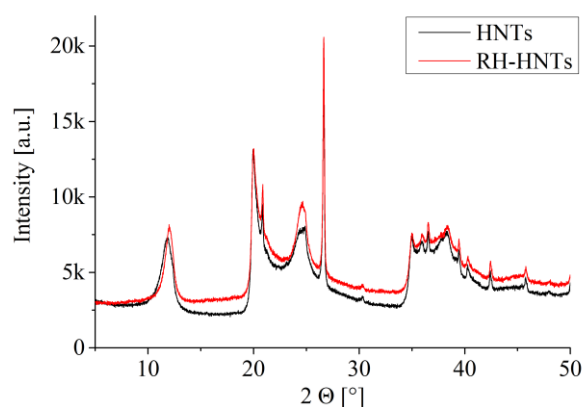


Figure 26. XRD patterns of p-HNTs and RH-HNTs.

The thermal decomposition of the p-HNTs and RH modified HNTs was examined by TGA (Figure 27). The weight loss of the HNTs at around 100 °C is attributed to the evaporation of

adsorbed water from the HNT surface. Both samples show a significant weight loss between 425 and 525 °C, which is ascribed to the dehydroxylation of Al-OH groups.<sup>[95]</sup> The decomposition of HNTs is completed at around 550 °C and with 82% residual weight. The decomposition of molecules belonging to the RH modification is observed in the temperature ranges of 100-425 °C and 525-1100 °C. The residual weight of the RH-HNTs (78%) is lower than that of the p-HNTs (82%) due to the decomposition of the RH moieties. The weight of the RH modification is calculated as 13 wt% relative to the weight of the HNTs.

The appearance of the HNTs was further examined by laser diffraction size analysis. As can be seen in Figure 28, HNTs and RH-HNTs showed monomodal distributions. Particles with sizes of up to 30 µm were detected, which indicates that the HNTs exist in aggregates and agglomerates. The lower count of the modified HNTs at particle sizes of <4 µm might be owed to the filtration step during the modification process, where smaller particles and aggregates were partially washed out.

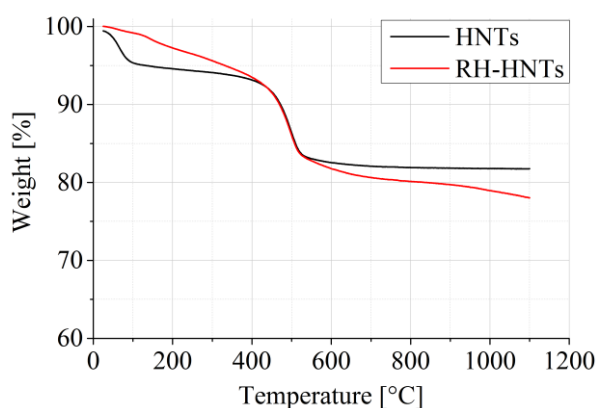


Figure 27. TGA curves of p-HNTs and RH-HNTs.

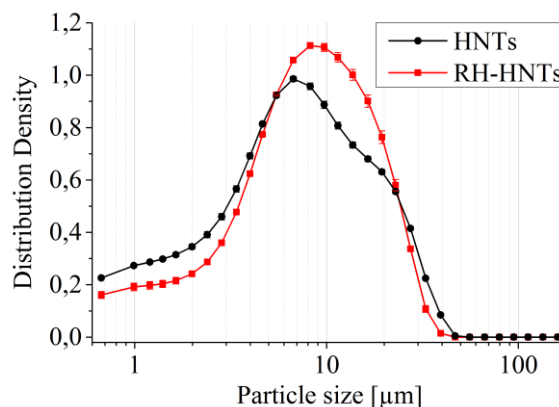


Figure 28. Size distribution of p-HNTs and RH-HNTs.

### 3.1.3 Carbon Nanotubes

With the use of CNTs as filler the generation of electrical conductivity in silicone rubber was intended. CNTs present an effective alternative for carbon black in rubbers. They offer better values in both mechanical and electrical performance. For example, natural rubber composites with 3 phr short CNTs were reported to show similar electrical conductivity values as composites with 52 phr carbon black.<sup>[96]</sup> Therefore, the use of CNTs provides a higher level of control over properties and the possibility to use multiple fillers without overloading the rubber matrix.

In this work, one type of single-wall carbon nanotubes (SWCNTs) and different multi-wall carbon nanotubes (MWCNTs) were applied for the preparation of silicone composites. The SWCNT type was Tuball from the manufacturer OCSiAl, the MWCNTs were K-Nanos 100P (K100P) and K-Nanos 210P (K210P) from Kumho Petrochemical Co., Ltd. as well as NC7000 from Nanocyl s.a. Apart from the number of walls the CNTs differ, according to the manufacturers, in their length, diameter, surface area, bulk density and carbon purity. The parameters of the applied CNTs are listed in Table 8. The aspect ratios are 158 for NC7000 and >3125 for Tuball. A modification was not carried out, because due to the chemical nature of CNTs a sufficient adhesion to silicone was expected. This adhesion is based on strong interactions between the CH- $\pi$  electrons of the silicone methyl groups and the  $\pi$ -electron rich surface of the CNTs.<sup>[97]</sup>

**Table 8. Technical data of the applied CNTs**

<b>Label</b>	<b>Type</b>	<b>Length [<math>\mu\text{m}</math>]</b>	<b>Diameter [nm]</b>	<b>Surface area [<math>\text{m}^2/\text{g}</math>]</b>	<b>Bulk density [g/L]</b>	<b>Carbon purity [%]</b>
<b>K-Nanos 100P</b>	MWCNT	10-50 (bundle)	8-15	-	15-30	90
<b>K-Nanos 210P</b>	MWCNT	10-80 (bundle)	8-15	-	15-30	90
<b>NC7000</b>	MWCNT	1.5	9.5	250-300	60	90
<b>Tuball</b>	SWCNT	>5	1.6	400	-	>85

The morphology of the applied CNTs was analysed using SEM. The aim was to evaluate the structure of the CNT agglomerates. The SEM images are shown in Figure 29-Figure 32.

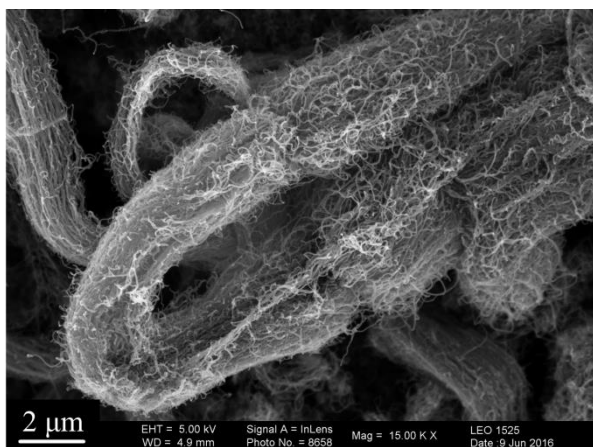


Figure 29. SEM image of K-Nanos 100P.

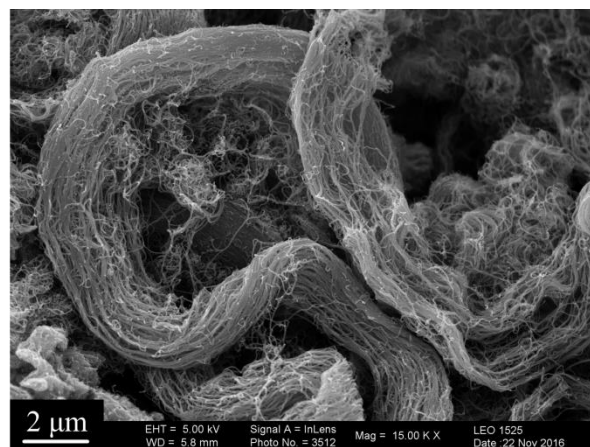


Figure 30. SEM image of K-Nanos 210P.

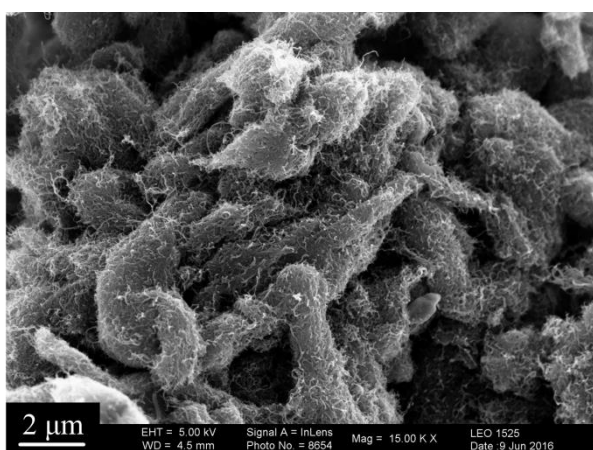


Figure 31. SEM image of NC7000.

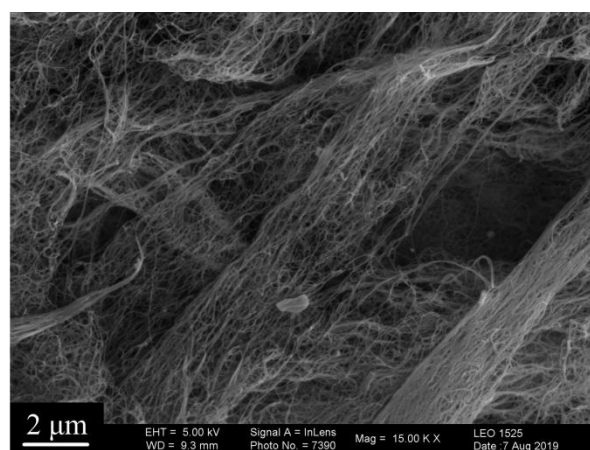


Figure 32. SEM image of Tuball.

The most common structure of K100P and K210P are highly aligned bundles of CNTs. NC7000 consists mostly of moderately ordered bundles. Compared to the bulky bundles of the K-Nanos, the bundles of NC7000 are rather compact, confirming the difference in the stated bulk densities. The bulk density serves as a criterion for dispersibility of the CNTs. Further, K210P and NC7000 exhibit a more porous bundle structure than K100P. Tuball shows mainly compact strands but also networks of individual CNTs.

### 3.2 Preparation of Rubber Compounds

In this work, commercially available, solid, high-temperature vulcanising (HTV) silicone rubber was used as a basis for the preparation of composites. The silicone type was a VMQ with a vinyl group content of 0.74%, which was determined by  $^1\text{H-NMR}$  spectroscopy, and a peroxide curing system. In this grade a certain amount of silica was dispersed in the rubber by

the manufacturer to obtain a Shore A hardness of around 80 in the vulcanised compound. This silicone rubber grade with relatively high silica content was chosen to test the applicability of the filler systems on a practical rubber compound and to keep the production costs low.

The heat resistance and thermal stability of the silicone rubber was analysed by thermogravimetric analysis (TGA). The TGA curve (Figure 33) shows, that the sample weight loss started at around 300 °C and that 62% of the sample decomposed before the temperature reached 700 °C. The residue after heating to 800 °C indicates that the silicone rubber contains  $\leq 37$  wt% silica as filler.

The differential scanning calorimetry (DSC) curve of silicone rubber (Figure 34) shows an exothermic crystallisation peak at -84 °C and an endothermic melting peak at -38 °C. The glass transition of vinyl methyl silicone rubber (VMQ) occurs, according to the literature, at a temperature lower than -120 °C and could not be determined using the instrument.<sup>[98]</sup> The results from TGA and DSC correspond with the data from the literature and confirm the wide application temperature range of silicone rubber.<sup>[99]</sup>

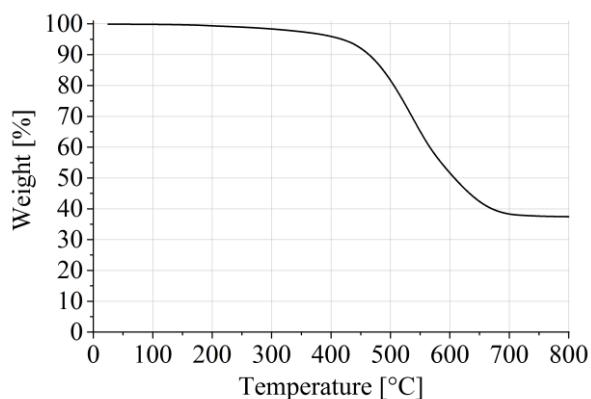


Figure 33. TGA curve for silicone rubber.

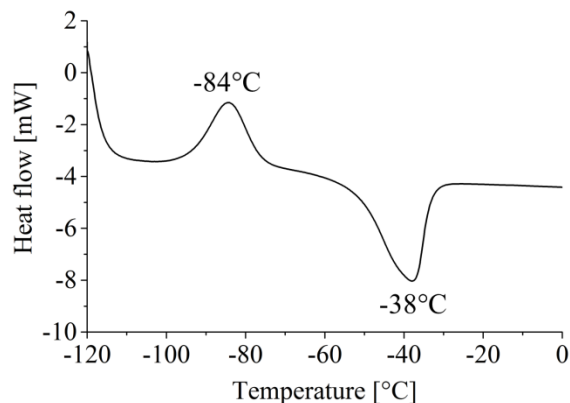


Figure 34. DSC curve for silicone rubber.

Compounds were prepared in an internal mixer using silicone rubber, different contents of AF, HNTs and CNTs and a peroxide crosslinking agent. Depending on the filler, the viscosity during the mixing process of the silicone compounds was affected to different degrees. The rheograms of the silicone compounds with 2 phr of the varying fillers are shown in Figure 35. The highest increase in viscosity was recorded for the compounds containing CNTs due to the high surface area and strong agglomeration of CNTs. The effect of the aramid fibres was also relatively high, presumably because of fibrillation. The torque values of the silicone HNT compound were similar to those of the unfilled compound, which indicates weak interaction between the HNTs and the silicone chains.

The torque during the mixing process also rose with increasing filler content. This was observed particularly for the CNTs, which can be attributed to their high surface area. The rheograms of the silicone compounds containing K100P are shown in Figure 36. The mean final torque of the compound with 8 phr CNTs was around 47% higher than that of the reference compound. In each case, the data was recorded after the addition of the CNTs and the curing agent. At this point the agglomerates and aggregates are broken down and dispersed in the silicone matrix. The torque approaches a constant value as the dispersion becomes more homogeneous.

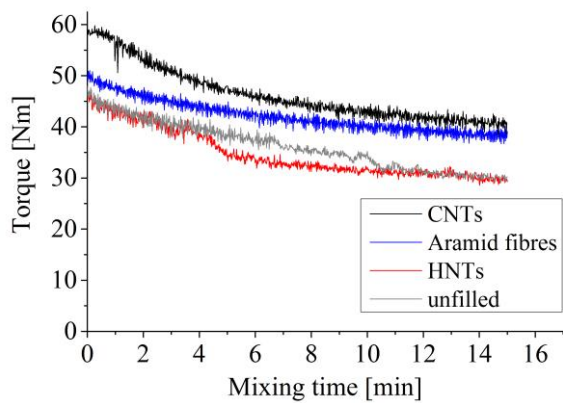


Figure 35. Rheograms of compounds with the different fillers used.

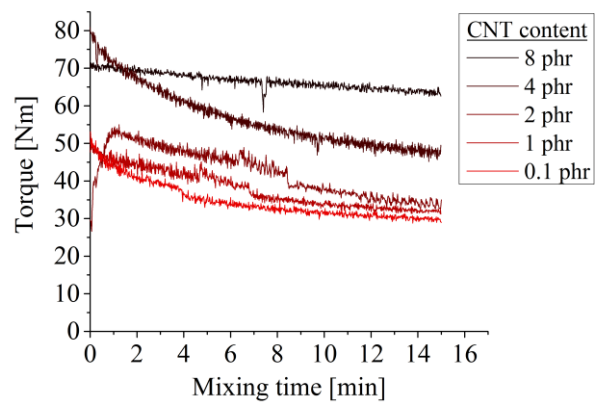


Figure 36. Rheograms of compounds containing different CNT contents.

### 3.3 Silicone Aramid Composites

#### 3.3.1 Vulcanisation behaviour

The effect of aramid fibres on the curing characteristics of silicone composites was examined by performing rheometric measurements at a constant temperature using composites with varying AF content. In Figure 37 the rheographs of the composites and the unfilled silicone compound are shown. It can be seen that the incorporation of AF leads to a significant increase in maximum torque, which is roughly proportional to the aramid content. Maximum torque represents the stiffness of the completely vulcanised samples at the curing temperature. The increment in torque indicates that the incorporated AF restricts the flow of the rubber, which results in more rigid vulcanisates.

Figure 38 shows the rheographs of composites with 3 phr pristine and modified aramid fibre, respectively. The composite with modified AF produces significantly lower torque than that with pristine AF. In fact, the values are close to those of the unfilled compound, which is an

indication for reduced crosslinking density. This might be a result of the consumption of the curing agent by the modifier groups without contributing to the overall polymer network.<sup>[100]</sup>

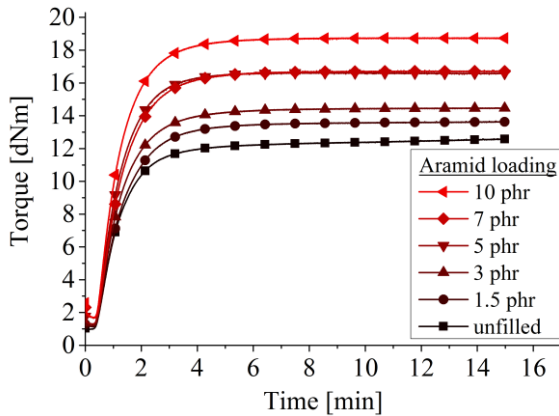


Figure 37. Rheographs of the silicone AF compounds.

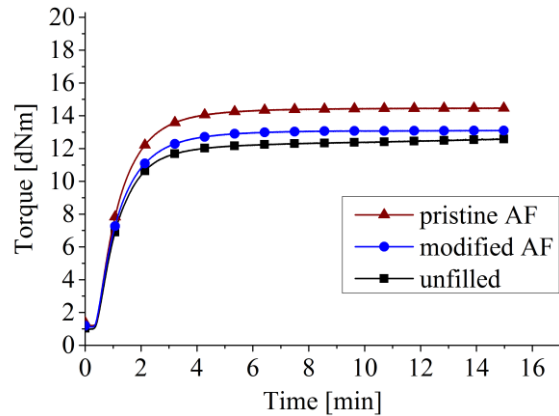


Figure 38. Rheographs of silicone compounds with 3 phr pristine and modified AF.

The scorch time, which is the time when the crosslinking begins and the torque increases, and the  $t_{90}$  time, which is the time required for the torque to reach 90% of the maximum value, were not particularly affected by the incorporation of the AF (Figure 39).

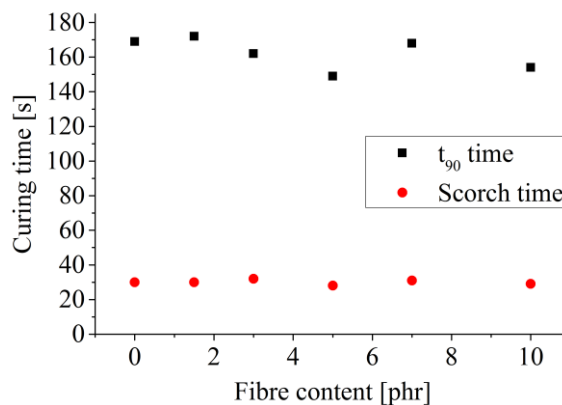


Figure 39.  $t_{90}$  times and scorch times of silicone AF compounds with varying aramid content.

Table 9 summarises the curing characteristics of the silicone AF compounds.  $M_H$  stands for maximum torque and  $M_L$  for minimum torque. The  $M_H-M_L$  values are a measure of the viscosity of the vulcanisates without the influence of filler-filler interactions and are thereby an indication of the crosslinking degree.<sup>[101,102]</sup> This includes both physical and chemical crosslinks. As can be seen, the  $M_H-M_L$  value rises with increasing fibre content, which can be ascribed to an interlocking between the fibre filaments and the crosslinked silicone chains.

The differences in the torque values of AF and m-AF suggest that the modification, in fact, reduces the crosslinking density. As described in chapter 3.1.1, the epoxy coating of AF was successful, while the PMA modification took place only to a small extent. This might result in an increase of reactive groups on the AF surface due to the epoxy modifier, which are not saturated by PMA. During the vulcanisation these groups react with the curing agent and thus affect the crosslinking. The influence of the modification on the vulcanisation times is negligible.

**Table 9. Curing characteristics of silicone AF compounds**

<b>Filler</b>	<b>M<sub>H</sub></b> <b>[dNm]</b>	<b>M<sub>L</sub></b> <b>[dNm]</b>	<b>M<sub>H</sub>-M<sub>L</sub></b> <b>[dNm]</b>	<b>Scorch time (t<sub>S1</sub>)</b> <b>[s]</b>	<b>t<sub>90</sub> time</b> <b>[s]</b>
<b>Unfilled</b>	12.6	1.0	11.6	30	169
<b>1.5 phr</b>	13.6	1.1	12.5	30	172
<b>3 phr AF</b>	14.1	1.2	12.9	32	162
<b>5 phr</b>	16.6	1.3	15.3	28	149
<b>7 phr</b>	16.8	1.7	15.1	31	168
<b>10 phr</b>	18.8	1.7	17.1	29	154
<b>3 phr m-AF</b>	13.1	1.1	12.0	29	164

### 3.3.2 Thermal properties

The effect of aramid fibres on the thermal stability of silicone composites was studied by performing TGA. As can be seen from the TGA curves, the addition of AFs caused the onset degradation temperature to shift from ~350 °C to ~300 °C (Figure 40). The degradation of the composites ended between 620 and 650 °C, that of the unfilled SiR at around 700 °C and the residual weight at 800 °C was about 2% lower for the composites. This effect was stronger with an increasing aramid content, still the difference is small. The higher degradation rate of the composites may be attributed to promoted outgassing of the material.



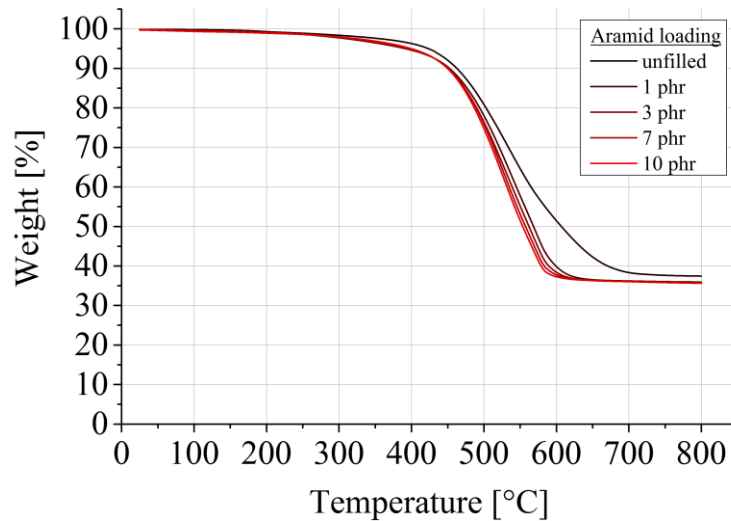


Figure 40. TGA curves of silicone AF composites and unfilled SiR.

### 3.3.3 Mechanical properties

The reinforcing effect of the aramid fibres on silicone rubber was examined on the basis of the material properties, such as hardness, Young's modulus, tensile strength, elongation at break, tear strength and compression set. The composites showed increasing hardness and Young's modulus with increasing fibre content (Figure 41, Figure 42), which is owed to reduced mobility of the polymer chains near the fibre surface. These findings are consistent with the results from the curing studies (Chapter 3.3.1). A sharp increase was noted between a fibre content of 2 and 3 phr, which apparently represents the mechanical percolation threshold for this rubber-filler system. Here, significantly more filler-filler interactions occur, which explains the sharp increase.

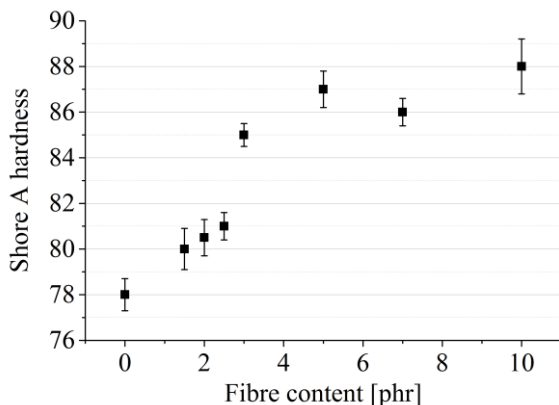


Figure 41. Hardness of silicone AF composites.

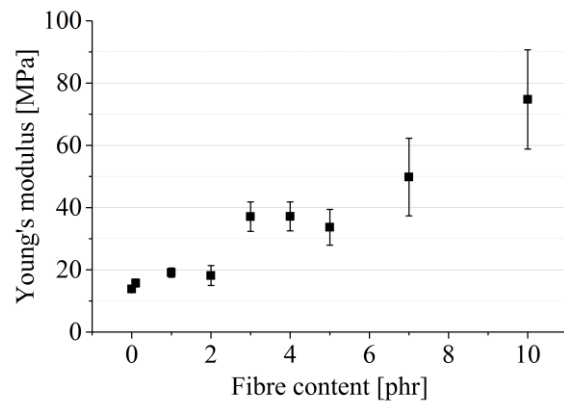


Figure 42. Young's modulus of silicone AF composites.

The tensile strength at break and elongation at break decreased with increasing fibre content, which is a common behaviour of composites without strong filler-polymer interaction. In this case, the load transfer from the rubber matrix to the filler is not possible, which results in decreased tensile properties.<sup>[103]</sup> Also insufficient dispersed fibres act as defects in the silicone matrix and cause a loss in elasticity. The decrease in tensile strength between 2 and 7 phr was roughly proportional to the fibre content (Figure 46). At loadings of 7 and 10 phr AF the composites showed very low elongation, which indicates an overloading of the rubber matrix.

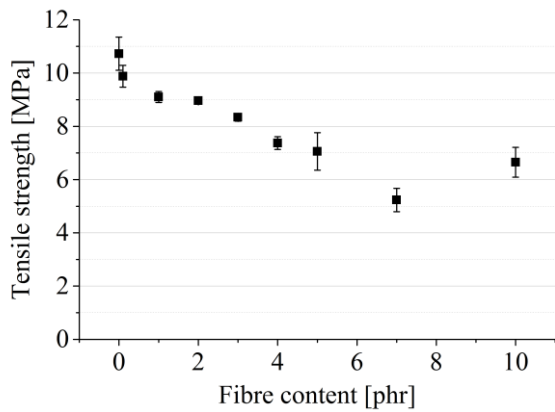


Figure 43. Tensile strength of silicone AF composites.

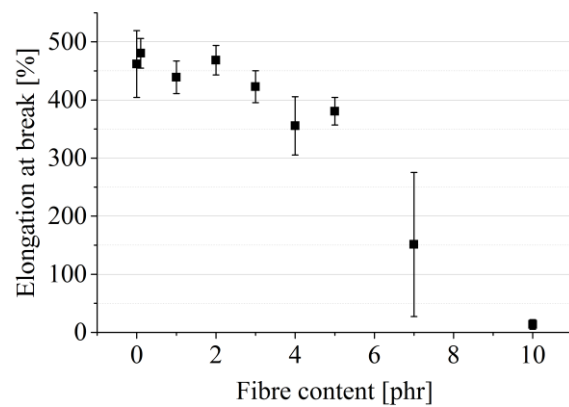


Figure 44. Elongation at break of silicone AF composites.

The aramid-silicone interface was examined using SEM. The SEM image of a silicone AF composite showed distinctive gaps between the aramid fibres and the silicone matrix, which displays the poor filler-polymer interaction (Figure 45).

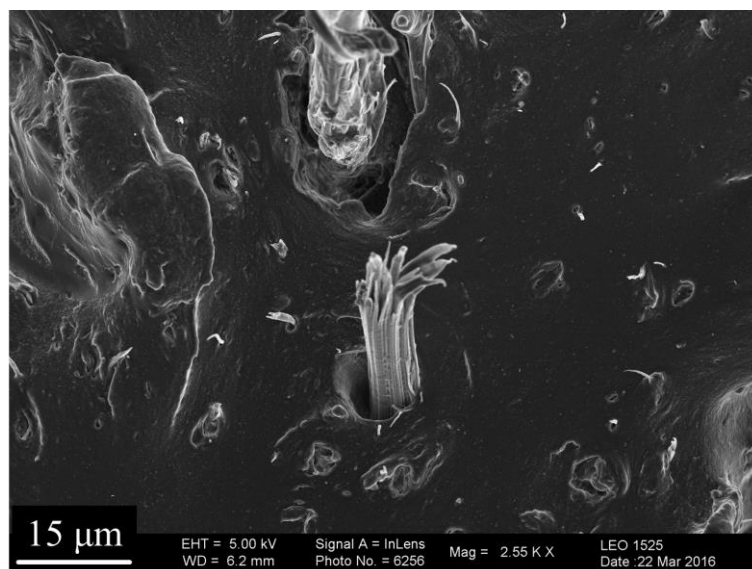
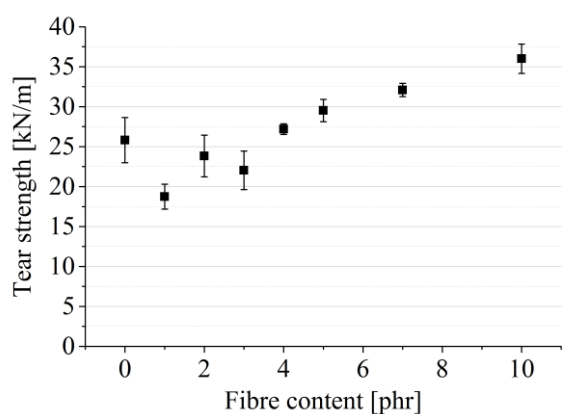


Figure 45. SEM image of a silicone AF composite.

The tear strength of the silicone AF composites with fibre contents between 2 and 5 phr showed no significant difference to the unfilled silicone compound (Figure 46). Apparently, a higher content of AF is required to limit the crack propagation, since with 7 and 10 phr AF loading the tear strength improved. Given the poor adhesion between aramid and silicone, this might be owed to the interlocking of the fibre filaments.

The compression set, which is the amount of permanent deformation after compression, also showed no significant difference at lower fibre contents and increased with 7 and 10 phr. The loss in elasticity that could be seen in Figure 44 is accompanied by an impairment of the compression set, which is attributed to chain slipping of the silicone molecules on the AF surface due to weak interaction.<sup>[104]</sup> In addition, a buckling of the fibres during the compression could also have an impact.<sup>[105]</sup>



**Figure 46. Tear strength of silicone AF composites.**

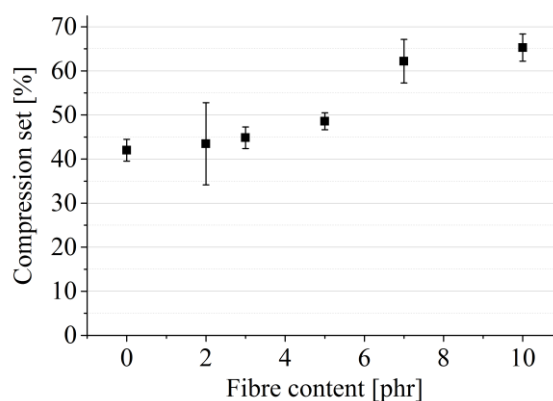


**Figure 47. Compression set of silicone AF composites.**

The performance of reinforced composites is strongly dependent on the filler-rubber interface. Strong interfacial bonding is required to ensure load transfer from the matrix to the filler. An improved adhesion between AFs and silicone rubber was expected by introducing methacrylate groups to the AF surface. The methacrylate groups are supposed to react like vinyl groups with the silicone molecules during the vulcanisation process and form covalent bonds between filler and rubber matrix (Figure 48).

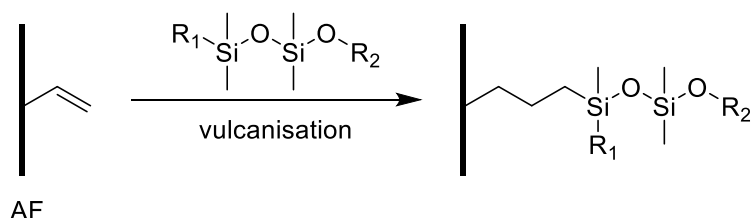


Figure 48. Reaction of modified AF reacting with silicone rubber in peroxide curing.

The effect on the mechanical properties of pristine (AF) and modified aramid fibres (m-AF) are compared using composites with 3 phr fibre content (Table 10). Compared to unfilled SiR, composites with 3 phr, AF showed increased hardness and Young's modulus without a significant loss in the other material properties. This fibre content in the range of the mechanical percolation threshold was also chosen because here the greatest differences could be expected.

Table 10. Mechanical properties of silicone AF composites with 3 phr pristine and silane modified AF

	Hardness (Shore A)	Young's modulus [MPa]	Tensile strength [MPa]	Elongation at break [%]	Tear strength [kN/m]	Compression set [%]
<b>unfilled</b>	78 ± 1	14 ± 1	10.7 ± 0.6	462 ± 58	26 ± 3	42 ± 3
<b>AF</b>	85 ± 1	37 ± 5	8.3 ± 0.1	423 ± 28	26 ± 2	45 ± 2
<b>m-AF</b>	84 ± 1	20 ± 1	6.8 ± 0.6	372 ± 57	31 ± 2	50 ± 2

The composites containing silane modified AF showed increased tear strength, however, this was accompanied by a significant loss in the other mechanical properties. These findings are consistent with those from the curing studies. As described in chapter 3.3.1, the incorporation of modified AF affects the crosslinking density of the composite and thus the mechanical properties.

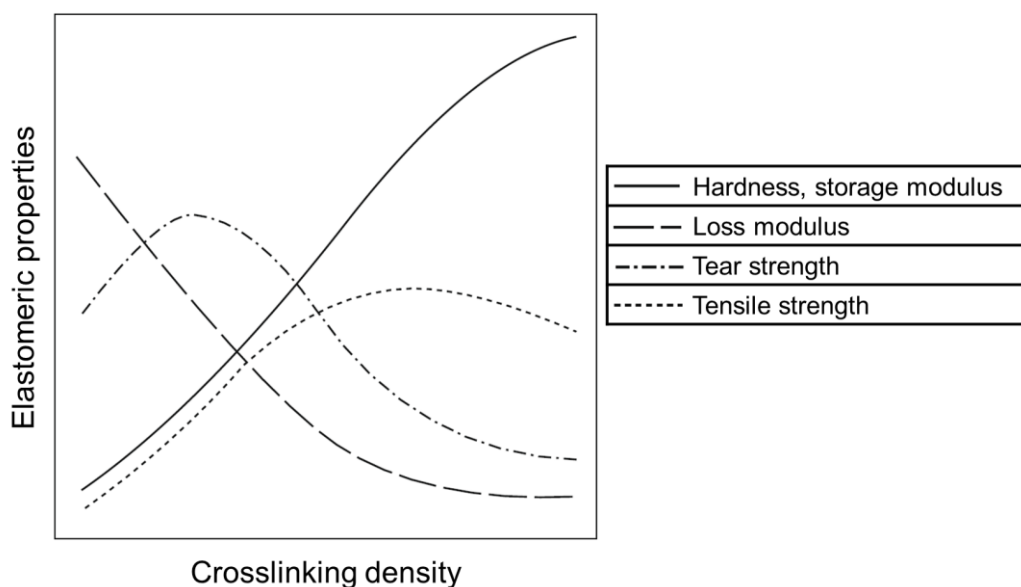


**Figure 49. Influence of the crosslink density on elastomeric properties.** <sup>adapted from [1]</sup>

Young's modulus, hardness and elasticity rise with increasing crosslinking density, while elongation at break, hysteresis, damping and compression set decrease. The curves of tensile strength and tear strength show a maximum at different crosslinking densities.<sup>[1,106]</sup> Accordingly, the crosslinking density in case of the composite with modified AF is reduced, whereby higher tear strength, adverse compression set and decreased tensile strength are obtained. The values of the hardness and elongation at break are within the range of error and do not provide further insight.

## 3.4 Silicone HNT Composites

### 3.4.1 Vulcanisation behaviour

The incorporation of HNTs into SiR has a strong impact on the vulcanisation behaviour of the compounds. In Figure 50 the rheographs of the pristine HNT composites with varying filler contents are presented. Compared to the unfilled SiR, the p-HNT composites showed significantly lower maximum torque. Thus, the presence of p-HNTs reduces the rigidity of the material. The data of the composite with 10 phr p-HNTs is considered as an outlier.

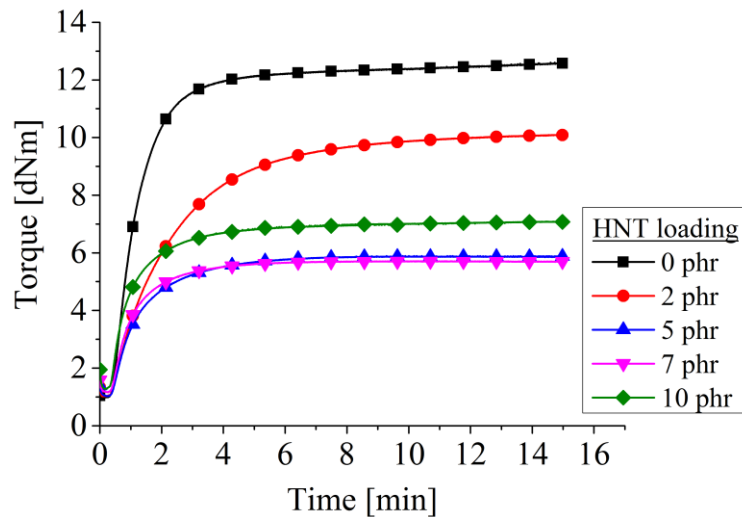


Figure 50. Rheographs of the p-HNT composites.

The presence of RH-HNTs causes an increase in maximum torque compared to the unfilled SiR, which indicates a higher rigidity of the vulcanisates (Figure 51). The increment in torque is owed to impaired mobility of the polymer chains by interaction between silicone chains and the modified HNTs. A steady increase of the maximum torque with increasing HNT loading was expected, because HNTs are a rigid powder and reduce the proportion of deformable rubber in the composites.<sup>[107]</sup> However, the composites with 7 and 10 phr RH-HNTs show lower maximum torque than the 5 phr composite. A larger proportion of the curing agent could react with groups on the increased surface area of HNTs, lowering the total number of crosslinks in the matrix.

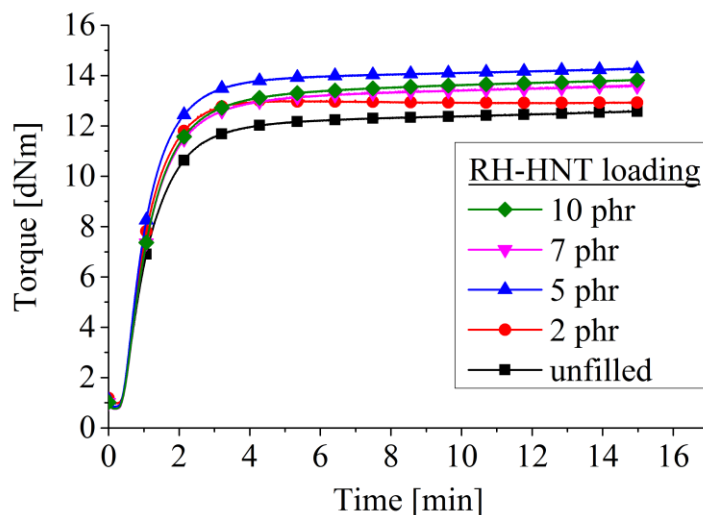
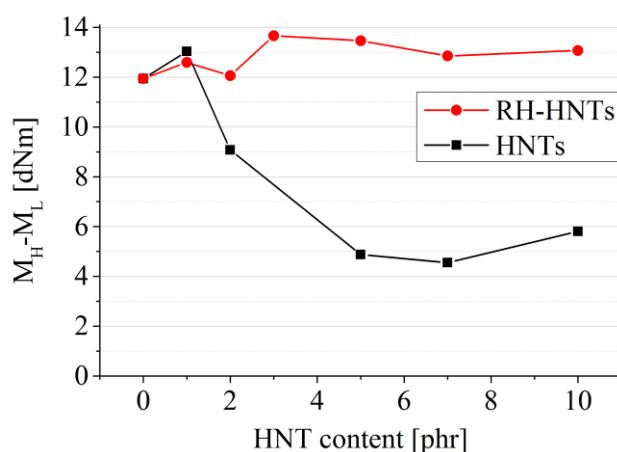


Figure 51. Rheographs of silicone RH-HNT composites and unfilled SiR.

In Figure 52, the maximal torque differences ( $M_H - M_L$ ) of the silicone HNT composites are presented. The difference is taken as a measure for the crosslink density of the matrix, i.e. interaction between filler and matrix are considered of zero importance for the effect. The crosslinking density slightly increases upon the incorporation of RH-HNTs, while the p-HNTs causes a substantial drop. The decrease is ascribed to the decomposition of the curing agent with the silanol and aluminol groups on the HNT surface.<sup>[107]</sup>

The presence of the RH complex induces an increase in crosslinking density, which levels off above 3 phr. The impact of RH-HNTs was expected to be more pronounced, especially at higher loadings. The measured values of RH-HNT composites might result from the combination of an increased crosslinking due to RH modification and a partial consumption of the curing agent. The efficiency of phenolic compounds as inhibitors of radical polymerisation is well-known.<sup>[108]</sup>



**Figure 52.** Maximal torque differences ( $M_H - M_L$ ) of the silicone HNT composites.

The incorporation of p-HNTs and RH-HNTs into silicone rubber also affected the curing kinetics. Regarding the scorch time, a delay of around 5 s for the composites containing between 2 and 7 phr p-HNTs was recorded, while there was a slight decrease of 1-2 s for the composites with RH-HNTs (Figure 53). Moreover, silicone composites with 2 and 5 phr HNTs showed significantly increased  $t_{90}$  times, while composites containing 1-5 phr RH-HNTs showed decreased  $t_{90}$  times (Figure 54). The delay in the curing process of composites containing p-HNTs is ascribed to an interaction of the curing agent with the silanol and aluminol groups on the HNT surface.<sup>[107]</sup> In case of the RH-HNTs, the interaction of the curing agent with the HNT surface is inhibited by the RH modification.

The decreased scorch time for the composites containing RH-HNTs is owed to the increased formation of crosslinks between the HNTs and the silicone matrix due to the RH modification. It has been reported that the RH complex accelerates the curing rate, which can also be confirmed for the  $t_{90}$  time.<sup>[85]</sup>

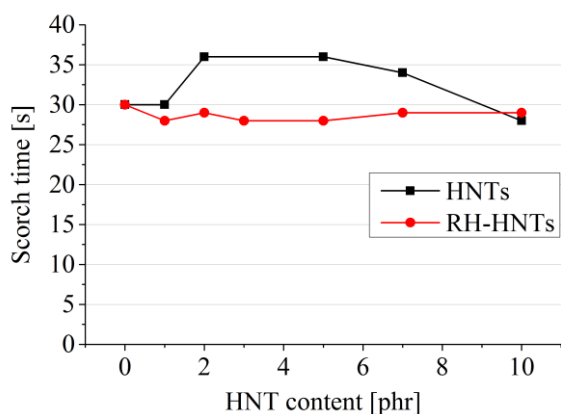


Figure 53. Scorch times of silicone HNT composites.

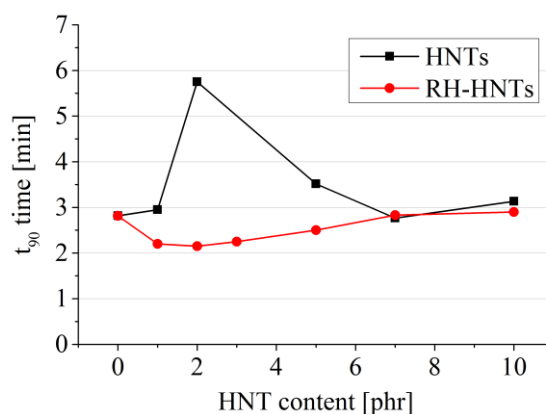


Figure 54.  $t_{90}$  times of silicone HNT composites.

### 3.4.2 Thermal properties

The thermal stability of the silicone HNT composites containing pristine HNTs or RH modified HNTs was examined by TGA. Figure 55 and Figure 56 show the corresponding TGA curves of the composites with varying HNT loadings. The composites containing p-HNTs show a two-step degradation behaviour, which is more pronounced with higher HNT content. The decomposition process of the composite with 2 phr p-HNTs is comparable to that of the unfilled silicone compound, while the degradation of the composites with 5-10 phr loading takes place at significantly lower temperatures. The first degradation step of the composites with higher loading starts between 250 °C and 300 °C and ends between 350 °C and 400 °C. This is presumably owed to the presence of vinyl entities, that remain after crosslinking due to the reaction of the curing agent with silanol and aluminol groups on the HNT surface.<sup>[107]</sup> The number of remaining vinyl groups corresponds with the CNT content in the composite, which agrees with the findings from the TGA curves. The second step is ascribed to the depolymerisation of the siloxane chains and ends between 625 °C and 675 °C.<sup>[109]</sup>

The incorporation of the RH modified HNTs decreased the thermal stability of the rubber compounds slightly. Even in case of the composites with higher loading, the decrease is minor. Here, the depolymerisation of the siloxane chains started between 400 °C and 500 °C and was completed between 650 °C and 675 °C.



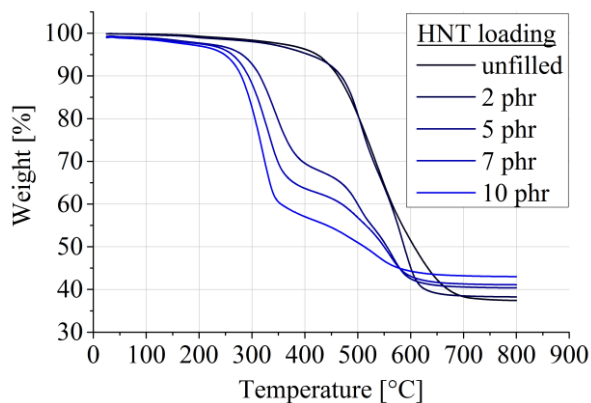


**Figure 55. TGA curves of silicone HNT composites and unfilled SiR.**

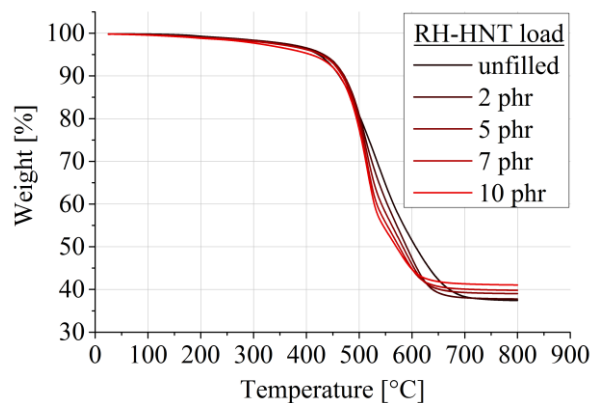


**Figure 56. TGA curves of silicone RH-HNT composites and unfilled SiR.**

The decomposition temperatures and the residual weights obtained from the TGA curves are summarised in Table 11.  $T_{5\%}$ ,  $T_{50\%}$  and  $T_{\text{final}}$  correspond to the temperatures at 5%, 50% and finalised weight loss, respectively. As can be seen from the data, almost all decomposition temperatures were reduced upon the incorporation of HNTs into the silicone compound. This effect was more pronounced with higher HNT loading. Only  $T_{5\%}$  was enhanced in case of the composites with 2-7 phr RH-HNTs. In addition, the composites with RH-HNTs consistently show higher decomposition temperatures than the composites with p-HNTs. Moreover, the residual weights of all tested silicone HNT composites are higher than that of unfilled SiR and rise with increasing HNT content.

**Table 11. TGA data of silicone HNT composites with varying loadings and unfilled SiR**

Filler	$T_{5\%}$ [°C]	$T_{50\%}$ [°C]	$T_{\text{final}}$ [°C]	Residue at 800 °C [%]
<b>Unfilled</b>	423	607	708	37.4
<b>2 phr p-HNTs</b>	407	588	656	38.3
<b>5 phr p-HNTs</b>	281	555	647	40.4
<b>7 phr p-HNTs</b>	263	550	641	41.1
<b>10 phr p-HNTs</b>	248	512	630	43.0
<b>2 phr RH-HNTs</b>	433	590	670	37.8
<b>5 phr RH-HNTs</b>	428	583	663	39.0
<b>7 phr RH-HNTs</b>	427	576	660	39.8
<b>10 phr RH-HNTs</b>	408	570	655	41.0

It was expected, that HNTs have a beneficial effect on the thermal stability of the rubber compounds due to several characteristics. For one thing, HNTs may delay the mass transport by entrapping decomposition products into their lumens.<sup>[40]</sup> HNTs further act as thermal barriers and restrain the heat flow in the polymer matrix.<sup>[110]</sup> Also, iron oxides like  $\text{Fe}_2\text{O}_3$  contained in the HNTs could trap radicals during the degradation process and thus act as a type of flame retardant.<sup>[40]</sup> Moreover, it is reported, that the formation of char hinders the vanishing of volatile substances during the decomposition process.<sup>[48]</sup> Finally, an increase in the thermal stability of SiR upon incorporation of RH modified HNTs up to a content of 10 wt% was reported.<sup>[91]</sup>

However, in this work the incorporation of pristine or RH modified HNTs into SiR did not result in an improvement of the thermal stability. In fact, the TGA derived thermal stability decreased substantially in case of composites with 5-7 phr p-HNTs. This decrease is probably owed to a good mass transfer resulting from an insufficient crosslinking due to the consumption of the curing agent on the HNT surface. This is also supported by the findings from the curing studies.<sup>[107]</sup> The displacement of the dispersed silica in the silicone compounds, which is already an effective thermal insulator, could also play a role.<sup>[111]</sup>

### 3.4.3 Mechanical properties

Various clays have been successfully used in the mechanical reinforcement of SiR.<sup>[112-115]</sup> A study reported on the reinforcement of liquid SiR with siloxane-modified montmorillonite clay. Here enhanced tear strength and compression set were achieved.<sup>[116]</sup> Additionally, an increase in Young's modulus and tensile strength of silicone rubber of different hardness through the incorporation of RH modified HNTs was reported.<sup>[91]</sup>

Depending on the content and modification, the incorporation of HNTs into silicone rubber affects the hardness of the composites to different degrees. While there is no major change in Shore A hardness at HNT loadings of 1-3 phr, with loadings of 5-10 phr a significant increase is observed (Figure 57). This is attributed to the high surface area of the HNTs that interacts with the polymer chains and reduces their mobility. The increment was far greater for the p-HNTs compared to the RH-HNTs.

The Young's moduli of the composites with 2 phr p-HNTs and across the whole content range of RH-HNTs show approximately the same value as the unfilled SiR (Figure 58). For the

composites containing 5-10 phr p-HNTs a sharp increase and larger deviations of the values are noted. This is likely owed to insufficient dispersion of the HNTs due to poor interaction with the matrix.

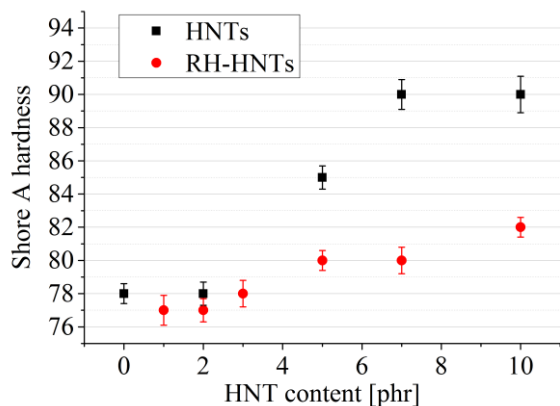


**Figure 57. Shore A hardness of silicone HNT composites.**

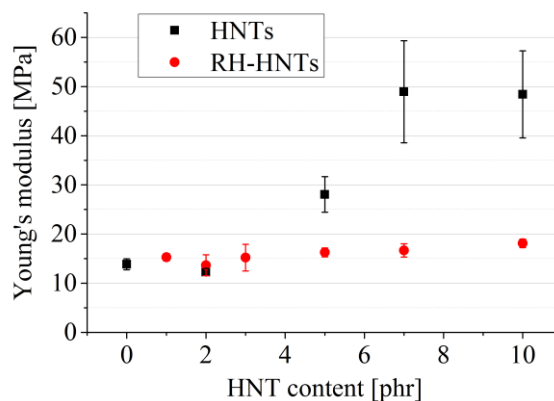


**Figure 58. Young's modulus of silicone HNT composites.**

The tensile strength of silicone composites with p-HNTs decreases with increasing HNT content up to a content of 7 phr (Figure 59). The composites containing 1-5 phr RH-HNTs show no significant change in tensile strength compared to the unfilled SiR. Simultaneously, with HNT contents of 7 and 10 phr a slight decrease is observed. Regarding the composites with 10 phr HNTs, the tensile strength is 55% higher in case of the RH-HNTs. This is owed to the reduced crosslinking density in the p-HNT composites on the one hand and the enhanced filler-polymer adhesion in case of the RH-HNTs on the other hand. The latter also results in a more homogeneous dispersion of the HNTs and thereby less defects in the polymer matrix. Also, a greater force is required to separate filler and polymer. These findings are not in agreement with the results from the literature, as here an increase in tensile strength upon the incorporation of RH modified HNTs into SiR was found.<sup>[91]</sup> However, the SiR grades used in the mentioned study are of considerably lower hardness (30, 40 and 50 Shore A) and lower reinforcing effects for the composites with higher initial hardness were reported. The dispersed silica of the SiR used here influences the proportion of the HNTs with regard to the total filler content. Accordingly, it is assumed that the lower reinforcing effect observed in this work is related to the higher amount of silica.

The elongation at break of the HNT composites, apparently, does not depend directly on the HNT content. The elongation at break values of the p-HNT composites did not show a steady trend with increasing HNT content and values also have comparably high errors (Figure 60). This is readily related to the reduced crosslinking density.<sup>[107]</sup> In case of the RH-HNT

composites, the values are equal to that of the unfilled SiR and do not change beyond the margin of error with increasing content. These findings indicate that the RH modification significantly improved the compatibility of the HNTs to the silicone matrix. As a result, a more homogeneous dispersion is achieved and thus even the highly filled composites exhibit no significant decrease in elongation at break.

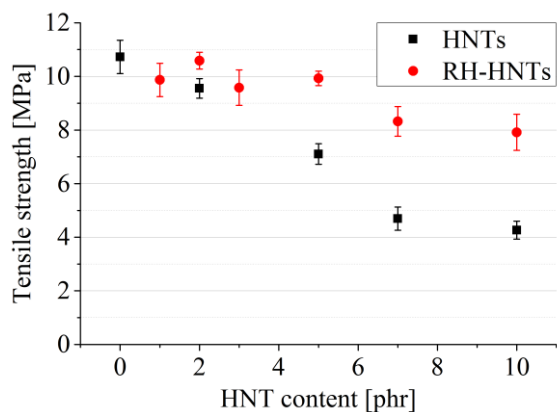


**Figure 59. Tensile strength of silicone HNT composites.**

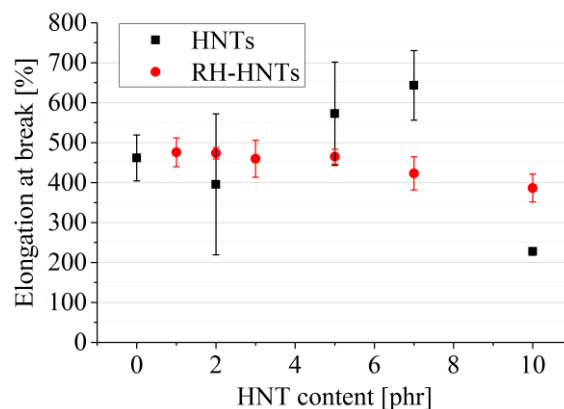


**Figure 60. Elongation at break of silicone HNT composites.**

Based on the tear strength data of the HNT composites, no profound evaluation of the reinforcing effects of the HNTs can be made (Figure 61). Most of the values for composites with p-HNTs and RH-HNTs, are within the error margin of the unfilled SiR. Only for the 2 phr HNT composite an increase of 16% was observed. However, the data indicates that a decrease in tear strength is not to be expected for composites with low loadings of 1-3 phr HNTs.

The impact of the RH modification on the mechanical properties is probably most evident in case of the compression set (Figure 62). Here, the incorporation of p-HNTs caused a significant increase (233% with 7 phr), while the composites containing 1-7 phr RH-HNTs show a decrease of 13-29%. Even with a loading of 10 phr there was no loss in compression elasticity of the RH-HNT composite. These findings are attributed to the enhanced interaction between the filler particles and silicone chains that causes a decreased chain slipping at the HNT surface. Chain slipping is considered as a main reason for the loss of elastic recovery.<sup>[117]</sup> The simultaneous improvement of tear strength and compression set is a highly desired feature of a filler and demonstrates the strong reinforcing effect of RH modified HNTs in SiR.

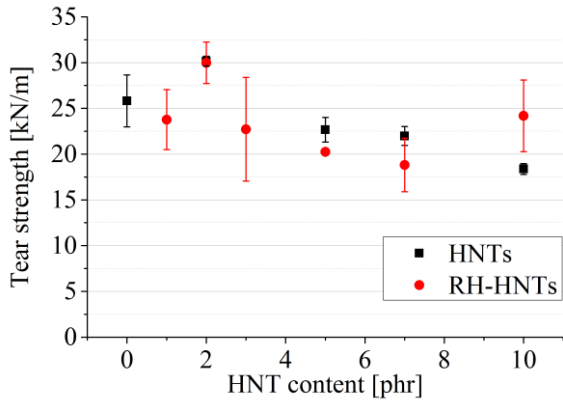


Figure 61. Tear strength of silicone HNT composites.

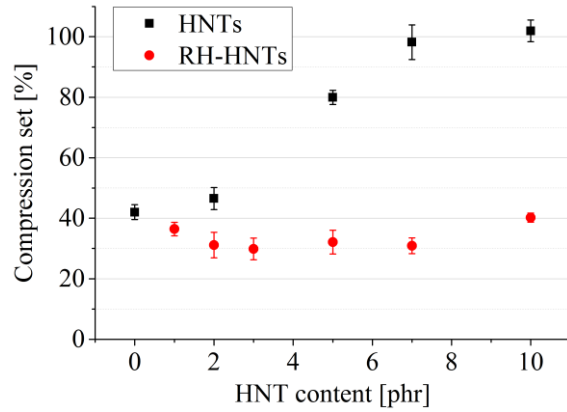


Figure 62. Compression set of silicone HNT composites.

The mechanical properties of the silicone HNT composites with 2 phr p-HNTs and RH-HNTs as well as the unfilled compound are summarised in Table 12. Overall, the mechanical properties of the RH-HNT composites are equal or superior to those of the corresponding p-HNT composites or the unfilled compound showing the reinforcing effect of the modified HNTs and thus the benefit of the modification.

Table 12. Mechanical properties of the composites with 2 phr p-HNTs or RH-HNTs

	Hardness (Shore A)	Young's modulus [MPa]	Tensile strength [MPa]	Elongation at break [%]	Tear strength [kN/m]	Compression set [%]
<b>unfilled</b>	78 ± 1	14 ± 1	10.7 ± 0.6	462 ± 58	26 ± 3	42 ± 3
<b>p-HNTs</b>	78 ± 1	12 ± 1	9.6 ± 0.4	396 ± 177	30 ± 1	47 ± 4
<b>RH-HNTs</b>	77 ± 1	14 ± 2	10.6 ± 0.3	474 ± 14	30 ± 2	31 ± 4

The result of the dispersion of the composites containing pristine or RH modified HNTs was examined using SEM images (Figure 63 and Figure 64). The p-HNTs occur in relatively large agglomerates, while the RH-HNTs are more finely dispersed. Moreover, gaps between the agglomerates and the silicone matrix can be detected frequently for p-HNTs, which displays the poor adhesion. In the RH-HNT composites gaps are less frequent.

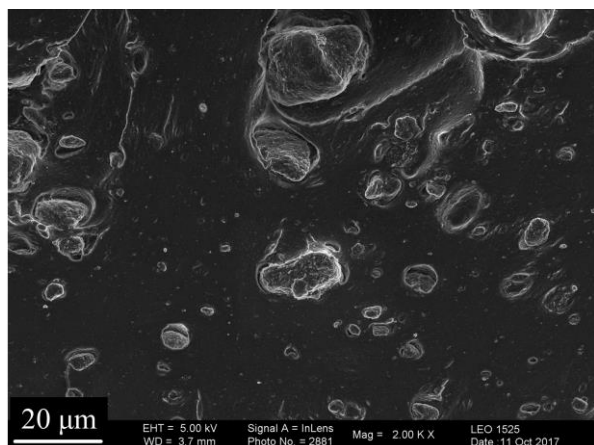


**Figure 63. SEM image of a silicone composite with p-HNTs.**

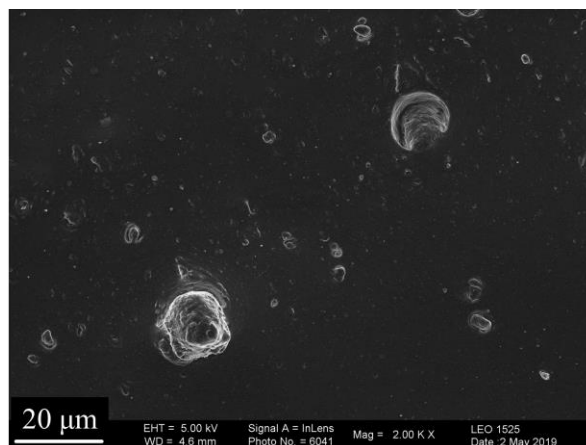


**Figure 64. SEM image of a silicone composite with RH-HNTs.**

The RH modification of the HNTs enhanced the filler-polymer interaction between the HNTs and the silicone rubber. This improvement is based on the formation of a phenol-formaldehyde resin at the interface and results in the throughout superior mechanical properties of the RH-HNT composites.

A reaction pathway of the RH complex as adhesion promoter for montmorillonite and NBR was proposed in literature.<sup>[89]</sup> A similar mechanism can be assumed for the RH promoted adhesion of HNTs to silicone due to the involved reactive groups. The reaction sequence is shown in Figure 65. In the first step, at temperatures above 110 °C, hexamethylenetetramine decomposes into formaldehyde and ammonia. In the second step, formaldehyde reacts with resorcinol to form 2,4-bis(hydroxymethyl)benzene-1,3-diol or 4,6-bis(hydroxymethyl)benzene-1,3-diol. These molecules react with each other in a polycondensation reaction to form the phenol-formaldehyde resin. Various polymerisation reactions are possible, but only one is shown for an easier access. The phenol-formaldehyde resin can also react with the silicone molecules by addition reaction to the vinyl groups. Also, the resin methylene groups could be involved in the vulcanisation reaction. The connection between the phenol-formaldehyde resin and the HNTs may take place through hydrogen bond formation between the present hydroxyl groups.

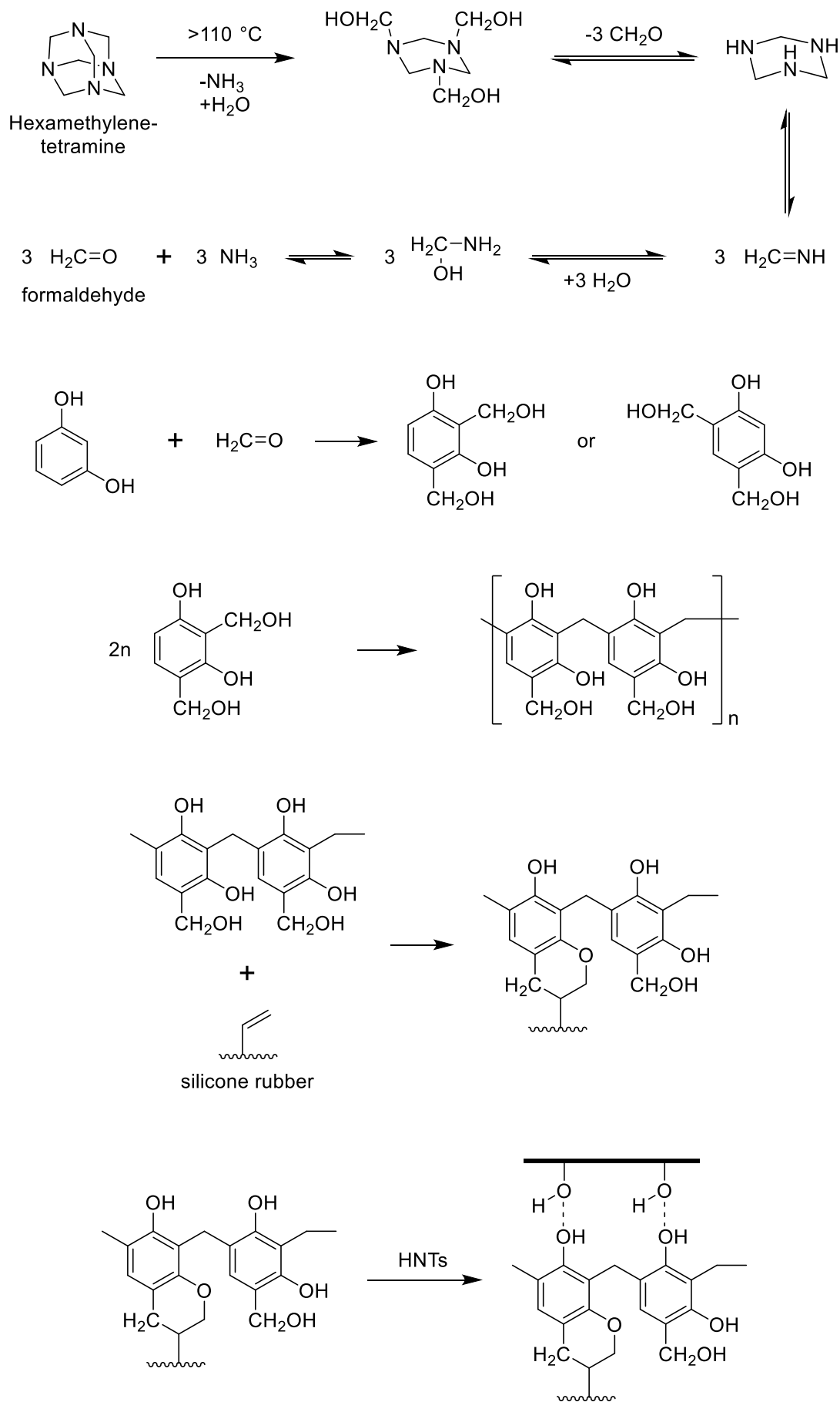


Figure 65. Reaction mechanism of RH promoted adhesion between silicone rubber and HNTs. [89,118]

## 3.5 Silicone CNT Composites

### 3.5.1 Vulcanisation behaviour

The effect of CNTs on the vulcanisation process was analysed using a concentration series of SWCNT in silicone rubber. The presence of CNTs causes a significant increase in torque even at low CNT loadings. Further a minor decrease of the scorch time and an increase of the  $t_{90}$  time, compared to the unfilled compound were observed (Figure 66).

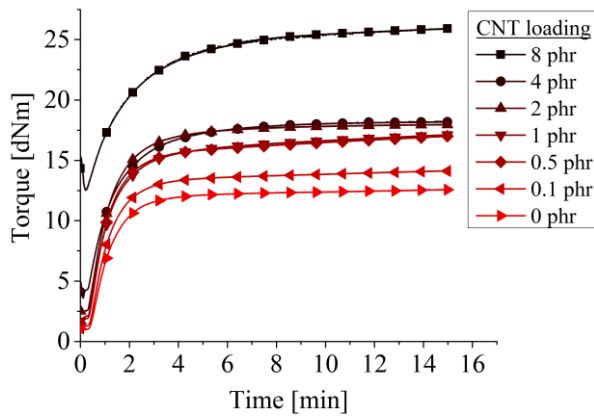


Figure 66. Rheographs of SWCNT silicone composites with varying CNT loadings.

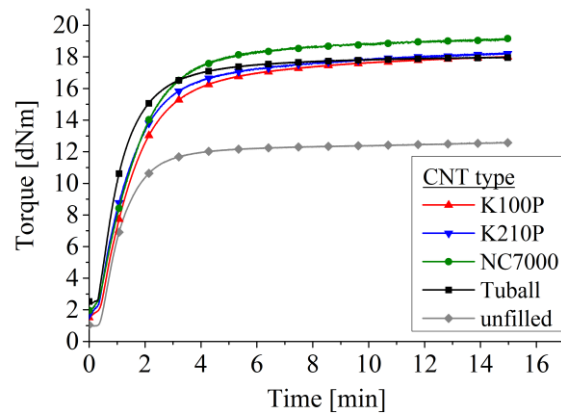


Figure 67. Rheographs of CNT silicone composites with 2 phr of varying CNT types.

The CNT type has a minor effect on the vulcanisation. An increase in torque and the  $t_{90}$  time as well as a small decrease in the scorch time can be observed for all 4 types of CNT composites compared to the unfilled compound (Figure 67, Table 13). The reduced scorch time of the composites can be attributed to a higher thermal conductivity due to the CNTs and to metal impurities that can provide a catalytic effect.<sup>[119]</sup> The noticeably short  $t_{90}$  time of the Tuball composites compared to the other CNT composites might be owed to a finer dispersion of the CNTs and the higher content of metal impurities.

Table 13. Curing times of the silicone CNT composites

CNT type	$M_H$ [dNm]	$M_L$ [dNm]	$M_H - M_L$ [dNm]	Scorch time ( $t_{S1}$ ) [s]	$t_{90}$ time [s]
K100P	18.0	1.6	16.4	28	267
K210P	18.2	1.7	16.5	23	250
NC7000	19.2	2.0	17.2	23	242
Tuball	18.0	2.4	15.6	23	185
unfilled	12.6	1.0	11.6	30	169



### 3.5.2 Thermal properties

The thermal properties of silicone CNT composites were studied by TGA and DSC. TGA curves of composites with varying content of K100P and unfilled SiR were recorded (Figure 68). It can be seen that the degradation of all samples started at around 300 °C and ended at approximately 700 °C. The addition of CNTs raised the onset degradation temperature. Also the proportion of residual weight at 800 °C rose with increasing CNT loading. The increased thermal stability of composites containing CNTs may be attributed to barrier effects and the limitation of the molecular mobility, which reduces the pyrolysis rate.<sup>[120]</sup>

In Figure 69 a selection of DSC curves is shown to provide a clearer overview. As can be seen in the DSC curves, the silicone CNT compounds undergo crystallisation between -97 and -87 °C (Figure 69). The crystallisation temperature  $T_C$  rises with increasing CNT loading. The dispersed CNTs might serve as nucleation seeds inducing further crystallisation.<sup>[120]</sup>

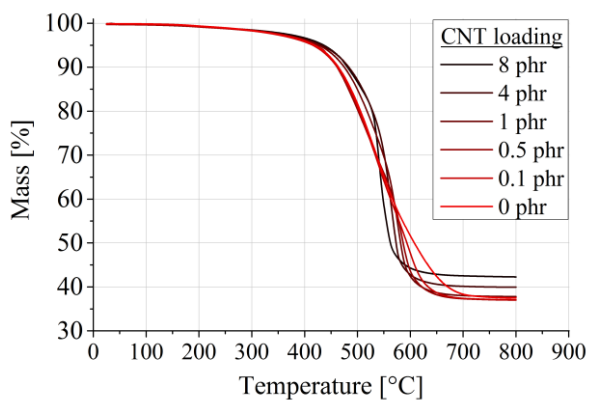


**Figure 68.** TGA curves of silicone CNT composites with varying K100P content.

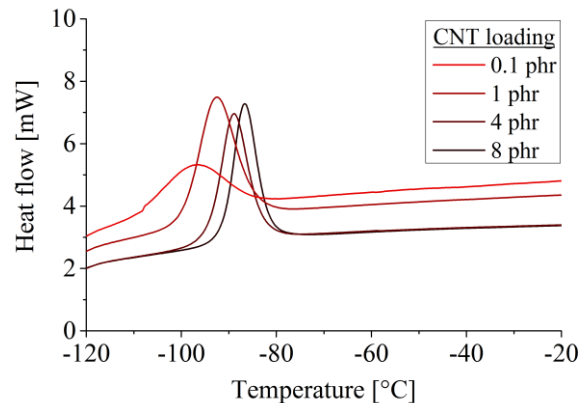


**Figure 69.** DSC curves of silicone CNT compounds with varying CNT loading in cooling state.

### 3.5.3 Electrical properties

As described in chapter 3.1.3, the CNTs differ in length, diameter, surface area and bulk density. These parameters affect the dispersion in the rubber matrix and thereby the electrical conductivity of the composites. With regard to SWCNT and MWCNTs, there is also a difference of several orders of magnitude in the inherent electrical conductivity.<sup>[56,121]</sup>

The minimal filler content required to obtain the first consistent conductive pathway through the matrix is the electrical percolation threshold. The curves for the electrical conductivity as

a function of the CNT content are presented in Figure 70, in which the inflection point of the sharp rise in the electrical conductivity represents the percolation threshold. It shows that the incorporation of different CNT types produces composites with different levels of conductivity.

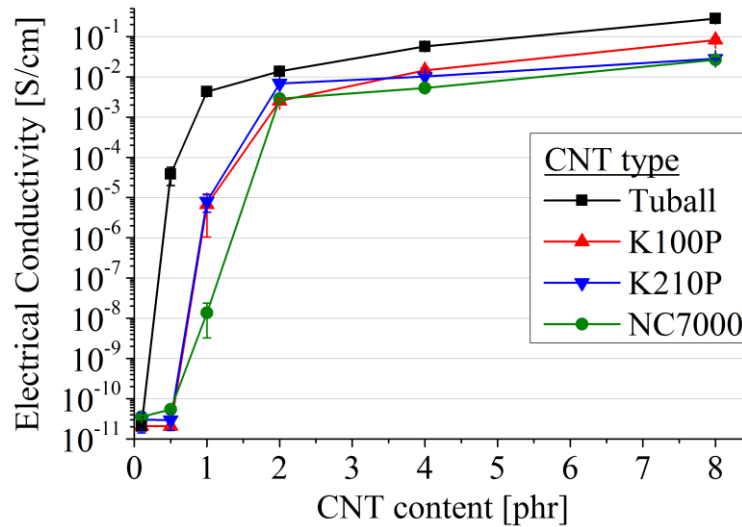


**Figure 70. Electrical conductivity of silicone CNT composites with varying CNT types and loading.**

The largest changes in electrical conductivity can be recognized around the percolation threshold. The electrical percolation threshold for the Tuball SWCNTs was  $<0.5$  phr, those for K100P and K210P were around 1 phr and that for NC7000 was between 1 and 2 phr. Below a CNT content of 2 phr the electrical conductivity values of the SWCNT composites are by several decades higher than those of the MWCNT composites. The curve of the Tuball silicone composite is marked by a steep rise in electrical conductivity, while the curves of the other composites increase more moderately. Additionally, the value for the conductivity at saturation is in case of the Tuball silicone composite 0.5-1 orders of magnitude higher than that of the other CNT silicone composites.

The disparity between the conductivity values of the different silicone CNT composites is for one thing ascribed to the different average diameters of the CNTs. The Tuball SWCNTs have much smaller diameters than the MWCNTs, leading to a higher number of CNTs per unit volume with the same sample weight. Further the higher aspect ratio of the SWCNTs increases the probability of particle-particle contact, which enables the formation of a conductive network with lower CNT content.<sup>[122]</sup> Moreover, the SWCNTs are more resistant to degradation during the mixing process, due to their higher flexibility. The different

compaction of the various CNT types will also have some impact on the dispersibility and in this way affect the conductivity.

The dispersion of the CNTs in silicone rubber was examined by SEM. After the mixing process the SWCNTs were found predominantly in agglomerates (Figure 71), which can be beneficial for the electrical conductivity, as the agglomerated CNTs can form pathways through the rubber matrix (kinetic percolation). In terms of mechanical properties, however, agglomerates might have an adverse impact.

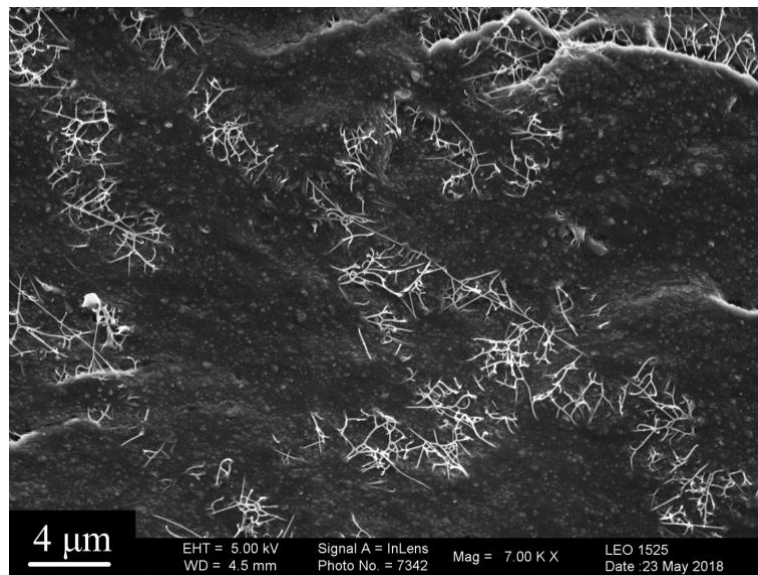


**Figure 71. SEM image of a Tuball silicone composite.**

### **3.5.4 Mechanical properties**

The silicone CNT composites were also compared regarding their mechanical properties. A CNT content of 2 phr, which is slightly above the percolation threshold, was chosen, because here the greatest differences were expected. This also ensured that an electrical conductive material is obtained. The mechanical data of these silicone CNT composites are listed in Table 14.

**Table 14. Hardness and mechanical properties of the silicone CNT composites with 2 phr CNTs**

<b>CNT type</b>	<b>Hardness (Shore A)</b>	<b>Young's modulus [MPa]</b>	<b>Tensile strength [MPa]</b>	<b>Tear strength [kN/m]</b>	<b>Compression set [%]</b>
<b>K100P</b>	83 ± 1	19 ± 1	9.1 ± 0.6	20 ± 2	70 ± 1
<b>K200P</b>	81 ± 1	22 ± 3	9.8 ± 0.5	27 ± 6	72 ± 4
<b>NC7000</b>	81 ± 1	20 ± 1	8.1 ± 0.4	21 ± 6	65 ± 1
<b>Tuball</b>	89 ± 2	49 ± 6	5.8 ± 0.7	33 ± 1	82 ± 1
<b>Unfilled</b>	78 ± 1	14 ± 1	10.7 ± 0.6	26 ± 3	42 ± 3

The silicone SWCNT composites showed higher electrical conductivity, hardness, Young's modulus and tear strength than the composites containing MWCNTs. The reinforcing effect of SWCNTs was examined in detail using a concentration series of Tuball in silicone rubber.

In case of hardness and Young's modulus a significant reinforcement was recorded. The hardness increased with the addition of CNTs even with low loadings (Figure 72). This can be ascribed to the high surface area of CNTs. A high filler surface area enhances the capability of immobilising molecules of the rubber matrix on its surface, leading to lower mobility of the polymer chains and reduced flexibility.<sup>[123]</sup> Therefore, the addition of all CNT types, especially the Tuball SWCNTs, leads to harder compounds. For the composite with 2, 4 and 8 phr Tuball no difference in hardness could be observed, which indicates an insufficient dispersion of the CNTs at higher loadings. Possibly, the dispersed silica in the green SiR affects the dispersion, as a steady increase in hardness with increasing CNT content was reported for silicone rubber with lower silica content.<sup>[120]</sup>

The increase in Young's modulus was similar to that in hardness (Figure 73) and confirms the rigidity of the composites. A sharp increase was observed at low CNT contents. The modulus reached a maximum at around 45 MPa and there was no significant difference between the composites with 2, 4 and 8 phr Tuball.

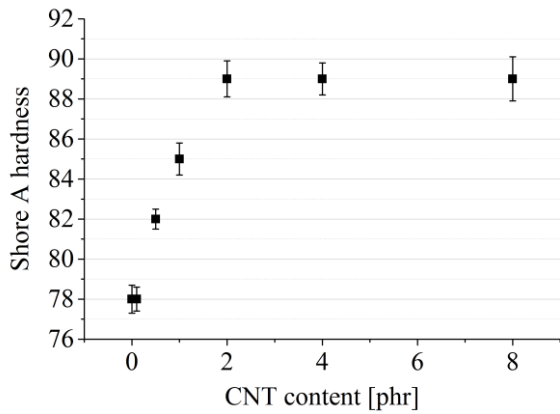


**Figure 72. Hardness of silicone SWCNT composites.**

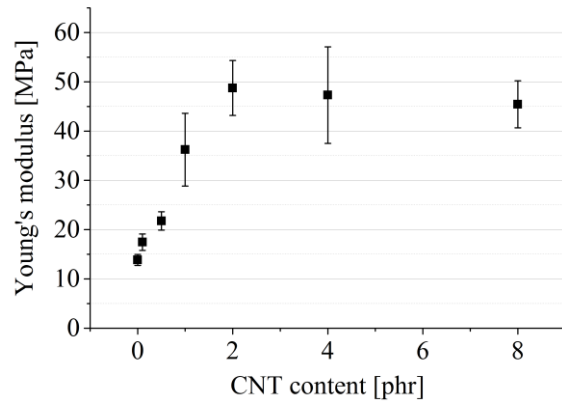


**Figure 73. Young's modulus of silicone SWCNT composites.**

The tensile strength was impacted negatively by the incorporation of CNTs. For the K-Nanos almost no significant change was noticed, while the incorporation of NC7000 led to a slight reduction. The most substantial loss was observed for the composites containing Tuball. The decrease is presumably the result of insufficient filler-polymer interaction, which impairs the deagglomeration of the SWCNT. The agglomerates act as defects in the rubber matrix and initiate the breaking of the material. The difference in the tensile strength of the NC7000 compared to the K-Nanos can be ascribed to a poorer dispersion on account of its higher bulk density. Due to their higher aspect ratio SWCNTs have a greater potential to form agglomerates, which explains their strong impact on the tensile strength. The Tuball SWCNTs caused a decrease in tensile strength with higher content (Figure 74).

CNTs are reported to increase the tensile strength of silicone rubber, which could not be confirmed in this work.<sup>[71,120,122,124,125]</sup> In these publications silicone rubbers with various compositions were used. Katihabwa et al. and Zimmermann et al., for example, used silicone rubber filled with fumed silica to yield a hardness of Shore B = 29 and Shore A = 40 respectively.<sup>[120,122]</sup> The silicone rubber in this work was designed for a Shore A hardness of 80, and thus had a significant higher content of silica. Consequently, the free volume capacity in the pristine rubber is smaller, which promotes the agglomeration of additional fillers.

The elongation at break also decreases with increasing CNT content (Figure 75), which is probably the result of insufficient filler-polymer interaction.<sup>[120]</sup> With 8 phr Tuball an elongation at break of around 10% was measured. Such low elongation at break values limit the possible applications of the material.

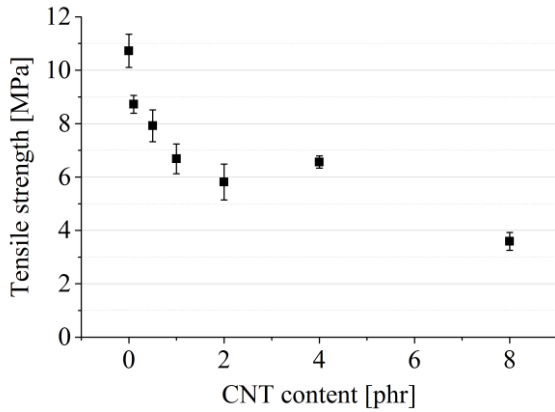


Figure 74. Tensile strength of silicone SWCNT composites.

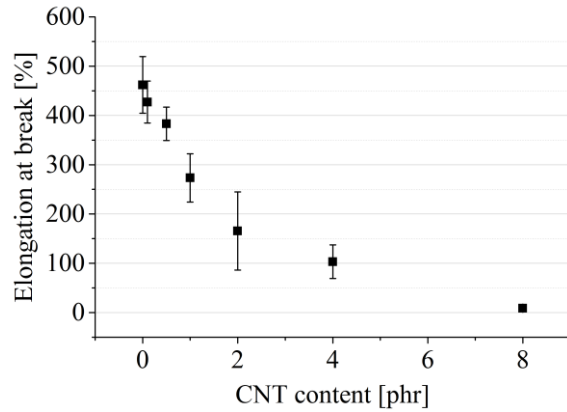


Figure 75. Elongation at break of silicone SWCNT composites.

The stress-strain curves of one sample of the composites with 2 phr of each CNT type are depicted in Figure 76. The curves show the reinforcing effect of the CNT types at lower strain, which is stronger for Tuball. However, the ultimate tensile strength was not improved using CNTs as fillers.

The stress required to produce a certain strain is a common criterion to evaluate and compare elastomers. 100% modulus or M100 refers to the stress value at 100% strain. In Figure 77 the 100% moduli for the silicone CNT composites are presented. The M100 values of Tuball composites increase gradually with increasing CNT content, which is proportional in the area of 0.1 to 2 phr. At 2 phr the M100 value is around 55% higher than that of the MWCNT types. This difference is ascribed to the higher surface area of the SWCNTs.

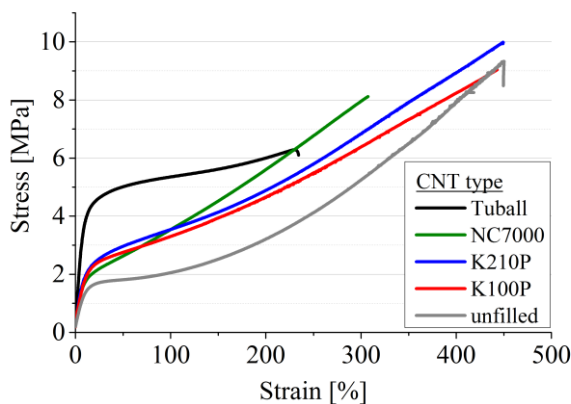


Figure 76. Stress-strain curves of silicone composites with 2 phr CNTs.

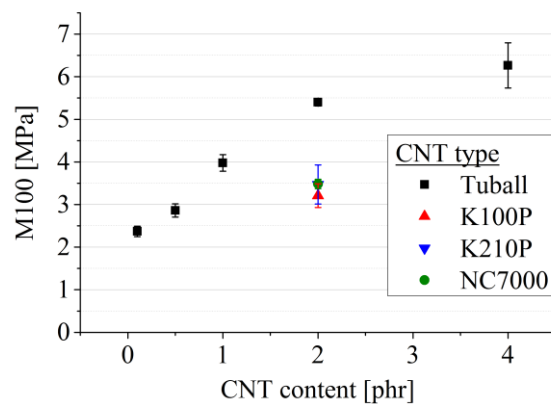
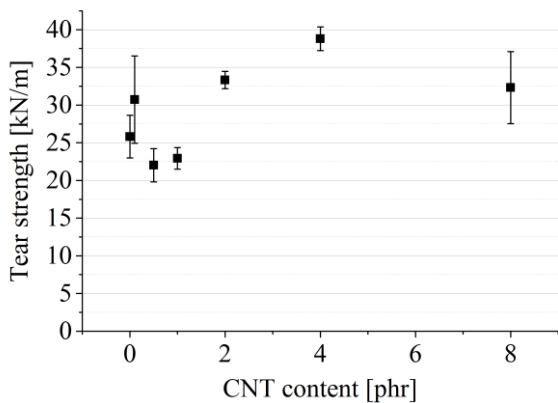


Figure 77. Stress at 100% strain of silicone CNT composites.

The change in tear strength showed no steady trend with increasing CNT content (Figure 78). For composites with a Tuball content below 2 phr the tear strength values were within the standard abbreviation of the unfilled silicone compound. The composites with 2 and 4 phr

Tuball showed improved tear strength compared to the unfilled compound. Given a homogeneous dispersion, the tear strength depends on the filler hardness and the filler-polymer adhesion.<sup>[126]</sup> Since hardness, adhesion and dispersion did not change within the concentration series, the composites with 2 and 4 phr Tuball apparently contain a sufficient amount of CNTs per unit volume to limit the crack propagation. The composites containing 2 phr of MWCNTs showed no improvement in tear strength. The different impact is owed to the higher surface area of the SWCNTs, which correlates with the filler-polymer interaction and thus with the tear strength.

The incorporation of CNTs into silicone rubber heavily impacted the compression set of the composites. The compression set increased from a value of around 40% for unfilled SiR with increasing Tuball content up to a value of around 90% (Figure 79). A compression set of 100% means that no recovery after the enforced compression took place. With a Tuball content of 0.5 phr, which is required to obtain an antistatic effect, a compression set of around 80% was measured. In case of the other CNT types the increase was less, but still severe (Table 14). The strong impact of CNTs on the compression set is probably owed to chain slipping along the CNT surface due to poor filler-polymer adhesion.<sup>[117]</sup> The unmodified formulation of the SiR obviously also results in a more regular network, probably with fewer dangling ends.



**Figure 78. Tear strength of silicone SWCNT composites.**

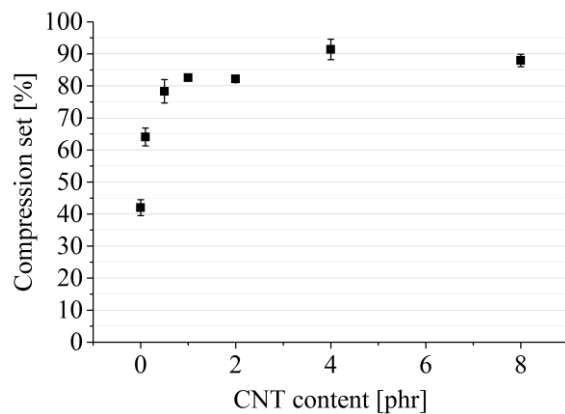


**Figure 79. Compression set of silicone SWCNT composites.**

### 3.6 Composites with Filler Combinations

This chapter describes the reinforcing effects of a selection of the used fillers in combination with each other. The influence on the vulcanisation behaviour and the mechanical properties has been examined, especially with regard to synergetic effects.

In the literature, similar studies have been described. For example, the reinforcement of SiR with a combination of montmorillonite clay and MWCNTs was studied.<sup>[127]</sup> The study revealed an improvement in tensile strength by 215% compared to the initial SiR, whereas the SiR containing clay or CNTs alone showed an improvement of 46 and 25%, respectively. The hybrid filler was prepared by grinding and showed an exfoliated structure. The nanocomposites were produced in solution.

Moreover, the effects of octadecylamine-modified montmorillonite clay in aramid short fibre-filled and carbon black-filled styrene butadiene rubber were described.<sup>[128]</sup> The highest tensile strength and elongation at break were found in clay filled composites. The composites were prepared on a two-roll mill.

In this work, aramid pulp (AF), RH modified HNTs and SWCNTs were used in combination for the preparation of composites containing multiple fillers. As seen in the previous chapters, the composites with 3 phr AF, 2 phr RH-HNTs and 2 phr SWCNTs, respectively, offer the most beneficial properties. Therefore, these filler contents were chosen for the preparation of the multi-filler composites. Since an improvement of both tear strength and compression set without affecting the other properties was accomplished in case of the 2 phr RH-HNT composite, this filler was combined with AF and SWCNTs to prepare the multi-filler composites. Since indications of overloading of the rubber matrix were observed at filler contents not lower than 7 phr AF and 8 phr SWCNTs, this was not expected here. The different fillers were consecutively incorporated into the green SiR formulation.

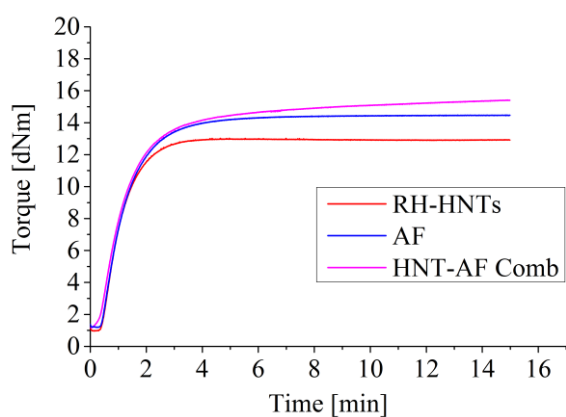
### 3.6.1 Vulcanisation behaviour

Figure 80 shows the rheograph of the compound containing RH-HNTs and AF in combination compared to those with HNTs and AF alone. The combination of the two fillers causes an increment in torque, which is due to the higher total filler content and thus more filler-rubber interaction. In contrast to the curing curves of the RH-HNT and AF compounds, that reach a plateau after 4 and 6 minutes, respectively, the HNT-AF compound shows a marching curve. This is attributed to the slower formation of additional crosslinks, probably between the RH resin and AF. These may be of physical rather than chemical origin.

The rheographs of the composites containing RH-HNTs and SWCNTs in combination and alone are presented in Figure 81. The torque values ( $M_H$  and  $M_L$ ) of the SWCNT compound



are significantly higher than those of the RH-HNT compound, which is owed to the high surface area of the CNTs. The combination of both fillers produces torque values that range between those of the single-filler compounds. The HNT-CNT compound also shows a marching curve, presumably also because of the formation of physical crosslinks between the RH resin and the CNTs. In this case the increase in torque is even more pronounced, resulting in a relatively high  $t_{90}$  time.



**Figure 80. Rheographs of the compounds with AF and HNTs alone and in combination.**

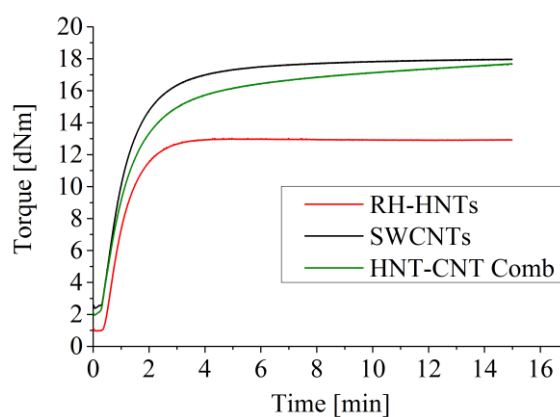


**Figure 81. Rheographs of the compounds with HNTs and CNTs alone and in combination.**

In Table 15 the curing characteristics of the compounds with filler combinations are listed. In both multi-filler compounds, the combination leads to a shorter scorch time and delayed  $t_{90}$  time compared to the single-filler compounds. It is noticeable that the  $M_L$  value of the SWCNT compound, which gives an indication of the filler content in the rubber,<sup>[129]</sup> is higher than that of the HNT-CNT compound. This may be related to the dispersion of the SWCNT being more compatible to the matrix than HNTs.

**Table 15. Curing characteristics of the compounds with filler combinations and with the fillers alone**

Filler	$M_H$ [dNm]	$M_L$ [dNm]	$M_H-M_L$ [dNm]	Scorch time ( $t_{S1}$ ) [s]	$t_{90}$ time [s]
RH-HNTs	13.1	1.0	12.1	29	129
AF	14.1	1.2	12.9	32	162
HNT+AF	16.8	1.2	15.6	26	171
SWCNTs	18.0	2.4	15.6	23	185
HNT+CNT	17.7	2.0	15.7	21	260

### 3.6.2 Mechanical properties

The stress-strain curves of the multi-filler composites, the corresponding single-filler composites and unfilled SiR are presented in Figure 82. As can be seen, the curves show a reinforcing effect of the combined fillers at low strain and a breakdown of these composites at lower values compared to unfilled SiR or the RH-HNT composite.

In Figure 83 the stress values at 100% strain of the multi-filler composites are shown. The increment in M100 of the HNT-AF composite compared to unfilled SiR is higher than the combined increments of the composites containing HNT and AF alone. In contrast, the HNT-CNT composite shows a lower M100 value than the composite containing only SWCNTs.

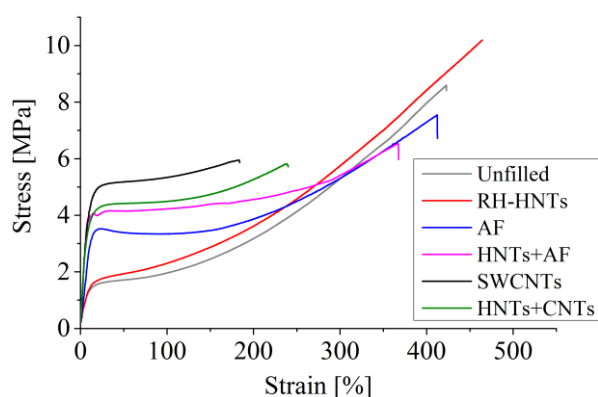


**Figure 82.** Stress-strain curves of multi-filler composites compared to those with single filler.

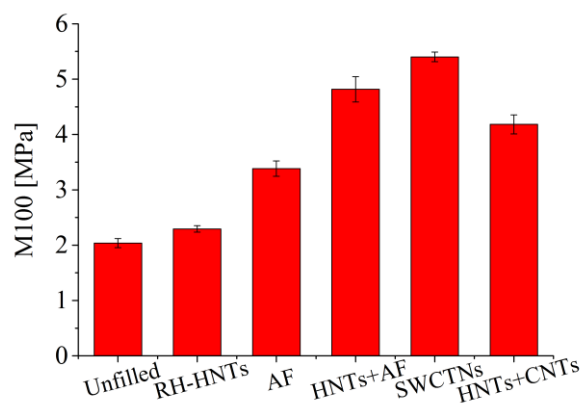


**Figure 83.** M100 values of multi-filler composites compared with those with single filler.

In Table 16 the mechanical properties of the HNT-AF composite, the HNT-CNT composite and the composites with the corresponding fillers alone are listed. The addition of RH-HNTs to the AF composite gives rise to an increase in hardness, Young's modulus and compression set as well as a decrease in tensile strength and elongation at break. The tear strength remains within the error margin. Similar values were found for the HNT-CNT composite as for the SWCNT composite. Only the compression set was improved slightly by the addition of RH-HNTs. The composite containing only RH-HNTs shows superior tensile strength, elongation at break and compression set. It follows that the reinforcing effect of the RH-HNTs does not suffice to compensate for the weaknesses of the insufficiently adhering properties or dispersion of the fillers.

Table 16. Mechanical properties of composites with filler combinations

<b>Fillers</b>	<b>Hardness (Shore A)</b>	<b>Young's modulus [MPa]</b>	<b>Tensile strength [MPa]</b>	<b>Elongation at break [%]</b>	<b>Tear strength [kN/m]</b>	<b>Compression set [%]</b>
<b>Unfilled</b>	78 ± 1	14 ± 1	10.7 ± 0.6	462 ± 58	26 ± 3	42 ± 3
<b>RH-HNTs</b>	77 ± 1	14 ± 2	10.6 ± 0.3	474 ± 14	30 ± 2	31 ± 4
<b>AF</b>	85 ± 1	37 ± 5	8.3 ± 0.1	423 ± 28	26 ± 2	45 ± 2
<b>HNTs+AF</b>	87 ± 1	50 ± 9	6.0 ± 0.4	336 ± 27	29 ± 2	62 ± 2
<b>SWCNTs</b>	89 ± 2	49 ± 6	5.8 ± 0.7	165 ± 79	33 ± 1	82 ± 1
<b>HNTs+CNTs</b>	87 ± 1	43 ± 5	5.7 ± 0.4	171 ± 89	32 ± 1	76 ± 3

## 4 Summary

HTV silicone rubber (SiR) was used in this work as a base material for the preparation of composites. According to TGA and NMR measurements, the SiR contained  $\leq 37$  wt% dispersed silica to yield a hardness of Shore A = 80 and had a vinyl content of 0.74%. The silicone compounds were prepared in an internal mixer with 1.2 phr of a peroxide curing agent and vulcanised using a hot press. Aramid fibres (AF), halloysite nanotubes (HNTs) and carbon nanotubes (CNTs) were used as fillers.

Untreated aramid fibres were incorporated into silicone rubber to produce composites with fibre contents in the range of 1 to 10 phr. The incorporation of the aramid fibres had no particular impact on the vulcanisation time and rendered the composites more susceptible to thermal degradation. Moreover, the hardness and the Young's modulus were increased compared to unfilled SiR by up to 13% and 101%, respectively. However, this was accompanied by a decrease in tensile strength and elongation at break, which is owed to the weak adhesion of the aramid fibres to the silicone matrix. The aramid fibres were chemically modified with an epoxy-silane coating in order to improve the silicone-aramid interaction. The epoxy coating was carried out successfully, whereas the silane coating took place only to a small extent. The coating caused a reduction in crosslinking density, which resulted in an increase in tear resistance of 22% compared to unfilled SiR. However, the other mechanical properties were adversely affected.

Composites with HNT contents in the range of 1 to 10 phr were prepared using pristine HNTs and HNTs modified with a complex based on resorcinol and hexamethylenetetramine. The composites containing the RH modified HNTs (RH-HNTs) showed consistently superior performance due to improved filler-rubber adhesion and higher crosslinking density. The vulcanisation process was accelerated by the incorporation of RH-HNTs, whereas the presence of pristine HNTs led to longer vulcanisation times. In addition, the RH-HNT composites showed a 35% lower compression set than unfilled SiR without impairing other mechanical properties.

Four different types of CNTs were used for the preparation of composites. Among them were three types of multi-wall CNTs (MWCNTs) and one type single-wall CNTs (SWCNTs). Composites with SWCNTs showed higher electrical conductivity and also higher tear strength than corresponding MWCNT composites, which is attributed to the significantly smaller

diameter of the SWCNTs and the larger surface area. Compared to unfilled SiR, the tear strength of composites containing 2 phr SWCNTs was improved by 29%. The thermal stability of the composites was gradually enhanced upon the addition of increasing amounts of CNTs.

Composites were prepared using the different fillers in combination. The RH modified HNTs were combined with untreated aramid fibres and SWCNTs, respectively. In the case of silicone-aramid-HNT composites, the increment in modulus at 100% strain was higher than those of the two single-filler composites combined. However, the ultimate tensile strength and the other mechanical properties turned out lower than those of the RH-HNT composite. The multi-filler composite containing RH-HNTs and SWCNTs showed a similar high tear strength as the RH-HNT composite. A further mechanical reinforcement was not achieved by the combination of RH-HNTs and SWCNTs. Compared to the SWCNT composite, the compression set was slightly decreased upon the addition of RH-HNTs.

The combination of the fillers did not result in synergetic effects or any further reinforcement of the composites. Rather, the reinforced composites were adversely affected by the fillers with insufficient adhesion or dispersion. Also, this could not be compensated for by the presence of a reinforcing filler.

## 5 Experimental Part

### 5.1 Materials and Chemicals

Solid silicone rubber (HTV) Elastosil R 401/80 was provided by Wacker Chemie AG. Curing agent Peroxan HX-45 SP (45% paste of 2,5-bis(tert-butylperoxy)-2,5-dimethylhexane in silicone rubber) was purchased from Pergan GmbH. Halloysite nanotubes Dragonite-HP were purchased from Applied Minerals, Inc. Multi-wall carbon nanotubes NC7000 were purchased from Nanocyl SA and K-Nanos 100P as well as K-Nanos 210P from Kumho Petrochemical Co., Ltd. Single-wall carbon nanotubes Tuball were purchased from OCSiAl. Dry *para*-aramid pulp Twaron 1095 was purchased from Teijin Aramid BV. The size of the aramid pulp was removed by Soxhlet extraction in ethanol prior to the experiments. All other materials were used without prior treatment.

Piperazine was purchased from Alfa Aesar. Docusate sodium, ethanol and hexamethylenetetramine were purchased from Sigma-Aldrich Chemie GmbH. Glycerol triglycidyl ether was purchased from Fluka Chemie AG. Glacial acetic acid and resorcinol were purchased from Merck KGaA. 3-(trimethoxysilyl)propyl methacrylate was supplied by Evonik Industries AG. Chloroform-*d* was purchased from Deutero GmbH. All chemicals were used without prior purification unless otherwise specified.

### 5.2 Filler Modification

#### Modification of aramid pulp

Piperazine (0.125 g, 1.45 mmol), docusate sodium (0.25 g, 0.56 mmol) and glycerol triglycidyl ether (7.5 g, 29 mmol) were dissolved in 250 mL demineralised water. Aramid pulp (4.5 g) was added and the slurry was stirred at room temperature for 45 minutes. The mixture was filtered and the treated aramid pulp was dried at 150 °C for 1 h. 250 mL demineralised water were adjusted to pH 3.5 with glacial acetic acid and 3-(trimethoxysilyl)propyl methacrylate (1 mL) was added. The pretreated aramid pulp was added to the solution and stirred at room temperature for 1 h. The mixture was filtered and the coated aramid pulp was stored overnight at room temperature. After drying at 175 °C for 30 minutes, the silane coated aramid pulp was obtained.

### **Modification of halloysite nanotubes (HNTs)**

Resorcinol (11.0 g, 0.10 mol) and hexamethylenetetramine (14.0 g, 0.10 mol) were dissolved under stirring in 125 mL demineralised water each. Both solutions were combined and heated to 50 °C. Then 25 g HNTs were dispersed under stirring in the solution and the suspension was stirred at 50 °C for 4 h. The mixture was cooled down to ambient temperature and filtered. The filter cake was dried in a vacuum oven at 50 °C for 48 h. The agglomerated solid was grinded in a ball mill and the RH modified HNTs were obtained as red brown powder.

## **5.3 Rubber Processing**

### **Preparation of rubber compounds**

The rubber compounds were prepared using a lab mixer (HAAKE Rheomix 3000 OS, tangential Roller Rotors) with varying rotor speed (30-90 U/min) and mixing time (15-30 min). The temperature of the mixing chamber was set to 25 °C. In most cases the rotor speed was set to 30 U/min and the mixing time was 15 min. After a 2 min plastification step, the peroxide curing agent and the fillers were added successively over a period of 1-3 min. The curing agent was added to the rubber compounds at a mass fraction of 1.2 phr. The process temperature was kept below 120 °C to avoid a premature start of the vulcanization.

### **Vulcanisation**

Vulcanised rubber sheets with 2 mm thickness and specimens respectively were prepared by compression moulding at 175 °C for 15 min as it is advised for the used silicone rubber type by Wacker Chemie AG. This was followed by a post curing step at 200 °C for 2 h.

## **5.4 Rubber Testing**

All vulcanised test specimens were conditioned for 24 h at  $20\pm 2$  °C before the tests. The tests were carried out at  $20\pm 2$  °C unless stated otherwise.

### **Vulcanisation studies**

Vulcanisation studies were performed using a moving die rheometer (MDR-A) from Beijing RADE Instrument Co., Ltd. at 175 °C for 15 minutes.

### **Hardness**

The hardness (Shore A) was determined in accordance to DIN ISO 7619-1 using a durometer from Albert Schumann GmbH. Five measurements were undertaken at different positions on stacks of three 2 mm specimens.

### **Compression set**

The compression set was determined at 175 °C for 24 h in accordance to DIN ISO 815-1 A. The test specimens were prepared via compression moulding.

### **Tear resistance**

Tear tests were performed according to DIN ISO 34-1 C using a Zwick Roell Z1.0. The test specimens were cut out from a 2 mm thick vulcanised rubber sheet.

### **Tensile testing**

Tensile tests were performed on a Zwick Roell Z1.0 with VideoXtens according to DIN 53504 (preload: 1 MPa, test speed: 50 mm/min). The test specimens were cut out from a 2 mm thick vulcanised rubber sheet.



### **Electrical properties**

The electrical conductivity of the vulcanised rubber compounds was determined using a MetrISO G1000<sup>+</sup> Insulation Tester. The test specimens (10 x 50 mm) were cut out from a 1 mm thick vulcanised rubber sheet.

### **Abrasion testing**

Abrasion tests were performed according to DIN ISO 4649 using a Rade DIN Abrasion Tester AT150. The test specimens were prepared via compression moulding.

## **5.5 Characterisation**

### **IR Spectroscopy**

IR spectroscopy was carried out on a Vertex 70v from Bruker and the spectra were analysed with Omnic 8.3.

### **Thermogravimetric analysis (TGA)**

TGA was performed using a TGA 1 from Mettler Toledo. The samples were heated from 25 °C to 800 or 1200 °C at a heating rate of 10 K/min under nitrogen atmosphere.

### **Differential scanning calorimetry (DSC)**

DSC was performed using a Mettler Toledo DSC 1 instrument calibrated with indium. The weight of samples sealed in an aluminium pan was about 10-15 mg.

### **Scanning electron microscopy (SEM) & Energy-dispersive X-ray spectroscopy (EDX)**

SEM images were taken with the field emission scanning electron microscope LEO 1525 Gemini at an acceleration voltage of 5 kV with an In-Lens detector. An Octane silicon drift detector from EDAX Inc. was used for energy dispersive X-ray spectroscopy.

### **X-ray powder diffraction (XRD)**

XRD patterns were recorded using a Panalytical MPD X'Pert Pro with Cu anode ( $\lambda = 1.54 \text{ \AA}$ ), scanning from  $5^\circ$  to  $50^\circ$ .

### **Laser diffraction size analysis**

Laser diffraction measurements were performed using a Helos KR sensor and a Rodos injection disperser from Sympatec GmbH. The data was processed with PaqXos 2.0 from Sympatec GmbH.














### **Element analysis**

The element analysis was carried out using a Euro EA Elemental Analyser with High-temperature Oxygen Analyser from HEKAtech GmbH.





### **Nuclear magnetic resonance (NMR) Spectroscopy**

$^1\text{H}$ -NMR spectra were recorded in chloroform-*d* ( $\text{CDCl}_3$ ) with tetramethylsilane as internal standard using a Bruker Avance 400 MHz spectrometer. The obtained data was analysed with MestReNova 14.0.

## 6 Safety Data

Substance	GHS pictograms	Hazard sentences	Precaution sentences
Acetic acid (≥ 99%)	 	H226, H290, H314	P210, P280, P303+P361+P353, P304+P340+P310, P305+P351+P338+P310, P370+P378
Chloroform- <i>d</i>	 	H302, H315, H319, H331, H351, H361d, H372	P260, P280, P301+P312+P330, P304+P340+P312, P305+P351+P338, P403+P233
Docusate sodium		H315, H318	P280, P305+P351+P338
Dragonite- HP™ (HNTs)	Not a hazardous substance or mixture according to Regulation (EC) No 1272/2008.		
Elastosil® R401/80 (silicone rubber)	Not a hazardous substance or mixture according to Regulation (EC) No 1272/2008.		
Ethanol	 	H225, H319	P210, P233, P280, P303+P361+P353, P337+P313, P370+P378
Glycerol triglycidyl ether	 	H302, H315, H319, H341, H361	P201, P202, P264, P270, P280, P301+P312, P330, P305+P351+P338, P308+P313, P321, P362+P364, P332+P313, P337+P313, P405, P501
Hexamethylene -tetramine	 	H228, H317	P210, P280, P333+P313
K-Nanos-100P (MWCNTs)		H315, H319	P264, P280, P302+P352+P332+P313+P362+P364, P305+P351+P338+P337+P313
K-Nanos-210P (MWCNTs)		H315, H319	P264, P280, P302+P352+P332+P313+P362+P364, P305+P351+P338+P337+P313

Safety Data

Substance	GHS pictograms	Hazard sentences	Precaution sentences
NC7000™ (MWCNTs)	not applicable	not applicable	P233, P260, P273, P280
Peroxan HX-45 SP		H242, H315	P210, P220, P234, P264, P280, P332+P313, P410, P411+P235, P420, P501
Piperazine		H314, H317, H334, H361fd	P261, P280, P305+P351+P338, P310
Resorcinol		H302, H315, H318, H400	P280, P301+P312+P330, P305+P351+P338+P310
3-(trimethoxysilyl)-propyl methacrylate	Not a hazardous substance or mixture according to Regulation (EC) No 1272/2008.		
Tuball® (SWCNTs)		H319	P264, P280, P305+P351+P338, P337+P313
Twaron® 1095 (aramid pulp)	Not a hazardous substance or mixture according to Regulation (EC) No 1272/2008.		

The CMR substances used in this work are listed in Table 17.

Table 17. Used CMR substances<sup>[130,131]</sup>

CAS-No.	Name	Procedure	Quantity	Category
110-85-0	Piperazine	Synthesis	7.5 g	Rep. 2
67-66-3	Trichloromethane- <i>d</i>	NMR measurements	12 mL	Carc. 2, Rep. 2

## 7 Bibliography

- [1] F. S. F. Röthemeyer, *Kautschuk-Technologie: Werkstoffe - Verarbeitung - Produkte*, Hanser, München, **2013**.
- [2] International Rubber Study Group, *Produktionsmenge von Kautschuk weltweit in den Jahren von 2000 bis 2018*, Statista GmbH, **2019**.
- [3] International Rubber Study Group, *Produktionsmenge von synthetischem Kautschuk weltweit in den Jahren von 2000 bis 2018*, Statista GmbH, **2019**.
- [4] International Rubber Study Group, *Weltweiter Verbrauch von Natur- und synthetischem Kautschuk in den Jahren 1990 bis 2018*, Statista GmbH, **2019**.
- [5] Ceresana, *Marktstudie Butadien-Kautschuk (BR)*, Ceresana eK, Konstanz, **2018**.
- [6] Ceresana, *Marktstudie Styrol-Butadien-Kautschuk (SBR)*, Ceresana eK, Konstanz, **2018**.
- [7] MarketWatch, *Silicone Market - Growth, Trends, and Forecast (2019 - 2024)*, **2018**, <https://www.marketwatch.com/press-release/the-silicone-elastomers-market-is-projected-to-grow-from-usd-638-billion-in-2018-to-usd-881-billion-by-2023-at-a-cagr-of-67-between-2018-and-2023-2018-10-01>. Accessed 02/2020.
- [8] V. D. J. Ackermann, *Chem. Unserer Zeit*, **1989**, *23*, 86.
- [9] CES Silicones Europe, *Silicone Manufacturing Process*, <https://www.silicones.eu/silicones/industry>. Accessed 02/2020.
- [10] *Silicone: Chemie und Technologie Symposium Papers*, Vulkan-Verlag, Essen, **1989**.
- [11] H. G. W. Hofmann, *Handbuch der Kautschuktechnologie*, Gupta, Ratingen, **2009**.
- [12] Bundesinstitut für Risikobewertung, *BfR-Empfehlungen zu Materialien für den Lebensmittelkontakt - Silicone*, **2017**.
- [13] H.-H. Moretto, M. Schulze, G. Wagner, in *Ullmann's Encyclopedia of Industrial Chemistry*, Vol. 2, Wiley-VCH Verlag GmbH & Co. KGaA, Weinheim, Germany, **2000**, p. 1289.
- [14] Umweltbundesamt, *Leitlinie zur hygienischen Beurteilung von Elastomeren im Kontakt mit Trinkwasser (Elastomerleitlinie)*, **2016**.
- [15] C. M. Harris, A. G. Piersol, *Harris' shock and vibration handbook*, McGraw-Hill, New York, **2002**.
- [16] R. Rotheron, *Fillers for Polymer Applications*, Springer International Publishing, Cham, **2017**.
- [17] W. B. Wiegand, *J. Ind. Eng. Chem.*, **1921**, *13*, 118.

- [18] J. Liu, H. Wan, H. Zhou, Y. Feng, L. Zhang, A. V. Lyulin, *RSC Adv.*, **2018**, 8, 13008.
- [19] M. Galimberti, in *Advanced Elastomers - Technology, Properties and Applications* (Ed.: A. Boczkowska), InTech, **2012**.
- [20] D. Ahmed, Z. Hongpeng, K. Haijuan, L. Jing, M. Yu, Y. Muhuo, *J. Appl. Polym. Sci.*, **2014**, 17, 1180.
- [21] M. G. Northolt, J. J. van Aartsen, *J. Polym. Sci. B Polym. Lett. Ed.*, **1973**, 11, 333.
- [22] M. Panar, P. Avakian, R. C. Blume, K. H. Gardner, T. D. Gierke, H. H. Yang, *J. Polym. Sci. Polym. Phys. Ed.*, **1983**, 21, 1955.
- [23] M. G. Dobb, D. J. Johnson, B. P. Saville, *J. Polym. Sci. Polym. Phys. Ed.*, **1977**, 15, 2201.
- [24] Teijin Aramid, *Twaron: A true all-round para-aramid performer*, **2018**.
- [25] Z. Denchev, N. Dencheva, in *Synthetic Polymer-Polymer Composites* (Eds.: D. Bhattacharyya, S. Fakirov), Carl Hanser Verlag GmbH & Co. KG. München, **2012**, p. 251.
- [26] W. Sweeny, *Poly-meta-phenylene isophthalamides*, US3287324, **1966**.
- [27] H. Blades, *Dry-Jet Wet Spinning Process*, US3767756, **1973**.
- [28] C. Cherif, *Textile Werkstoffe für den Leichtbau*, Springer, Berlin, Heidelberg, **2011**.
- [29] E. M. Abdel-Bary, E. M. El-Nesr, F. M. Helaly, *Polym. Adv. Technol.*, **1997**, 8, 140.
- [30] T. R. I. Orlob, *GAK Gummi Fasern Kunststoffe*, **2011**, 64, 94.
- [31] P. Pittayavinai, S. Thanawan, T. Amornsakchai, *Polymer Testing*, **2017**, 64, 109.
- [32] G. S. Shibulal, K. Naskar, *Polym. Compos.*, **2014**, 35, 1767.
- [33] P. A. Tarantili, A. G. Andreopoulos, *J. Appl. Polym. Sci.*, **1997**, 65, 267.
- [34] G. Markl, *Minerale und Gesteine*, Springer, Berlin, Heidelberg, **2015**.
- [35] P. Yuan, P. D. Southon, Z. Liu, M. E. R. Green, J. M. Hook, S. J. Antill, C. J. Kepert, *J. Phys. Chem. C*, **2008**, 112, 15742.
- [36] B. Singh, *Clays and Clay Minerals*, **1996**, 44, 191.
- [37] M. Makaremi, P. Pasbakhsh, G. Cavallaro, G. Lazzara, Y. K. Aw, S. M. Lee, S. Milioto, *ACS applied materials & interfaces*, **2017**, 9, 17476.
- [38] M. Fizir, P. Dramou, N. S. Dahiru, W. Ruya, T. Huang, H. He, *Mikrochimica acta*, **2018**, 185, 389.
- [39] S. Satish, M. Tharmavaram, D. Rawtani, *Nanobiomedicine*, **2019**, 6, 1-16.
- [40] M. Du, B. Guo, D. Jia, *European Polymer Journal*, **2006**, 42, 1362.
- [41] Z. Jia, Y. Luo, B. Guo, B. Yang, M. Du, D. Jia, *Polymer-Plastics Technology and Engineering*, **2009**, 48, 607.

- [42] D. Marney, L. J. Russell, D. Y. Wu, T. Nguyen, D. Cramm, N. Rigopoulos, N. Wright, M. Greaves, *Polymer Degradation and Stability*, **2008**, *93*, 1971.
- [43] T. Kim, S. Kim, D. K. Lee, B. Seo, C.-S. Lim, *RSC Adv*, **2017**, *7*, 47636.
- [44] Y. Ye, H. Chen, J. Wu, L. Ye, *Polymer*, **2007**, *48*, 6426.
- [45] B. Guo, F. Chen, Y. Lei, X. Liu, J. Wan, D. Jia, *Applied Surface Science*, **2009**, *255*, 7329.
- [46] B. Guo, Y. Lei, F. Chen, X. Liu, M. Du, D. Jia, *Applied Surface Science*, **2008**, *255*, 2715.
- [47] H. Ismail, H. S. Ahmad, *Journal of Elastomers & Plastics*, **2014**, *46*, 483.
- [48] H. Ismail, P. Pasbakhsh, M. A. Fauzi, A. Abu Bakar, *Polymer Testing*, **2008**, *27*, 841.
- [49] K. Waesateh, S. Saiwari, H. Ismail, N. Othman, S. Soontaranon, N. Hayeemasae, *International Journal of Polymer Analysis and Characterization*, **2018**, *23*, 260.
- [50] S. Yellampalli, *Carbon Nanotubes - Polymer Nanocomposites*, InTech, Rijeka, **2011**.
- [51] O. V. Kharissova, B. I. Kharisov, *RSC Adv*, **2014**, *4*, 30807.
- [52] Eric Wieser, *A multi-walled armchair carbon nanotube, rendered in POVray*, **2010**, [https://commons.wikimedia.org/wiki/File:Multi-walled\\_Carbon\\_Nanotube.png](https://commons.wikimedia.org/wiki/File:Multi-walled_Carbon_Nanotube.png). Accessed 08/2019.
- [53] Paul Wagner, *DSIAC Journal*, **2014**, *1*, 5.
- [54] S. Iijima, *Nature*, **1991**, *354*, 56.
- [55] M.-F. Yu, O. Lourie, M. J. Dyer, K. Moloni, T. F. Kelly, R. S. Ruoff, *Science*, **2000**, *287*, 637.
- [56] T. W. Ebbesen, H. J. Lezec, H. Hiura, J. W. Bennett, H. F. Ghaemi, T. Thio, *Nature*, **1996**, *382*, 54.
- [57] M.-F. Yu, B. S. Files, S. Arepalli, R. S. Ruoff, *Phys. Rev. Lett.*, **2000**, *84*, 5552.
- [58] N. Hamada, S. Sawada, A. Oshiyama, *Phys. Rev. Lett.*, **1992**, *68*, 1579.
- [59] G. Fugallo, A. Cepellotti, L. Paulatto, M. Lazzeri, N. Marzari, F. Mauri, *Nano letters*, **2014**, *14*, 6109.
- [60] P. Kim, L. Shi, A. Majumdar, P. L. McEuen, *Physical review letters*, **2001**, *87*, 215502.
- [61] T. R. Anthony, W. F. Banholzer, J. F. Fleischer, Lanhua Wei, P. K. Kuo, R. L. Thomas, R. W. Pryor, *Phys. Rev. B*, **1990**, *42*, 1104.
- [62] J. Prasek, J. Drbohlavova, J. Chomoucka, J. Hubalek, O. Jasek, V. Adam, R. Kizek, *J. Mater. Chem.*, **2011**, *21*, 15872.

- [63] A. Jorio, G. Dresselhaus, M. S. Dresselhaus, *Carbon Nanotubes: Advanced Topics in the Synthesis, Structure, Properties and Applications*, Springer-Verlag Berlin/Heidelberg, Berlin, Heidelberg, **2008**.
- [64] P. M. Ajayan, O. Stephan, C. Colliex, D. Trauth, *Science (New York, N.Y.)*, **1994**, 265, 1212.
- [65] M. T. Byrne, Y. K. Gun'ko, *Adv. Mater.*, **2010**, 22, 1672.
- [66] A. J. Mertens, S. Senthilvelan, *Proceedings of the IMechE*, **2018**, 232, 669.
- [67] H. Wang, Z. Li, K. Hong, M. Chen, Z. Qiao, Z. Yuan, Z. Wang, *RSC Adv.*, **2019**, 9, 29087.
- [68] L. Bokobza, *Polymer*, **2007**, 48, 4907.
- [69] N. Girun, F.-R. Ahmadun, S. A. Rashid, M. Ali Atieh, *Fullerenes, Nanotubes and Carbon Nanostructures*, **2007**, 15, 207.
- [70] S.-W. Han, N.-S. Choi, S.-R. Ryu, D.-J. Lee, *J Mech Sci Technol*, **2017**, 31, 4073.
- [71] T. A. Kim, H. S. Kim, S. S. Lee, M. Park, *Carbon*, **2012**, 50, 444.
- [72] Z. Peng, C. Feng, Y. Luo, Y. Li, Z. Yi, L. X. Kong, *J. Appl. Polym. Sci.*, **2012**, 125, 3920.
- [73] A. Das, K. W. Stöckelhuber, R. Jurk, M. Saphiannikova, J. Fritzsche, H. Lorenz, M. Klüppel, G. Heinrich, *Polymer*, **2008**, 49, 5276.
- [74] Y. Nakaramontri, C. Kummerlöwe, C. Nakason, N. Vennemann, *AMR*, **2013**, 844, 301.
- [75] R. J. Brown, R. M. Sriver, *Rubber containing aramid pulp reinforcement, US 4871004*, **1989**.
- [76] V. Demétrio da Silva, Í. R. d. Barros, D. K. S. d. Conceição, K. N. d. Almeida, H. S. Schrekker, S. C. Amico, M. M. Jacobi, *J. Appl. Polym. Sci.*, **2020**, 137, 48702.
- [77] C. Hahn, *Journal of Industrial Textiles*, **2000**, 30, 146.
- [78] V. Demétrio da Silva, M. M. Jacobi, H. S. Schrekker, S. C. Amico, *J. Appl. Polym. Sci.*, **2018**, 135, 46693.
- [79] Teijin Aramid, *Technical Data Sheet Twaron 1095*, **2016**.
- [80] D. F. M. Michiels, *Composite Article and its Manufacture, US 7404989 B2*, **2008**.
- [81] Y. Iyengar, *J. Appl. Polym. Sci.*, **1978**, 22, 801.
- [82] H. Zhang, J. Zhang, J. Chen, X. Hao, S. Wang, X. Feng, Y. Guo, *Polymer Degradation and Stability*, **2006**, 91, 2761.
- [83] S. Kasetaitė, J. Ostrauskaitė, V. Grazulevičienė, D. Bridziuvienė, R. Budreckienė, E. Rainosaló, *Reactive and Functional Polymers*, **2018**, 122, 42.

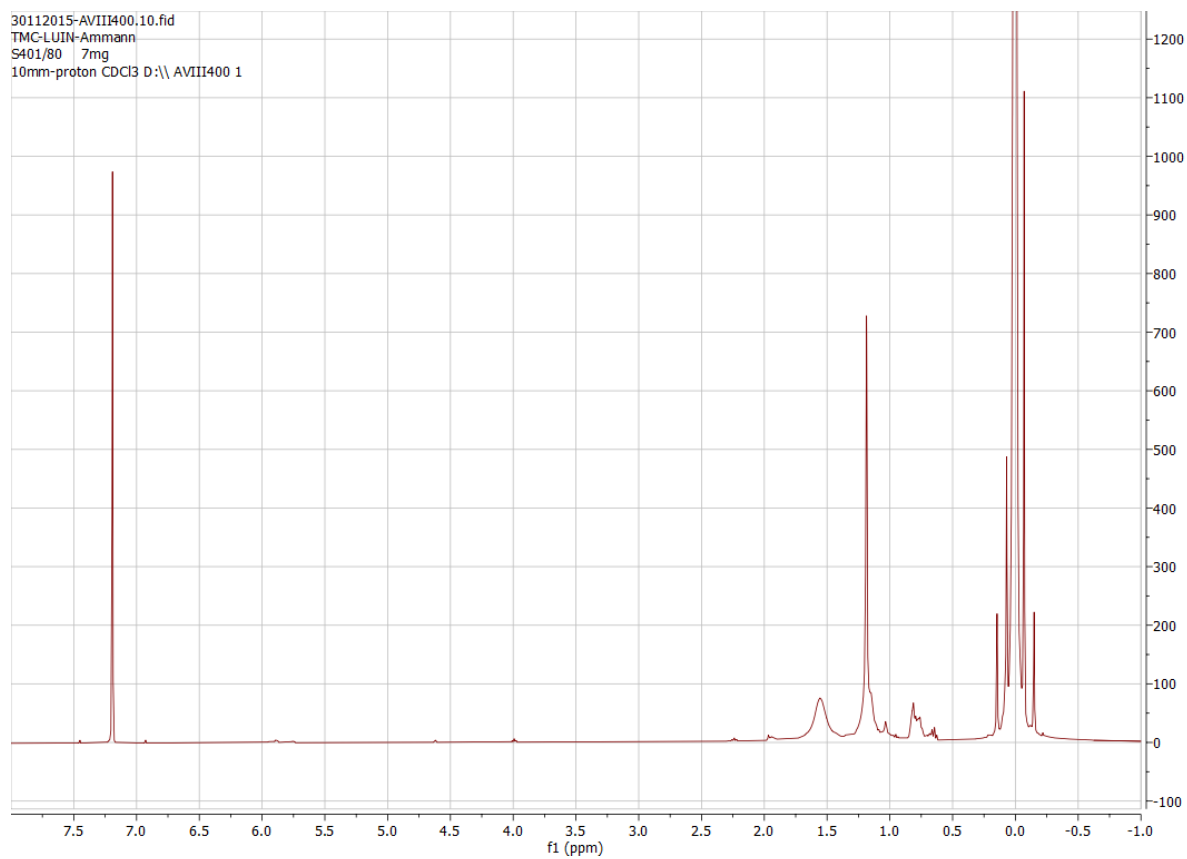


- [84] M. Masudul Hassan, M. R. Islam, M. A. Khan, *Journal of Adhesion Science and Technology*, **2003**, *17*, 737.
- [85] Z. Jia, B. Guo, D. Jia, *Journal of nanoscience and nanotechnology*, **2014**, *14*, 1758.
- [86] Applied Minerals Inc., *Dragonite - Halloysite Clay*, **2016**,  
[http://appliedminerals.com/images/uploads/Dragonite\\_Overview.pdf](http://appliedminerals.com/images/uploads/Dragonite_Overview.pdf). Accessed 01/2017.
- [87] R. Jain, G. B. Nando, *Rubber World*, **1988**, *199*, 40.
- [88] Z. Jia, Y. Luo, S. Yang, B. Guo, M. Du, D. Jia, *Chinese J. Polym. Sci.*, **2009**, *27*, 857.
- [89] L. Liu, D. Jia, Y. Luo, B. Guo, *J. Appl. Polym. Sci.*, **2006**, *100*, 1905.
- [90] S. Varghese, B. Kuriakose, S. Thomas, A. T. Koshy, *Journal of Adhesion Science and Technology*, **1994**, *8*, 235.
- [91] R. Berahman, M. Raiati, M. Mehrabi Mazidi, S. M. R. Paran, *Materials & Design*, **2016**, *104*, 333.
- [92] M. Logvinova, E. V. Sakharova, A. V. Krylov, E. E. Potapov, G. A. Khlebov, V. F. Kablov, L. M. Inzhinova, *International Polymer Science and Technology*, **2013**, *40*, 35.
- [93] X. Li, I. Nikiforow, K. Pohl, J. Adams, D. Johannsmann, *Coatings*, **2013**, *3*, 16.
- [94] H. Lun, J. Ouyang, H. Yang, *RSC Adv*, **2014**, *4*, 44197.
- [95] P. Sun, G. Liu, D. Lv, X. Dong, J. Wu, D. Wang, *RSC Adv.*, **2015**, *5*, 52916.
- [96] S. Matchawet, A. Kaesaman, P. Bomlai, C. Nakason, *Polym. Compos.*, **2017**, *38*, 1031.
- [97] A. Beigbeder, M. Linares, M. Devalckenaere, P. Degée, M. Claes, D. Beljonne, R. Lazzaroni, P. Dubois, *Adv. Mater.*, **2008**, *20*, 1003.
- [98] B. Pradhan, S. K. Srivastava, *Polym. Int.*, **2014**, *63*, 1219.
- [99] E. S. Kim, E. J. Kim, J. H. Shim, J.-S. Yoon, *J. Appl. Polym. Sci.*, **2008**, *110*, 1263.
- [100] G. Martin, C. Barrès, P. Cassagnau, P. Sonntag, N. Garois, *Polymer*, **2008**, *49*, 1892.
- [101] A. Ciesielski, *Introduction to Rubber Technology*, ISmithers Rapra Publishing, Shrewsbury, **2001**.
- [102] K. N. Madhusoodanan, S. Varghese, *J. Appl. Polym. Sci.*, **2006**, *102*, 2537.
- [103] R. S. S. Thomas (Ed.), *Rubber nanocomposites: Preparation, properties, and applications*, John Wiley & Sons, Singapore, Hoboken, NJ, **2010**.
- [104] K. G. Gatos, N. S. Sawanis, A. A. Apostolov, R. Thomann, J. Karger-Kocsis, *Macromol. Mater. Eng.*, **2004**, *289*, 1079.
- [105] V. M. Murty, S. K. De, *J. Appl. Polym. Sci.*, **1982**, *27*, 4611.
- [106] G. Abts, *Einführung in die Kautschuktechnologie*, Hanser, München, **2019**.

- [107] H. Ismail, S. Z. Salleh, Z. Ahmad, *Polymer-Plastics Technology and Engineering*, **2011**, *50*, 681.
- [108] F. Lartigue-Peyrou, in *The Roots of Organic Development*, Vol. 8, Elsevier, **1996**, p. 489.
- [109] G. Camino, S. Lomakin, M. Laguard, *Polymer*, **2002**, *43*, 2011.
- [110] J. W. Gilman, C. L. Jackson, A. B. Morgan, R. Harris, E. Manias, E. P. Giannelis, M. Wuthenow, D. Hilton, S. H. Phillips, *Chem. Mater.*, **2000**, *12*, 1866.
- [111] H. C. Bidsorkhi, H. Adelnia, R. Heidar Pour, M. Soheilmoghaddam, *J Mater Sci*, **2015**, *50*, 3237.
- [112] L. Bokobza, *J. Appl. Polym. Sci.*, **2004**, *93*, 2095.
- [113] J. Dai, *Applied Clay Science*, **1999**, *15*, 51.
- [114] E.-S. Kim, E. J. Kim, T. H. Lee, J.-S. Yoon, *J. Appl. Polym. Sci.*, **2012**, *125*, E298-E304.
- [115] J. Ma, Z.-Z. Yu, H.-C. Kuan, A. Dasari, Y.-W. Mai, *Macromol. Rapid Commun.*, **2005**, *26*, 830.
- [116] M. W. Simon, K. T. Stafford, D. L. Ou, *J Inorg Organomet Polym*, **2008**, *18*, 364.
- [117] K.-W. Park, G.-H. Kim, S. R. Chowdhury, *Polym. Eng. Sci.*, **2008**, *48*, 1183.
- [118] D. Zhu, J. Hou, Q. Wei, X. Wu, B. Bai, *Energy Fuels*, **2017**, *31*, 1519.
- [119] M. P. Wagner, *Rubber Chemistry and Technology*, **1976**, *49*, 703.
- [120] A. Katihabwa, W. Wang, Y. Jiang, X. Zhao, Y. Lu, L. Zhang, *Journal of Reinforced Plastics and Composites*, **2011**, *30*, 1007.
- [121] B. Marinho, M. Ghislandi, E. Tkalya, C. E. Koning, G. de With, *Powder Technology*, **2012**, *221*, 351.
- [122] H. Zimmermann, R. H. Schuster, *Kautschuk-Gummi-Kunststoffe*, **2011**, *9*, 40.
- [123] V. M. Litvinov, P. A. M. Steeman, *Macromolecules*, **1999**, *32*, 8476.
- [124] N. Iqbal, M. B. Khan, S. Sagar, A. Maqsood, *J. Appl. Polym. Sci.*, **2013**, *128*, 2439.
- [125] Y. Li, M. Li, M. Pang, S. Feng, J. Zhang, C. Zhang, *J. Mater. Chem. C*, **2015**, *3*, 5573.
- [126] M. Pittolo, R. P. Burford, *J Mater Sci*, **1984**, *19*, 3330.
- [127] B. Pradhan, S. Roy, S. K. Srivastava, A. Saxena, *J. Appl. Polym. Sci.*, **2015**, *132*.
- [128] S. Praveen, P. K. Chattopadhyay, S. Jayendran, B. C. Chakraborty, S. Chattopadhyay, *Polym. Int.*, **2009**.
- [129] M. Jacob, S. Thomas, K. T. Varughese, *Composites Science and Technology*, **2004**, *64*, 955.

- [130] Deutsche Gesetzliche Unfallversicherung e.V., *Liste der krebserzeugenden, keimzellmutagenen und reproduktionstoxischen Stoffe (KMR-Stoffe)*, **2020**, <https://publikationen.dguv.de/widgets/pdf/download/article/3517>. Accessed 04/2020.
- [131] Sigma-Aldrich, *Safety Data Sheets*, **2020**, [www.sigmaaldrich.com](http://www.sigmaaldrich.com). Accessed 04/2020.

## 8 Appendix



**<sup>1</sup>H-NMR spectrum of Elastosil 401/80 (HTV silicone rubber)**

## **Declaration on Oath**

I hereby declare on oath, that I have written the present dissertation by my own and have not used other than the acknowledged resources and aids. I hereby declare that I have not previously applied or pursued for a doctorate (Ph.D. studies).

Hamburg,